FR-28855
21 December 2020

CONTINUOUS LOWER ENERGY, EMISSION, AND NOISE (CLEEN II)

HIGH-PERFORMANCE CORE, ULTRA-HIGH BYPASS RATIO, GEARED DUCTED PROPULSION SYSTEM

FINAL REPORT — PUBLIC RELEASE

PERIOD OF PERFORMANCE: 10 OCTOBER 2015 TO 31 DECEMBER 2020

Prepared for

Federal Aviation Administration
800 Independence Ave SW
Room 406
Washington, DC 20591
Attention: Levent Ileri

Prepared by

Pratt & Whitney, a division of Raytheon Technologies Corporation
400 Main Street
East Hartford, CT 06118 USA

In Response to
Contract No. DTFAWA-15-A-80010

TECHNICAL CONTACT: Stephen Gatto
TELEPHONE: (860) 565-8266
EMAIL: stephen.gatto@prattwhitney.com

CONTRACTS CONTACT: Kim Sansone
TELEPHONE: (860) 565-2690
EMAIL: kimberly.sanone@prattwhitney.com

GO BEYOND

Published by BACE Editing, Graphics, and Publishing

EXECUTIVE SUMMARY

Pratt & Whitney (P&W) successfully concluded all activities included as part of the technology maturation efforts covered by the Federal Aviation Administration's (FAA) Continuous Lower Energy, Emissions, and Noise (CLEEN) II Program as outlined in DTFAWA-15-A-80010. This proposal addresses the FAA's objective to develop continuous lower energy, emissions, and noise technologies for civil subsonic airplanes under the CLEEN II program, which is a follow-on to CLEEN I program.

P&W's intent with this program was to further develop, design, and validate advanced core-engine technologies that were aimed at improving the thermal efficiency of the current generation of the PurePower® Geared Turbofan™ (GTF) engine, as well as the next generation (NextGen) of GTF engines. The core improvements, when integrated with the ultra-high bypass (UHB) ratio GTF Propulsor previously developed under the FAA CLEEN I program, is estimated to deliver a total of 25% fuel burn reduction, relative to a year 2000 best in-class aircraft, such as the Boeing 737-800. This represents a significant contribution to the achievement of FAA CLEEN Program fuel burn reduction goals.

The contracted work included development of compressor and turbine technologies that will enable higher overall pressure ratio (OPR), higher compressor exit temperature (T3), and higher turbine inlet temperature (T4) for future GTF engines. These characteristics enable the advanced cycle and unique architecture that, when combined with the innovative, UHB ratio GTF Propulsor and result in a gas turbine engine that has the best-in-class thermal and propulsive efficiencies.

Specifically, P&W was successful with the development and demonstration of advanced turbine engine core technologies — even in the face of a global pandemic — achieving all program goals for technology advancement on-time and on-budget in the following areas:

- Compressor aero-efficiency technology for a higher polytrophic efficiency to TRL-6 under the CLEEN II contract and to TRL-7 under a continued P&W initiative
- High-OPR, high-T3 compressor technology for higher temperatures and core thermal efficiency
- Turbine aero-efficiency technology for a higher turbine adiabatic efficiency to TRL-6
- Application of advanced materials technologies and an innovative design that supports non-film cooled turbine design technology to TRL-5, enabling the removal of a significant amount of cooling (about 50%) and corresponding losses to achieve a higher thermal efficiency and corresponding fuel burn benefit.

The high compressor aero-efficiency development objectives to characterize inlet flow, determine sensitivities relative to distortion, bleed, Reynolds number, vane design and their impacts to transient operability of the compressor were validated in both a 2016 full-scale rig and both a ground and flight engine demonstrator. These compressor efficiency improvements were concluded in 2019 with an on-time flight test in an existing GTF product line asset demonstrating 2.2% performance improvement, 0.5% efficiency improvement, and a high power stability improvement of as much as 7%.

Under the CLEEN II contract, P&W initiated conceptual design of the advanced adiabatic turbine system. The program validated a new turbine blade concept technology, initiated in 2015, with two single element cascade rigs before finalizing single element casting designs that were procured in expectation of a full-scale single stage turbine test that completed in late 2020. This full-scale testing was completed at the new state of the art turbine test facility designed, built and commissioned under this FAA CLEEN II contract at the Pennsylvania State University (PSU). The Steady Thermal Aero Research Turbine (START) facility is a high-speed aero durability single stage test asset with unique and innovative measurement capability that yields high fidelity, pressure and thermal measurements.

In all, the FAA CLEEN II scope executed by P&W, with the support of the FAA, offered a strategy that helped develop advanced, aerodynamic-efficiency-related technologies that have been applied to current and planned future products for improved fuel burn. Some of the aforementioned technologies have already made environmental impacts on the current fleet of NGPF aircraft. The successful CLEEN II technologies developed under this contract can enable product improvement capability and environmental benefits for future propulsion impacting impacting 2025+ Entry Into Service (EIS) commercial programs with 1.4% fuel burn benefit expecting a reduction of more than 29,000 gallons of fuel per plane annually.

CLEEN II success, even under 2020 unprecedented circumstances, demonstrates P&W's commitment to continued technology advancements, environmental responsibility, and customer expectations. Achievement in these areas are supporeted by P&W's long term committed technology programs, such as FAA CLEEN, tremendous personnel with experience and expertise using the most advanced computational tools, processes, and validation facilities.

P&W's succesful completion of the CLEEN II program is another key step in P&W's and the overall aviation industry's advancement toward cleaner, more environmental responsibility flight, we look forward to future opporopportunities with the FAA to make a meaningful impact on a sustainable aviation market that benefits civil transportation while reducing the ecological footprint.

CONTENTS

Section *Page*

FIGURES

Figure ***Page***

Figure ***Page***

TABLES

ACRONYMS

A

AWS	Aft Wheel Space

B

BOAS	Blade Outer Air Seal

C

CFD	Computational Fluid Dynamics
CLEEN	Continuous Lower Energy, Emissions, and Noise

D

DDP	Durability Design Point
DOE	Design of Experiments

E

EDM	Electric Discharge Machining
EIS	Entry Into Service
EWC	Endwall Contouring

F

FAA	Federal Aviation Administration
FBR	Fuel-Burn Reduction

G

GIS	Geographic Information Systems
GTF	Geared Turbofan

H

HPC	High Pressure Compressor
HPT	High Pressure Turbine

I

IMC	Intermediate Case
IR	Infrared

K

KE	Knife-Edge
KMPS	Kulite Miniature Pressure Scanner

L

LPC	Low-Pressure Compressor

M

MRL	Manufacturing Readiness Level

N

NextGen	Next Generation
NGPF	Next Generation Product Family
NOx	Nitrogen Oxide
nvPM	Nonvolatile Particulate Matter

O

OPR	Overall Pressure Ratio

P

P/S	Pressure Side
P&W	Pratt & Whitney
PLC	Programmable Logic Control
PoE	Power Over Ethernet
PR	Pressure Ratio
PRT	Platinum Resistance Thermometer
PSU	Pennsylvania State University
Pt	Total Pressure
PTFE	Polytetrafluorotheylene

R

RPCL	Rapid Prototype Casting Lab
RTRC	Raytheon Technologies Research Center

S

SEC	Single-Element Cascades
SP	Speed Parameter
START	Steady Thermal Aero Research Turbine
SVS	Stator Vane Schedule

T

TDC	Top-Dead-Center
TOBI	Tangential On-Board Injection
TRL	Technology Readiness Level
Tt	Total Temperature

U

UHB	Ultra-High Bypass
UT	Ultrasonic

1. INTRODUCTION

1.1 OVERVIEW OF CORE TECHNOLOGIES

Under the FAA's CLEEN II effort, P&W conducted rig testing of new engine core technologies within the High-Pressure Compressor (HPC) and the High-Pressure Turbine (HPT).

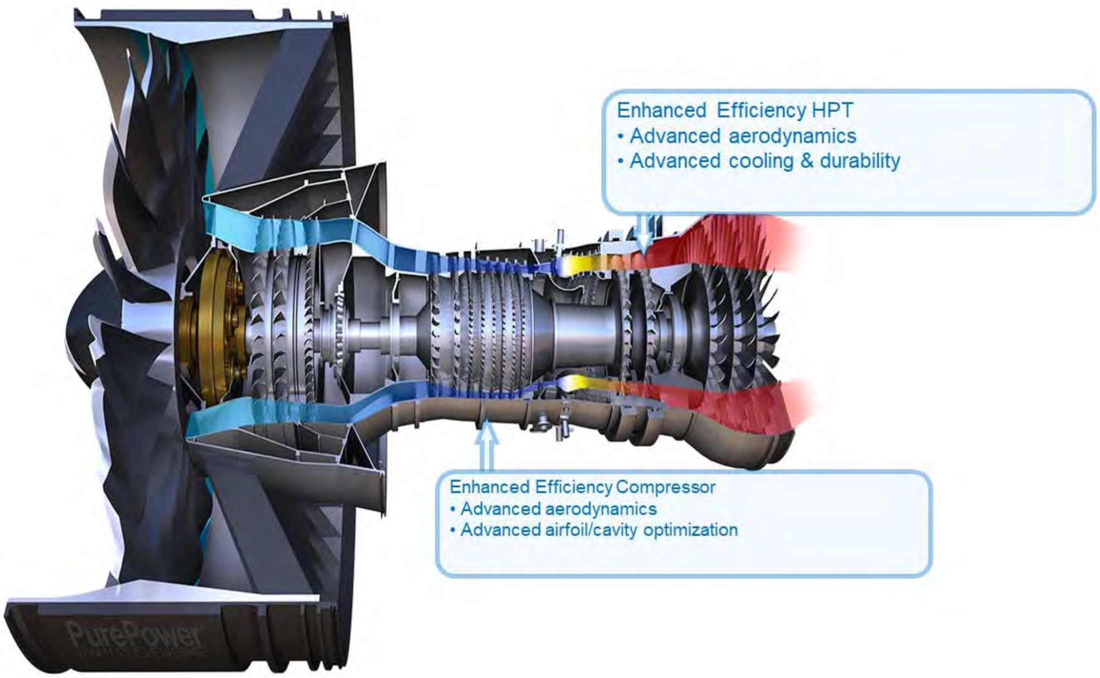

Figure 1-1. *Pratt & Whitney's Geared Turbo Fan Engine with CLEEN II Core Technologies*

The technology suite for the HPC consisted of optimizing the shape for the HPC blades and vanes as well as the cavities located between stages in order to minimize aerodynamic losses. The estimated target fuel burn benefit at the start of the program was a 0.8-1.0% reduction at the system level.

Prior to the FAA CLEEN II contract, P&W had been developing the conceptual and detailed design for a new HPC architecture and configuration. With the help for the FAA, P&W was able to validate the technologies in a module rig test.

The technology suite for the HPT consisted of integrating new concepts in cooling circuitry, cooling hole shape optimization, and new aerodynamic shapes. The estimated target fuel burn benefit at the start of the program for the HPT technologies was also 0.8 to 1.0% reduction at the system level.

With the help of the FAA, P&W designed, built, and tested scaled airfoils with novel cooling hole shapes to tailor film cooling effectiveness for the internal environment of the turbine. Using new methods of instrumentation, P&W was able to quantify film cooling effectiveness. This allows for future designs to reduce the amount of film cooling air necessary in order to effectively protect turbine blades from degradation. Thus reducing overall fuel consumption at the system level.

Also performed under this effort was the design, manufacture and testing of full-scale hardware embodying advances in internal cooling circuitry design and external aerodynamic shapes. The CLEEN II Technology Blade progressed advancements in manufacturing using a new method of creating internal cores for single crystal casting manufacturing. Using the new methods, P&W was able to integrate extremely detailed core features. This directly paves the way for integrating novel manufacturing methods into our production for future product offerings.

Integrated into the Technology Blade design was a 3-dimensional optimized airfoil that took advantage of new core designs to effect cooling efficiency over the surface of the airfoil.

These HPT technologies, combined with the HPC module technologies, enables P&W to offer future products that reduce effort required to compress flow as well as required cooling flow so that the engine can run more efficiently with less fuel consumed.

1.2 COLLATERAL BENEFITS

The compressor and turbine technologies funded with help by the FAA CLEEN II program have improved the way P&W designs commercial products. Module level validation has and will continue to prove out technologies to Technology Readiness Level (TRL)-6 and enables higher efficiency compressors and turbines for a successful entry into service for the next commercial product offering by P&W. Those same analytical tools and design practices used for the design and validation of the CLEEN-funded compressor and turbine demonstrations are also being used to expand the envelope on military engines.

Also with the assistance of the FAA under the CLEEN II program, P&W has been able to make advancements in manufacturing readiness Level (MRL) for advanced turbine hardware casting and machining. Inclusion of new methodologies and technologies necessary to create the advanced HPT blade used in the START rig were made possible by the CLEEN II program. The application of these benefits is not limited to the GTF engine, but across all of P&W's future product lines.

1.3 PROGRAM EXECUTION

The FAA CLEEN II program spanned from October 2015 to December 2020. The original plan was for the program to close in September of 2020; however, a three-month facility shutdown at PSU in mid-2020 due to the COVID-19 pandemic forced the program to be extended by the same duration. Even with this delay, the program completed on-budget and compliant to the 50/50 cost share split with all technical milestones successfully met. The timeline in ***Figure 1-2*** shows the revised schedule due to the COVID-19 impacts.

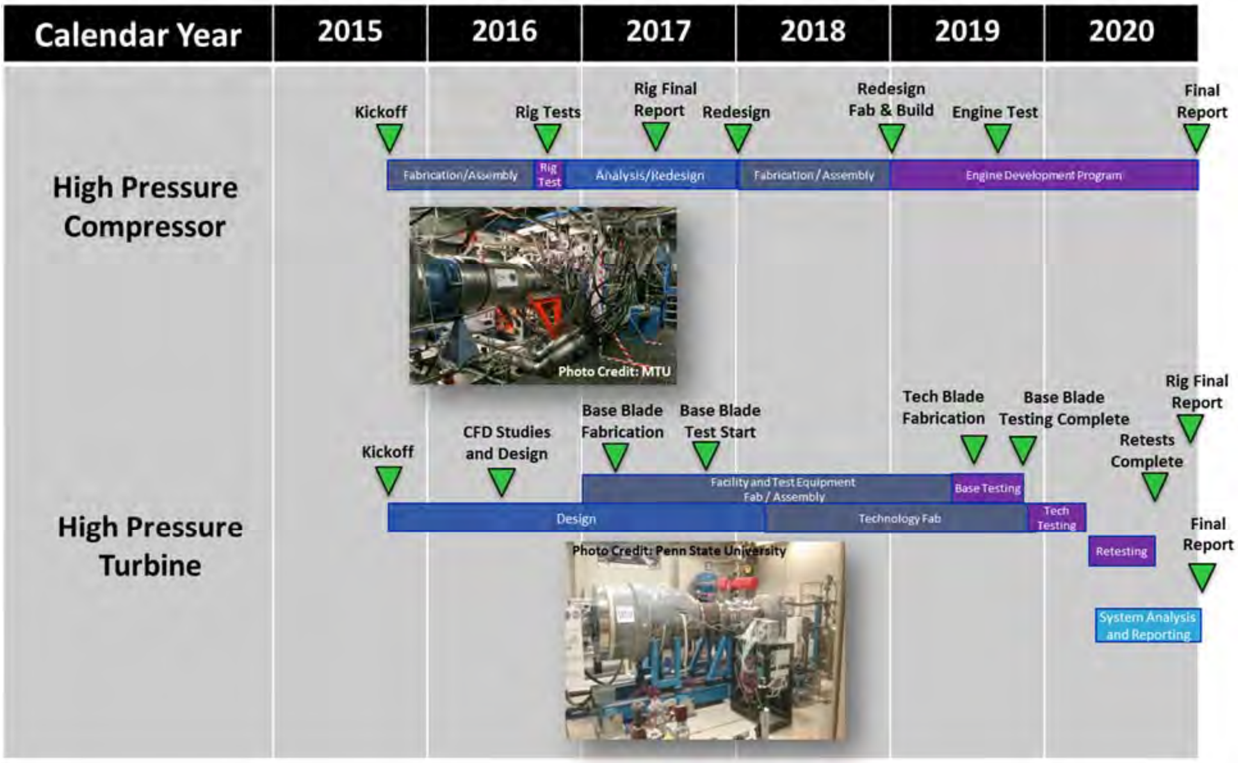

Figure 1-2. *CLEEN II Program Schedule*

2. HIGH-PRESSURE TURBINE CORE TECHNOLOGIES TESTING

2.1 INTRODUCTION

The cooling of the airfoils within a modern HPT presents a formidable challenge due to the high operating temperatures needed to support optimized cycles for reduced fuel burn. So, as engines become more fuel efficient, turbine inlet temperatures continue to increase beyond the temperature capability of turbine airfoil materials. It is therefore necessary to have effective cooling designs in order to protect turbine components from the hot mainstream gases. The air used for cooling purposes is extracted from the high-pressure-compressor stages, which results in a performance penalty because the cooling air bypasses some of the work extraction of the first turbine stage. Therefore, for optimum performance, it is necessary to minimize the amount of turbine cooling.

The portion of the CLEEN II program detailed here focuses on the design and testing of new HPT air-foil-cooling and design philosophies in order to demonstrate their improved efficacy and advance their TRL in preparation for product applications. In order to minimize the cooling air required to meet life and efficiency metrics, both passive- and active-cooling methods were utilized during the design of the CLEEN II HPT. Passive methods comprise modifications of the airfoil profile/geometry to reduce the external connective heat-load distribution, while active methods typically entail internal convective and external film-cooling mechanisms.

The design of film-cooling configurations for HPT airfoils is inherently a multi-disciplinary endeavor. Two of the main disciplines involved are turbine durability and aerodynamic performance. Turbine durability relies on film-cooling to effectively protect the metal surface from the hot mainstream gases and reduce the overall part temperature and subsequently maximize the life of the turbine. Moreover, it is desirable that any mixing losses or additional profile losses caused by film-cooling are minimized in order to achieve optimal aerodynamic performance. There exists a vast parameter space associated with film-cooling performance (including blowing rates, hole geometry, and airfoil loading, to name a few) which has led to various experimental studies which focus on either heat transfer and/or aerodynamic performance optimization for film cooling.

The investigation of the durability and aerodynamic aspects of the new technologies tested under CLEEN II took place in two main phases: small-scale, Single-element Cascade (SEC) testing, and full-scale rotating rig testing. Theoretical and design work had already been largely completed prior to the CLEEN II contract, and so will not be detailed in this section. The main facilities used were the Raytheon Technologies Research Center (RTRC) and the START Rig at PSU, both of which provide state-of-the-art testing capabilities.

2.2 TEST PLANNING AND EXECUTION

Completion of the planned test program required manufacture of a set of technology blades (hereafter referred to as the tech blades) as well as the design, manufacturing, and integration of upgrades to the START Rig to allow for the necessary data gathering. Two important upgrades were the addition of an Infrared (IR) camera system to allow for thermal imaging of airfoil surfaces for durability analysis as well as a 360-degree traversing set of pressure and temperature rakes (hereafter called the 360 degree Traverse) to allow for high fidelity performance measurements. The challenges associated with these prerequisite sets of equipment largely drove the scheduling efforts for the entire program.

The baseline set of turbine blades (rotating airfoils) comprised a set of production blades and so did not require special design, manufacturing, or procurement efforts. The tech blades however, incorporated new cooling and aerodynamic features. PSU and P&W worked to streamline the testing process in order to minimize the effect of hardware availability on the whole program schedule. This was largely successful as significant amounts of time were cut from the originally planned testing period.

Finally, after all components were manufactured and testing was completed, challenges relating to malfunctioning instrumentation discovered during the last planned set of tests, along with the COVID-19 pandemic and ensuing facility shutdown, resulted in the need to add an additional set of tests later in 2020. This represented an approximate 3-month extension of the period of performance (equivalent to the length of COVID facility shutdowns) and two new sets of aero-efficiency tests in August and September of 2020. ***Figure 2-1*** and ***Table 2-1*** represent the final executed CLEEN II program schedule and milestones.

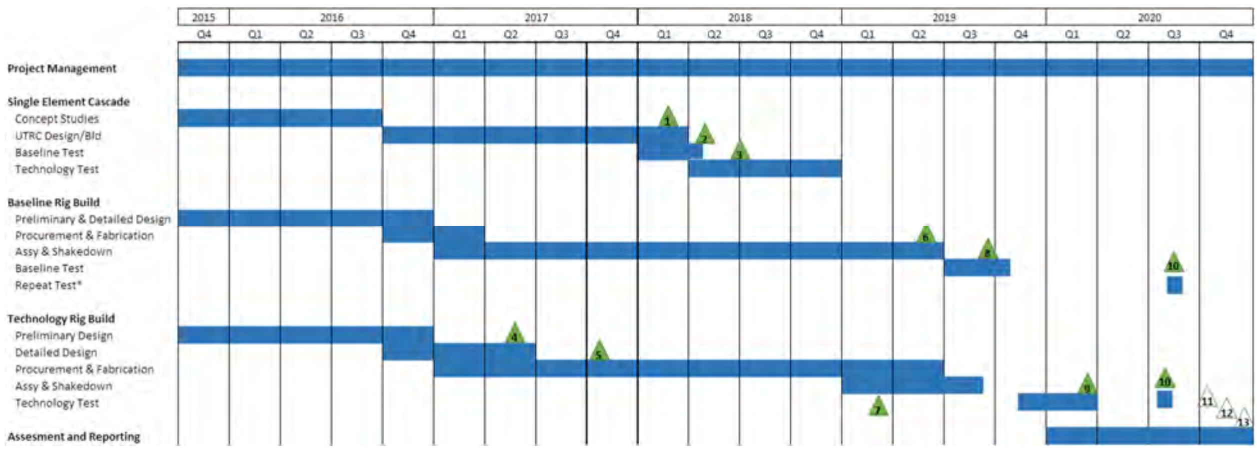

Figure 2-1. *Final Overall CLEEN II HPT Schedule With Milestones*

Table 2-1. *Final Overall CLEEN II HPT Milestone Dates*

Milestones	***Planned Date***	***Complete Date***
1. Cascade Build Complete	2/9/2018	2/9/2018
2. Cascade Test 1	4/13/2018	4/13/2018
3. Cascade Test 2	6/30/2018	6/28/2018
4. Rig PDR	5/19/2017	5/19/2017
5. Rig DDR	10/26/2017	10/26/2017
6. Rig Baseline Testing Start	9/1/2017	8/30/2017
7. Rig TRR	2/26/2019	2/26/2019
8. Baseline testing complete	12/17/2019	12/17/2019
9. Tech blade testing complete	3/12/2020	3/11/2020
10. Repeat efficiency testing complete	9/25/2020	9/22/2020
11. Informal Test Review	11/16/2020	11/16/2020
12. Test Report	11/30/2020	11/30/2020
13. System Level Assessment	12/15/2020	12/15/2020

2.3 FACILITY AND RIG

2.3.1 Overview

As previously mentioned, the CLEEN II HPT testing was conducted at the START laboratory located at the Pennsylvania State University within the University Park campus in State College, Pennsylvania. The Penn State turbine facility supports testing of true-scale, rotating engine hardware with continuous and steady air flow at elevated pressures and temperatures to provide aerodynamic- and thermal-condition similitude to the engine. This world-class research facility was established in 2011 as a collaboration between U.S. academia, industry, and government to further advance the development of modern gas turbine engines and support the aircraft propulsion and land-based power generation industries. Funding was provided to construct the facility and rig from three primary research sponsors including Penn State University, Pratt & Whitney, and the Department of Energy - National Energy Technology Laboratory.

The pursuit of ever-increasing engine efficiency has driven core temperatures higher and higher. Core temperatures in modern engines are often well above the thermal capabilities of the materials involved. Safely operating such an engine requires the use of active cooling to protect these materials and ensure longevity and durability of the relevant engine components. Therefore, the engines are designed to transfer a certain amount of relatively cool, high-pressure air directly to the turbine section through a series of secondary paths and cavities that are located radially inward and outward from the main gas path annular walls. This cooler airflow (termed secondary air) originates from the upstream compressor section, where a portion of the compressor main air flow is strategically bypassed around the combustion chamber. Within the turbine, the cooling air is used to thermally protect the metal hardware including the stationary vanes, platforms, rotating blades, and disks. The cooling air is also employed to reduce or eliminate ingestion of the hot main-gas-path flow into the cavity spaces between adjacent stationary and rotating hardware. This requirement for secondary air extraction for cooling reduces the overall cycle efficiency of the engine through the loss of air from the main gas path as well as creating avenues for leakages in the routing of airflow amongst rotating and stationary hardware. So, with these complex, multi-disciplinary considerations in mind, the PSU START rig facility was designed to support the study of product-relevant improvements.

The START research facility was specifically designed to focus on these important turbine aerodynamic and heat-transfer challenges by providing a heated, engine-relevant environment with the necessary cooling and data-gathering capabilities to study a large variety of different test objectives. Design studies were first conducted to establish the requirements for the necessary engine-relevant conditions to support the capture the most useful data possible. These design studies also helped determine the rig-infrastructure power requirements, which were substantial and required extensive equipment and power grid modifications to support. These substantial power requirements necessitated integration of advanced safety and control systems to maintain the turbine shaft speed and allow the turbine blades to operate at engine-relevant ratios of axial to circumferential air-flow velocities. All of these facility-design measures helped to ensure fundamental aero- thermal parameters, such as Reynolds numbers and Mach numbers, were matched to the engine-relevant conditions.

Prior to construction, a facility like the START lab did not exist at a university in the United States, representing a major deficiency in the ability for U.S. industry and academic institutions to study and understand these topics. The ultimate result of such a deficiency is a competitive disadvantage in the design and manufacturing of the most efficient and highest-performing turbine engines possible. With its establishment and commissioning, the START laboratory at Penn State represents a major achievement for the U.S. to support its competitive edge in turbine engine development. It also represents a fantastic incubator of knowledge for continuing generations of engineers and scientists to study these topics, as evidenced by the great number of Ph.D. and graduate students assisting with the CLEEN II work, as well as the large number of research activities slated for future study in the START rig.

2.3.2 Facility Construction

Facility construction began with site selection in 2011. A site was selected within an existing Penn State research facility, an approximately five-minute drive from the main campus (***Figure 2-2***). Plans were then created to renovate the space for the required research and support equipment. Both indoor and outdoor equipment would be needed.

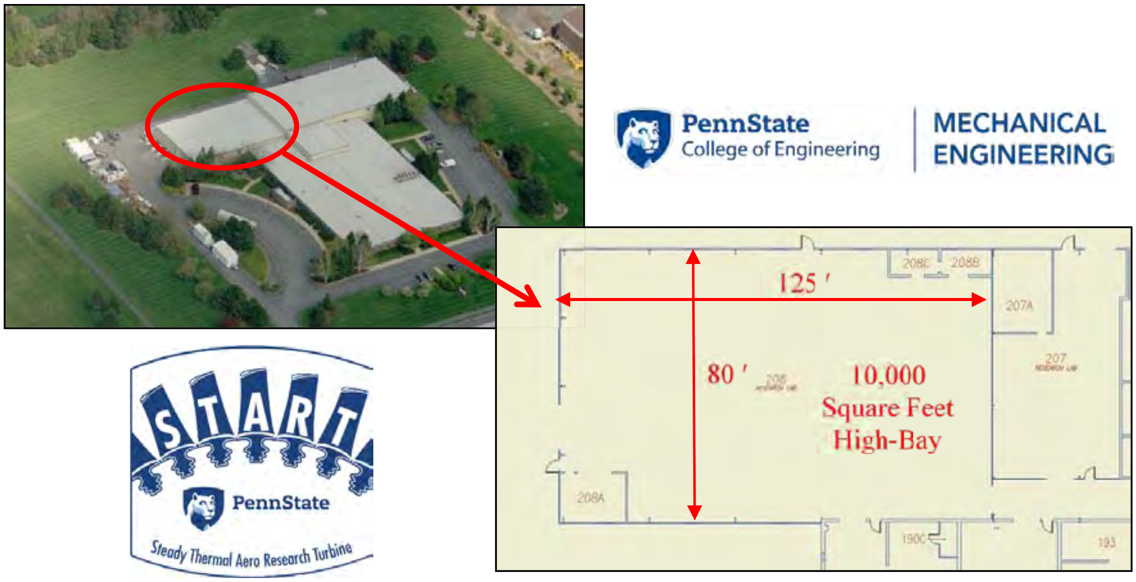

Figure 2-2. *Aerial View of the START Facility Prior to Construction*
A high-bay area in the back of this building was selected for renovation into the START facility. Location: State College, PA

Three primary rooms were planned in order to isolate the turbine test area from both the air flow source equipment and the human command center. The facility design plan consisted of an air compressor room, turbine test room, and a control room, as shown in ***Figure 2-3***. The rooms were sized appropriately to incorporate the necessary equipment and support equipment and infrastructure, as well as human access and support. The command center was designed with safety as a main focus, incorporating the use of ballistic windows.

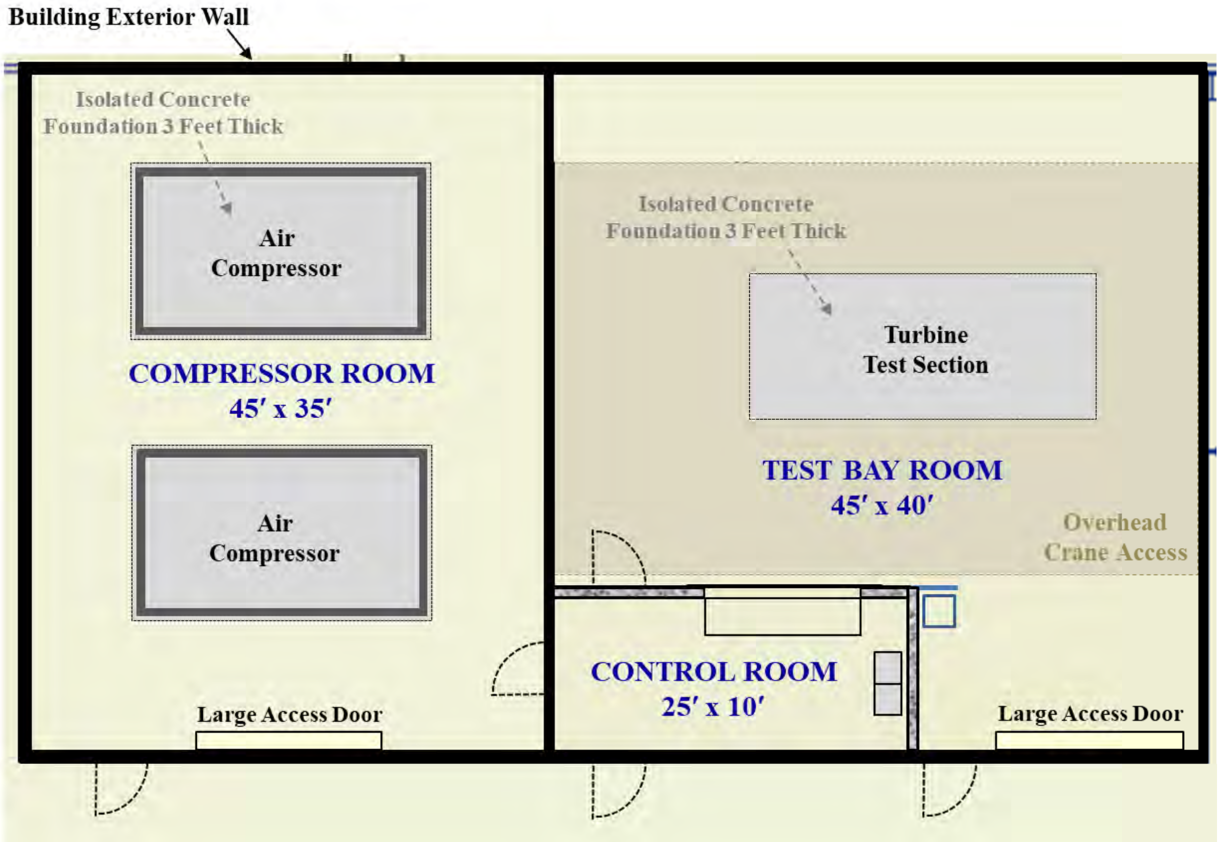

Figure 2-3. *Layout of START Facility Rooms*

The walls of the new facility were specially designed to help contain the sound levels from the rig from spreading throughout the building. Additionally, three isolated concrete foundations were poured to separate the rooms from each other and from the main building. These foundations were a special design feature, which included steel-reinforced concrete slabs approximately three feet thick. The intent was to create very large and strong slab masses that are decoupled from the building concrete floor to eliminate vibration transmission to and from the high-speed rotating hardware within the air compressors and the test turbines. Vibration-isolation joints were also incorporated within all four perimeter seams of each foundation. The renovation of the rooms and space were completed in mid-2012 (***Figure 2-4***) and included the addition of an overhead crane for use in equipment installation as well as rig-configuration teardowns and changeovers. The completed state of the test-facility space is shown in ***Figure 2-5***.

Figure 2-4. *Renovation and Construction Work Performed at the START Facility Building in 2012 Within the Large High-bay Room. Image credit: PSU*

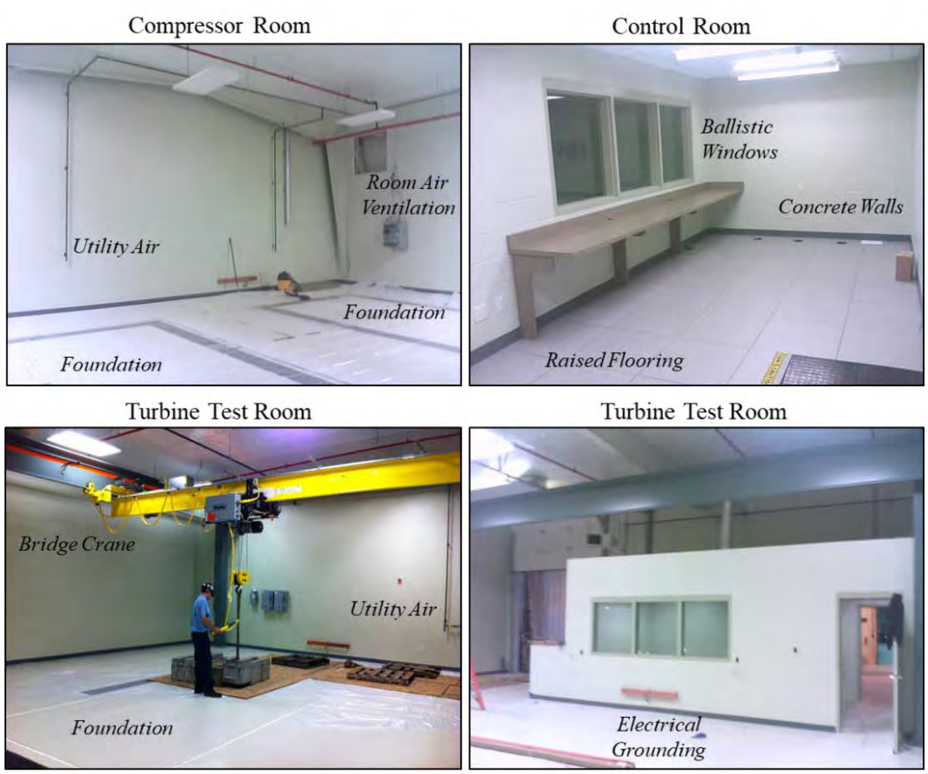

Figure 2-5. *Renovation Completed at the START Facility In mid-2012 Including the Compressor Room, Control Room, and Turbine Test Room. Image credit: PSU*

Upon completion of the test facility space, the sourcing and procurement of test equipment and infrastructure began in the second half of 2012. It was initially planned to first fully integrate one compressor, along with its testing and commissioning, before continuing with the second compressor and additional components. This first compressor, a centrifugal style two-stage machine, was delivered in 2012, with the final completion of piping, fittings, and other necessary equipment being finished in 2014. A single compressor can discharge air at a rate up to approximately 11,000 SCFM. The electrical power requirement to operate a single compressor was approximately 1.1 MW. After incorporation of this first air compressor, it was planned to demonstrate its capabilities by supplying compressed air flow to a test turbine with partial-span vanes and blades (relatively short in height).

With the single air compressor integrated into the facility and successfully demonstrating its use to supply air flow to the preliminary, partial-span test turbine, a second air compressor was acquired. The second air compressor was delivered to the START facility in 2014 and its integration was completed in 2016, including its piping system and electrical equipment. The addition of the second air compressor raised the air flow rate capacity of the facility to approximately 22,000 SCFM. The electrical power requirement to simultaneously operate both compressors was therefore also raised to nearly 2.2 MW. ***Figure 2-6*** shows the stages of compressor procurement and integration.

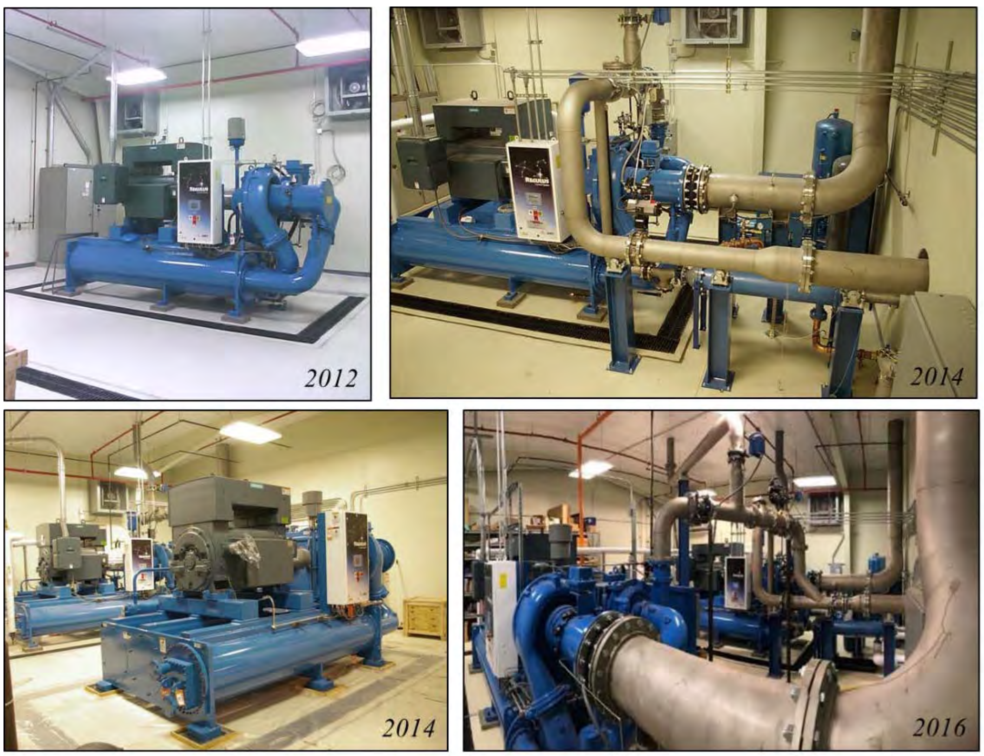

Figure 2-6. *Compressor Room at Different Stages of the START Facility Evolution. Image credit: PSU*
Showing the first air compressor system delivered in 2012 (upper left) and its air piping connections completed in 2014 (upper right); the second air compressor system delivered in 2014 (lower left), and both air compressor systems fully integrated with piping into the rig in 2016 (lower right).

As capabilities of the START facility continued to expand, so too did the infrastructure demands necessary to support the system. Among the required upgrades were electrical additions of a new dedicated 46 kV electrical power line and substation (***Figure 2-7***), a significant increase to automated air-handling capacity in the compressor rooms, and a continuous supply of cooling fluid circulated to critical sub-system components (including an inter-stage air heat exchanger, an oil heat exchanger, and the necessary sub-components). This cooling system is sized to circulate approximate 250 gallons per minute of a water-glycol mixture to cool critical components while transferring the heat outdoors through a system of fans located 50 feet from the building (indoor pumps and equipment are shown in ***Figure 2-8***, while outdoor equipment is shown in ***Figure 2-9***). Also shown in ***Figure 2-9*** are an outdoor process chiller and underground water tank system. These systems are specifically dedicated to the test turbine operation and will be discussed in more detail in Section 2.3. The process chiller system was used specifically to thermally condition the turbine cooling air flowing through the secondary air system. The underground water tank and pump vault system were used specifically to circulate water to a dynamometer, mounted on the turbine test stand and coupled to the turbine shaft. The dynamometer and water system controlled and maintained the turbine operating speed.

Figure 2-7. *Dedicated Electrical Infrastructure Installed at START in 2013 Including a 46kV Electrical Line and Substation to Solely Support the Air Compressor Operation. Image credit: PSU*

Figure 2-8. *Indoor Circulation System for the Air Compressor Cooling Fluid Installed for the START Facility During 2013-2016. Image credit: PSU*

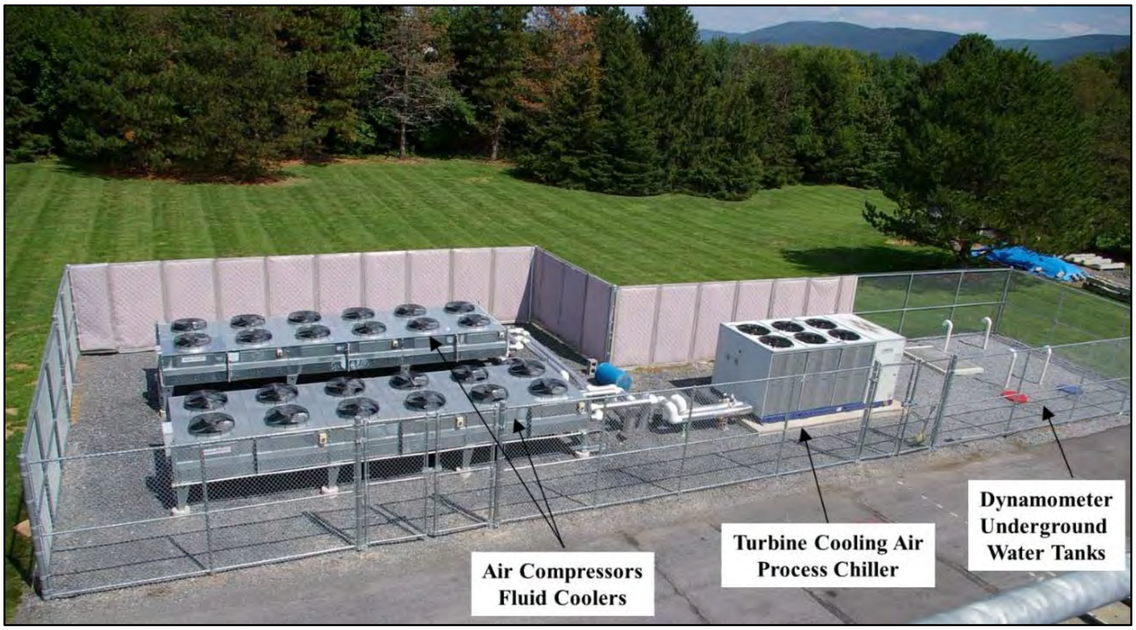

Figure 2-9. *Outdoor Large Cooling Systems for the Compressors and Test Turbines, Including an Underground Water Tank System, Installed for the START Facility During 2013-2016. Image credit: PSU*

To establish the elevated air temperatures passing through the main gas path and entering the test turbines, a natural gas delivery system was installed, as shown in ***Figure 2-10***. The natural gas system provided the necessary fuel required to operate a combustion-based heating chamber upstream of the turbine test section. The natural gas system and heater were both sized to adequately heat the combined total discharge flow from both air compressors up to a maximum temperature of 750°F (675°K). This heating system ensured that the main gas path air flow entering the test turbines would be at a high enough temperature to provide meaningful testing and heat transfer research. The two photographs located at the top of ***Figure 2-10*** show the natural gas delivery system, while the two lower photographs show the combustion-based heating chamber that conditions the air flow prior to the air flow entering the turbine test section.

Figure 2-10. *Natural Gas Delivery System Installed at START During 2016 and the Combustion-based Heater Chamber. Image credit: PSU*

The facility also incorporated a large steel platform that was installed above the compressor room on the building roof, as shown in ***Figure 2-11***. The platform was designed to support two inlet-filter weather hoods (one per air compressor), as well as a series of four industrial-grade exhaust silencers that reduced the sound levels of the exhausting flow. The inlet-filter weather hoods remove dirt and particulates from the air and were piped directly to the inlet of the air compressors. Two exhaust silencers were connected directly to the rig piping located downstream of the turbine test section, and the other two exhaust silencers were each piped directly to the unloading valves of the air compressors.

Figure 2-11. *Outdoor Roof Platform Installed Above the START Facility Compressor Room. Image credit: PSU*
Including the air flow intake systems and turbine exhaust silencers for a single air compressor operation in 2014 (left) and for dual air compressor operation in 2016 (right)

The facility control room was designed to incorporate the necessary operational equipment, as shown in ***Figure 2-12***, as well as advanced data acquisition and monitoring systems.

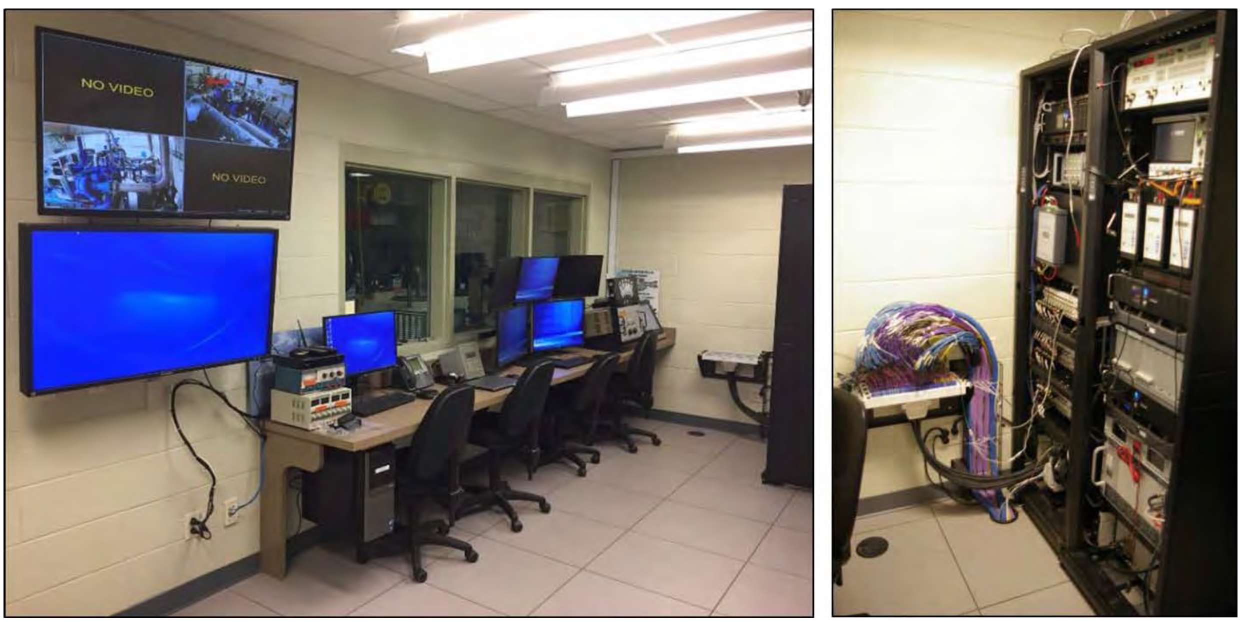

Figure 2-12. *START Facility Control Room Showing the Test Command Center and Data Systems. Image credit: PSU*

2.3.3 Test Rig Equipment

2.3.3.1 Rig Test Conditions

Throughout the process of designing and constructing the test rig and facility, primary focus was placed on sizing and selecting equipment to support test section conditions that offered the best engine representative environment and would produce the most meaningful learning of aerodynamic and heat transfer topics. The main gas path at the inlet of a high-pressure turbine is typically characterized by the air flow conditions that exit the combustor section of the engine in terms of air pressure, temperature, and flow rate. The secondary air system that supplies cooling air to the turbine section is characterized by the conditions present within the turbine disk cavity region in terms of air pressure, temperature, flow rate, and also turbine disk rotational speed.

Through this attention to the necessary rig operating performance characteristics, the non-dimensionalized fluid mechanics parameters are brought to similar levels as in a real world engine. For instance, the air density ratio as measured between main gaspath airflow and secondary airflow (primarily a function of pressure and temperature) are in a similar range of around 2. This parameter directly impacts the sizing of the compressors (supplying air pressure), heaters (heating the main gas path), and chillers (cooling the secondary air). These air conditions and the following appropriate rig and equipment design resulted in properly scaled parameters and a test section analogous to typical engine conditions.

2.3.3.2 Rig Mechanical Design and Function

The basic function and operation of the START Rig will be described briefly here, followed by a discussion of the test section equipment. Outdoor atmospheric air is first pulled into the rig by two centrifugal compressors that then discharge directing the combined flow towards the main turbine test section, after which the air flow is exhausted back outdoors to atmosphere.

Upon exiting the two compressors, the air flow is thermally conditioned. Both the main gas path air flow temperature (which is raised in the heater chamber) and the secondary path air temperature, which is split off prior to the heater chamber (then lowered in temperature in the chiller/heat exchanger), are thermally conditioned at this stage. The rig also includes a series of valves that are used within the air piping circuit to control the air flow rate and pressure passing through each component. Precision flow control valves operate with relatively slow actuation to manage the primary air exchange process during normal testing operation. A settling chamber is located between the main gas path heater chamber and the turbine test section in order to ensure the air flow pressure and temperature are spatially mixed and uniform prior to the air flow entering the test turbine.

Air flow rate is measured as it passes into the turbine through the main gas path and each secondary cooling air path. It is also measured when combined upon exiting the turbine. The turbine shaft power and speed are measured using a torque meter and a dynamometer that are coupled to the end of the turbine shaft. The cooling equipment and dynamometer water system components located outdoors serve primarily to reject the large heat load from the rig to atmosphere. A solid model view and photograph of the turbine room are shown in ***Figure 2-13*** and ***2-14*** that provide context to the physical scale of the rig components and their arrangement, including integrated instrumentation and data systems that will be described in the next report section.

Figure 2-13. *Solid Model Rendering of the Turbine Test Rig Within the START Facility. Image credit: PSU*

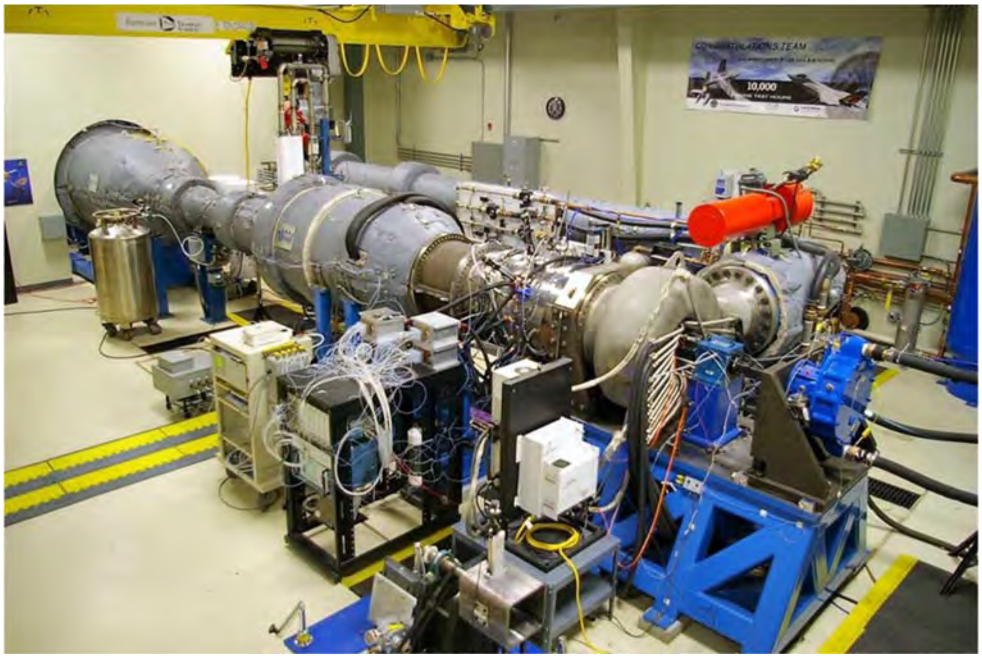

Figure 2-14. An Overview Photograph of the Turbine Room Taken During the Testing Campaigns Showing the Rig and Many of the Test Section Components Including Instrumentation Systems. Image credit: PSU

2.3.3.3 Turbine Test Section

The primary test section of the START rig includes a single stage turbine consisting of one row of stationary vanes followed by one row of rotating blades. The rotating assembly is characterized by an overhung turbine including the disk and blades that are mounted towards the upstream end of the shaft.

The bearing structure and table consist of relatively thick and heavy metal components that serve to provide stiff and rigid supports to the rotating turbine assembly. The two main bearings are located at the forward end of the rotor shaft and at the aft end of the rotor shaft. The two bearings operate using magnets that levitate the main shaft in the radial direction approximately 0.010 inch such that a zero-friction and contactless boundary condition is established for the turbine rotor. The zero-friction operation of the shaft during testing increases the accuracy of determining the true lossless power generation of the turbine rotor system. The magnetic bearing system also includes high frequency response sensors that are used to monitor shaft speed and control shaft position. The position sensors can detect shaft position to within less than 0.001 inch at all speeds. Additionally, the magnetic bearings are actively tunable that allow the user to adjust the stiffness and damping associated with shaft vibration and rotor dynamics, which was performed for the current test program to ensure any critical speeds and vibrational modes were safely managed.

After passing through the turbine test section, the air flow enters a downstream settling chamber in which the air flow passes through a baffle system and is then directed towards the rig downstream Venturi meter and exhaust system.

2.3.3.4 Controls and Safety

The design of the START facility and rig was performed with the safety of the personnel and hardware in the absolute highest priority. The safety plan that was ultimately developed was designed and thoroughly reviewed by the Penn State START team, the P&W CLEEN II team, and the P&W engineering test and safety teams. Safety precautions included simple limitations on personnel, such as the prohibition of personnel to be in the test room when the rig is rotating, as well as two-person sign-off procedures to ensure that any inspection or assembly activities had been performed correctly.

To further protect the turbine hardware during testing, certain operational limits to the test turbine and rig equipment were first identified and then incorporated into an advanced programmable logic control (PLC) computer system that is used during all operation and designed to trigger an emergency shutdown should a critical parameter stray from its safe operating range. Some examples of the primary operational safety limits related to the test turbine itself include the turbine shaft speed, torque, position, and axial force load. Other examples of monitored parameters include those critical to the function of the supporting equipment, such as coolers, chillers, water pumps, etc. A suite of instrumentation sensors is used to actively monitor the critical safety parameters continuously in real time at high frequency responses (kHz).

2.3.4 Instrumentation

Because the START facility operates on a steady, continuous-operation principle, it is critical that the test section reaches a thermally saturated, steady-state condition to ensure thermal boundary conditions are repeatable for test operations and to reduce measurement variability in aero efficiency and durability tests. To determine when a thermally saturated state is achieved during rig testing, a series of efficiency measurements were collected during the shakedown process. During these tests, temperatures near the outer diameter wall at the turbine inlet plane, on the outer skin of the test section hardware, and other locations of interest (defined in ***Figure 2-15***(a)) were recorded versus time. Using these data, an assessment of the startup time required to thermally saturate the rig was defined such that the temperature measurement T-P1-R2 (shown in ***Figure 2-15***(b)) exhibits a temperature change of less than 1°R/min.

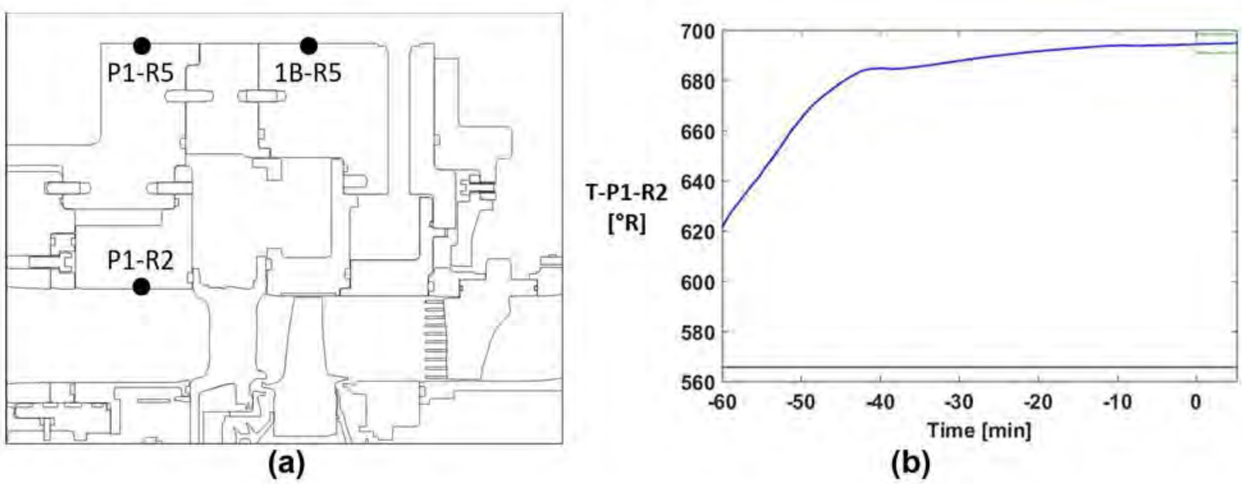

Figure 2-15. *Thermal Soak Criteria Definition*

(a) primary monitor locations; (b) Example time history for temperature monitor location P1-R2, the test period begins at time zero, and the duration of the specified test point is identified by the boxed time interval

2.3.4.1 Efficiency Instrumentation

Turbine efficiency measurements were characterized using stage inlet and exit parameters. Inlet parameters were measured upstream of the vane, and stage exit parameters are measured by a state-of-the-art 360-degree circumferential traversing system downstream of the blades. For program tests that did not require efficiency measurements, the stage exit rakes were removed. In that case, stage parameters, such as stage total pressure ratio, were calculated from a fixed-probe measurement downstream of the blade.

2.3.4.1.1 Turbine Inlet Measurements

Stage-inlet measurements were characterized using six circumferentially distributed exposed bead Type E thermocouples in fixed locations at the midspan upstream of the vane. These thermocouple probes were calibrated using an end-to-end approach maintaining standard wire and channel connections from typical test configurations. Through this wire calibration process, temperature measurement accuracy better than 0.1°R was achieved. Total-pressure probes with 0.125-in. Kiels were equally spaced at the location, however offset from the temperature probes by 30 degrees in the circumferential direction.

These six fixed thermocouples positioned at mid-span provide an understanding of circumferential total temperature variations around the inlet of the turbine test section. A representative example of circumferential temperature variation at the inlet is presented in ***Figure 2-16***(a). In ***Figure 2-16***(a), the temperatures at the aerodynamic design point (ADP) conditions are shown as a difference relative to the arithmetic mean. The measured temperature distortion is highly repeatable and represents the influence of natural convection cooling around the test section. As shown in ***Figure 2-16***, the circumferential temperature distortion is within ±1°R (approximately 0.1% of the ADP set point of 750°R). At elevated Durability Design Point (DDP) temperatures, the distortion is approximately ±1.6°R, or 0.2% of the DDP set point of 860°R.

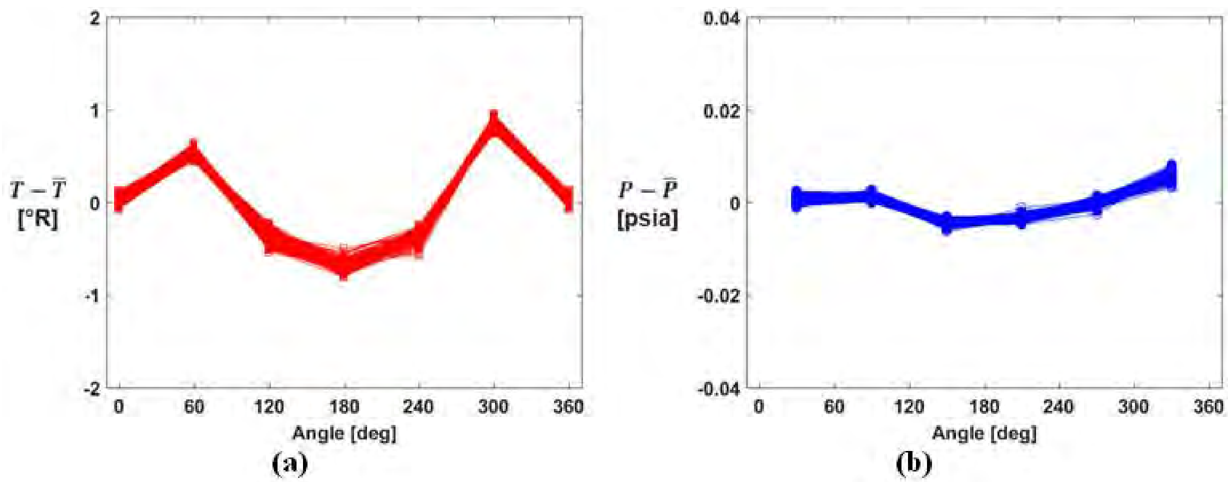

Figure 2-16. *Representative Circumferential Variation of Turbine Inlet Conditions Relative to the Mean at Upstream Plane P0 for ADP Operation: (a) Total Temperature; (b) Total Pressure.*

Similarly, the circumferential distortion of total pressure for the upstream measurement location is shown in ***Figure 2-16***(b). The maximum pressure distortion is shown to be within ±0.007 psia (approximately 0.02% of the ADP setpoint of 41 psia; approximately half of the uncertainty for the pressure measurement itself). Finally, the circumferential pressure distortion was found to be unaffected by temperature increases introduced for DDP operation.

In addition to the midspan inlet measurements, radial profiles of total pressure and total temperature were collected upstream of the vane. Radial profiles of pressure were collected using a United Sensor CA-type three- hole cobra probe with 0.028-in. diameter pressure tubes ***Figure 2-17***(a). Total temperature profiles were measured using a custom Kiel probe with an exposed 28 AWG Type E thermocouple wire (***Figure 2-17***(b)). Representative temperature and pressure profiles for the ADP test condition are shown in ***Figure 2-18***. Here, the experimental measurement points are identified by filled circles. Ultimately, the radial profiles were synchronized with the circumferential measurements of the fixed inlet probes at midspan. It is worth noting that using only midspan data at the inlet rather than the integrated radial profile leads to an over-prediction of stage efficiency.

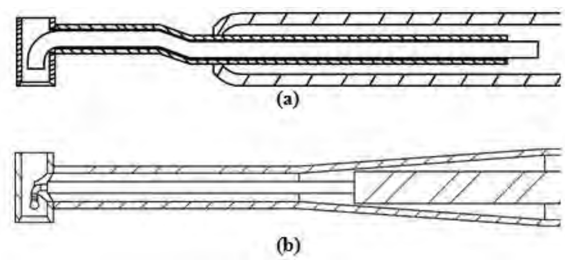

Figure 2-17. *Radial Traversing Probe Designs: (a) Total Pressure Probe; (b) Total Temperature Probe*

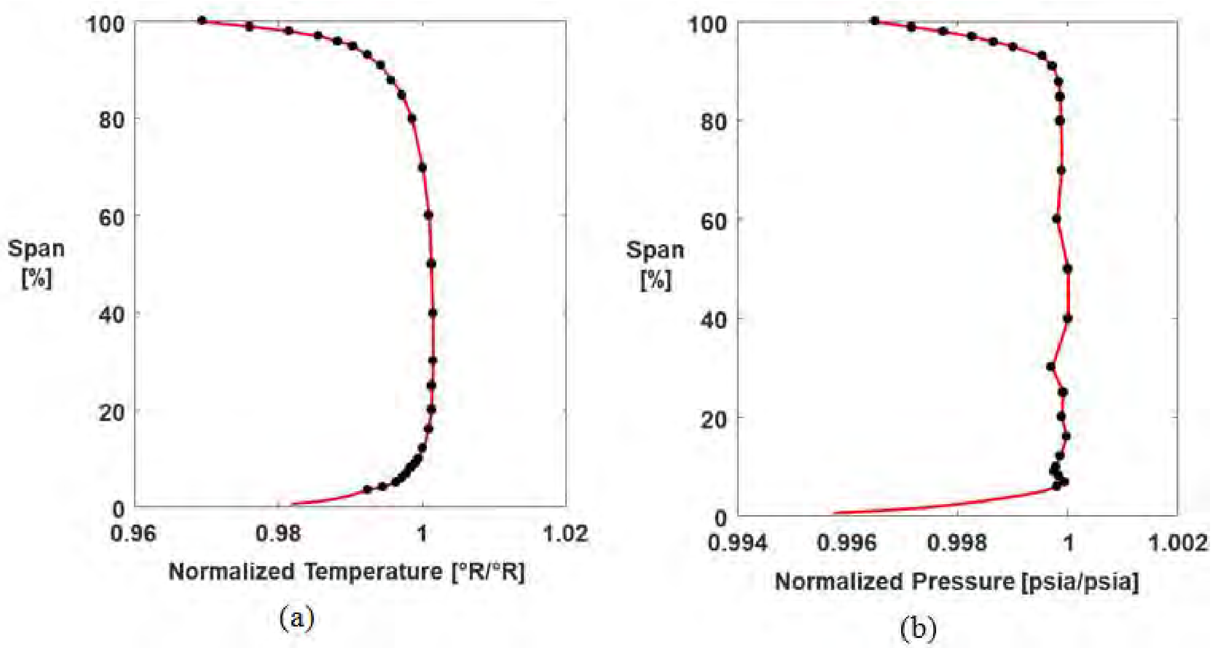

Figure 2-18. *Radial Profiles of Turbine Stage Inlet Parameters at ADP Condition: (a) Total Temperature Profile; (b) Total Pressure Profile*

Additional turbine inlet parameters were characterized using measurements of turbulence intensity with a constant temperature anemometry (CTA) system. Turbulence intensity (TI), is defined using Equation 1, for velocity V, average velocity $\overline{V}$, and fluctuating velocity component, v'.

$$TI=\frac{v'}{\overline{V}}$$

$$V=\overline{V}+v'$$

Equation 1

A TSI hot-film probe with a 0.002-in. diameter sensing element was positioned at midspan upstream of the vane. CTA bridge circuitry was completed using a TSI IFA-100, and frequency response of the system was estimated to be 60 kHz using a square-wave response test. Through this technique, the turbulence intensity was calculated to be 2.4% for a bandwidth up to 20 kHz at operating conditions representative of the current test program.

2.3.4.1.2 Turbine Exit Measurements (360 Degree Traverse)

The Turbine Exit Measurements used for aero-efficiency calculations on the START rig feature a unique, state-of-the-art rotating piece of equipment referred to as the *360 degree traverse*. Many rig-test arrangements employ a set of fixed locations for stationary pressure and temperature rakes. In contrast, the 360 degree traverse allows for unprecedented data gathering of the full circumference of turbine exit duct. What will follow is a brief review of the instruments followed by a discussion of the rotating equipment.

Exit Rake Design

Turbine stage exit conditions were measured using a set of four rakes with equally-distributed Kiels: one 10-element total pressure rake (Pt-10), one 10-element total-temperature rake (Tt-10), one 9-element total-pressure rake (Pt-9), and one 9-element total pressure rake (Tt-9). The rakes of similar types (i.e., Pt-10 and Pt-9; Tt-10 and Tt-9) were installed opposing each other 180 degrees apart. The radial placements of Kiels are arranged such that the Kiels from similar rake types (i.e., both total pressure rakes) alternate span-wise locations to provide maximum spatial resolution once the data from each rake are combined. This arrangement is akin to two combs with the same tooth spacing, but radially offset from each other by half the tooth spacing. The radial placements of the rake Kiels are outlined in ***Table 2-2***.

Table 2-2. *Stage Exit Rake Kiel Measurement Locations (% Span)*

Kiel ID	*Pt-10 or Tt-10 [% Span]*	*Pt-9 or Tt-9 [% Span]*
1	5	10
2	15	20
3	25	30
4	35	40
5	45	50
6	55	60
7	65	70
8	75	80
9	85	90
10	95	-

Each kielhead has a unique angle (see ***Figure 2-19***) associated with its spanwise position. These angles were chosen to follow the CFD-predicted flow angles at the measurement-plane location. It is important to note that, due to the nature of Kiel-probe designs, the pressure and temperature measurements are insensitive to off-incidence flow angles between -20 and +20 degrees.

360 Degree Traverse Rotating Equipment

The 360-degree traverse system represents a collaborative design effort integrating resources from P&W PSU, and Belcan Engineering. In principle, the system operates with the aforementionedfour fixed rakes (i.e. ***Figure 2-19***) equally spaced at 90-degree intervals. Each temperature rake has a dedicatedmulti-cable assembly (two thermocouple cables in total) egressing Type-E thermocouple wires. Each pressure raketerminates flexible tubing to channels of a Kulite KMPS-4 miniature digital pressure scanner (two 16-channel modules, one dedicated to each rake; additional pressure ports are reserved for other traverse-related pressure not connected

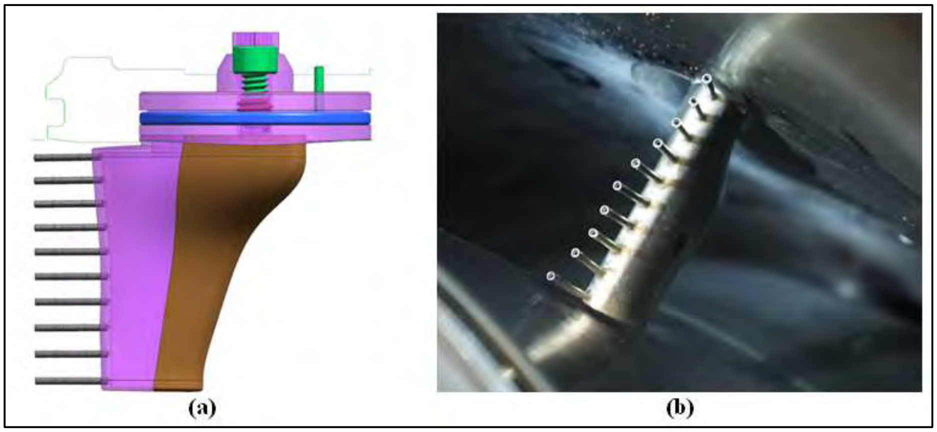

Figure 2-19. *Turbine Stage Exit Measurement Rake*
This view also shows noticeable probe angle changes with span

to rake hardware). Signals from the KMPS module egress from the traverse hardware using one Ethernet cable, including Power Over Ethernet (PoE) provisions to power the device.

To facilitate egress of these wires during the rotational motion of the traverse system, a series of auto-retraction cable housings were designed. These auto-retraction devices use power springs to rewind the cables onto their respective cable coil components. In total, there were three wire-retraction housings to accommodate each egress cable (two multi-channel thermocouple cables and one Ethernet cable for the pressure scanner).

The motion of the traverse assembly through 360 degrees was provided using a stepper motor driving a pinion gear. A belt connected the pinion gear to a large drive gear encompassing the entire traverse assembly. Through this design, the traverse ring to which the rakes are mounted moves, whereas all other surrounding components are stationary. Belt tensioning devices ensured contact is maintained between the pinion and the drive gear. An encoder attached to the common motor drive shaft provided real time feedback of the traverse ring position.

A variety of Kapton-insulated wires (for thermocouples) and PTFE tubing (for pressure rakes) were used with in the housing to facilitate egress.

For the thermocouple rakes, the 0.040-in. MgO thermocouple wires transitioned to Kapton-insulated wires for flexibility. The high quantity of wiring and pressure tubing, thermocouple connectors, and placement of pressure scanner modules all required significant wire and tube management to ensure measurement integrity without damage to equipment. ***Figure 2-20*** highlights the access requirements and distribution of these wires and tubes in the internal traverse cavity.

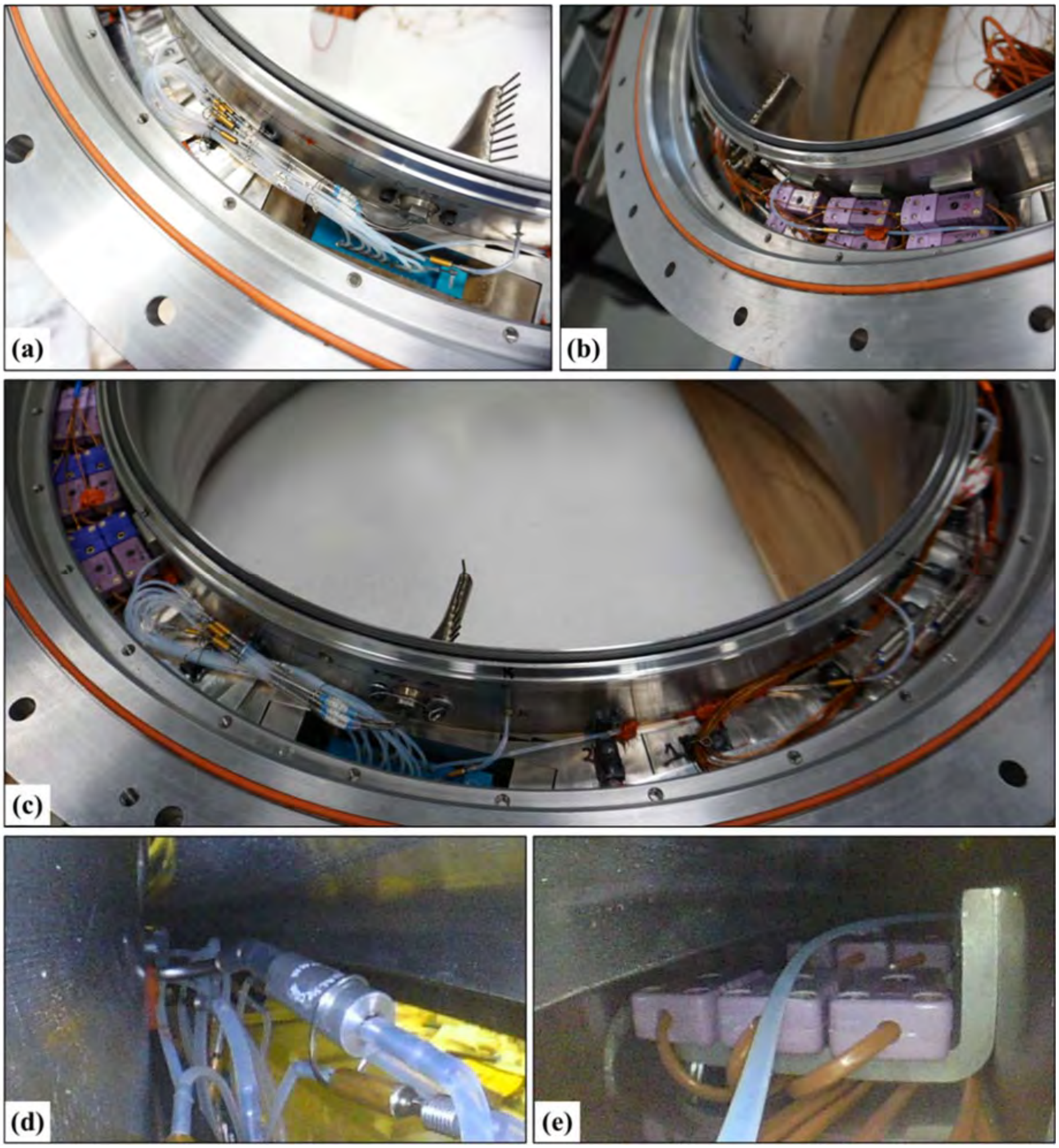

Figure 2-20. *Internal Wire and Tube Management for Turbine Exit Traverse Assembly*
(a-c) View With Open Assembly; (d-e) Borescope Photos of Closed Assembly

As the internal diameter of the 360 degree traverse shared its wall section with the OD of the main gas path test section, steps were taken to ensure thermal protection of the equipment in the traverse. This included selection of equipment for its temperature capabilities, mounting components with a gap between instrumentation/wiring and the wall of the traverse cavity, and providing compressed cooling air (shop air) into the internal cavity during testing (see ***Figure 2-21***).

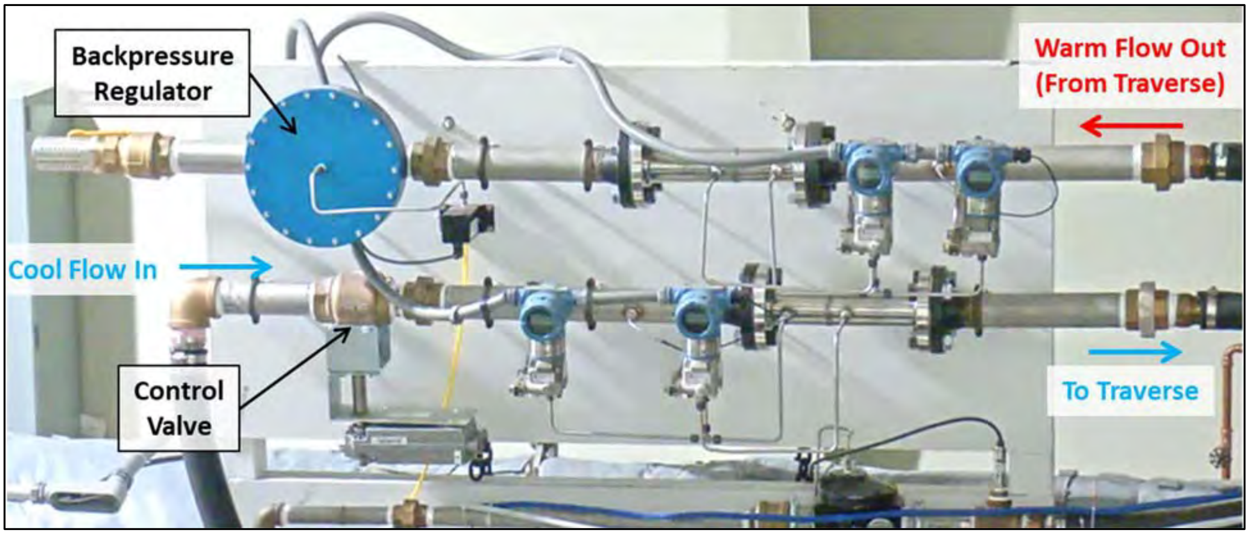

Figure 2-21. *Traverse Cooling Air System*

2.3.4.1.3 Additional Information to Support Efficiency Measurements

Blade tip clearances were measured using a turnkey Capacisense system. This system has a 400 kHz bandwidth, though it was operated with a 200 kHz bandwidth due to magnetic bearing noise. A custom probe that accepts the threaded capacitance sensor was designed to accommodate the thermal growth of the BOAS and case. Four probes were placed in the BOAS, circumferentially located at 3 deg, 99 deg, 183 deg, and 279 deg clockwise from TDC aft-looking-forward. A 0.001-in. tip clearance measurement resolution is achieved with this system. The custom probe and spring assembly is shown in ***Figure 2-22***.

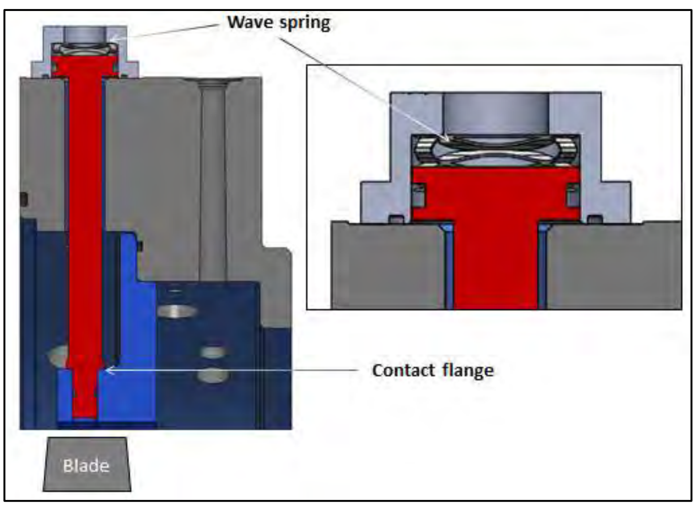

Figure 2-22. *Custom Probe Assembly, Shown in Red, Which Accepts Threaded Sensors*

In order to verify the correct pressure distribution on the vane airfoil surfaces, four vanes were additively manufactured to include internal passages for surface static pressure measurement. Pressure and temperature instrumentation in the vane cavities and upstream of the TOBI allowed for measure the supply conditions of the cooling flows required to calculate the mixed efficiency defined in Section 2.6.3.2.

2.3.4.2 Durability Instrumentation

The selected detector for IR measurements was similar to a camera previously used by P&W so it was possible to leverage some of the learning from that program for thenew START rig instrumentation.

The FAA-CLEEN II program had several IR-related advancements relative to previous engine programs, which included:

1. Improved position accuracy through better rotor shaft indicators
2. Ability to rotate probes for different targets
3. Ability to raise and lower probes
4. Reuse of same probes in multiple locations.

In essence, the IR camera attaches to the rig and accesses the test section where it is able to take several images of the pressure side (P/S) of the turbine blades while running. As noted above, it is movable to allow image capture of different regions of the blades, so that thermal data for nearly the entire surface may be compiled.

Additively Manufactured Vane Doublets

A modified vane doublet to accommodate the IR probe was additively manufactured. This IR doublet is located at top dead center. P&W's Turbine Durability and Aerodynamics groups performed the bulk of the doublet design and came up with a solution that preserves the total flow through the doublet with minimal disruption to the vane aerodynamics. This was in part accomplished by thickening the vane which housed the IR probe while the adjacent vane was thinned.

IR Shakedown Testing

A spin rig was created to be used for preliminary testing of various instrumentation applications before final execution in the START rig. The rig consists of an electric motor driving a shaft connected to an aluminum bladed disk used to simulate turbine blade passing. This spin rig was used to shakedown the synchronization of the IR camera with the once-per-revolution laser tachometer to produce phase-locked images at rotational speeds up to 6,500 rpm. Paint dots were applied to the blade portions in order to study the effect of rotational speed and camera integration time on image blurring. Several more disks were also used to study IR camera performance on even higher linear speeds, properly simulating rig conditions.

2.3.4.2.1 IR Camera Measurements

The amount of radiant energy collected by an IR detector is affected by both the surface temperature and the background temperature. The impact of the background temperature may be minimized by maximizing the emissivity of the blade surface.

When adding a coating to the blade surface, both the radiative heat transfer and conductive heat transfer can be affected. A coating on the surface can in some cases act as an insulator, increasing the blade surface temperature. This effect was quantified during calibration and that the coating procedure had minimal impact on a blade's internal cooling operation.

A need for contrasting features on the blade was identified for the 2D-to-3D image mapping process which was achieved by using a low-emissivity metallic paint without affecting the aero-thermal performance of the blades.

The infrared camera was calibrated using a bench-top setup, before inserting the camera into the START rig. This involved the use of a plate with embedded thermocouples and in the same high emissivity coating as the blades, which could be used to correlate IR images to directly measured temperatures. This calibration ensured a very high degree of precision in the thermal data that was gathered during testing.

2.3.4.3 Instrument Calibration

Thermocouple wire calibration is performed with an oil bath with a temperature stability of better than +/- 0.03°F. The reference sensor is a platinum resistance thermometer (PRT) and is measured by a thermometer read-out. The manufacturer's stated uncertainty for this PRT at the tested temperature is +/- 0.03°F which includes uncertainty due to 100 hour drift and three thermal cycles from the min-to-max temperature range for hysteresis effects.

An aerodynamic recovery calibration was performed. A total of 12 Mach calibrations and one yaw calibration were performed for the temperature rakes at room temperature conditions. A single yaw calibration was performed for the pressure rakes.

Pressure devices are calibrated against a reference pressure generated by a pneumatic pressure controller. The Scanivalve pressure modules have a built in CALZ command which is used at least once per day to perform a zero offset calibration. Calibration of these Scanivalve modules are conventionally performed using the built in calibration ports.

The Kulite Miniature Pressure Scanner (KMPS) that measures the exit traverse pressures is calibrated in a two-step process. The KMPS is first calibrated in increments at room temperature in order to adjust the gain value of each sensor. The second step of the calibration is to account for measurement sensitivity due to temperature effects.

Capacitance tip clearance probes were calibrated using the actual test rotor on PSU's balance machine. The tip clearance probe was mounted onto a traverse system in order to determine the true axial position of the probe relative to the blade leading edge and also to define the zero position of the probe tip to the blade tip, i.e. when the probe head is in contact with the blade tip. Typical calibration variability is less than 0.001 inches. Probes are calibrated with their respective tri-axial cable, coaxial cable, and oscillator and demodulator setup.

2.3.4.4 Data Acquisition

Rig operation, facility monitoring, and primary data acquisition is performed with LabVIEW. The LabVIEW front panels are divided into three screens dedicated to traverse controls, facility monitoring, and test section monitoring and cooling flow control. These three panels are updated to the facility operator effectively at 1 Hz. Voltage signals, thermocouple signals, and pressure signals, are sampled at rates from a few Hz to a few kHz. These sample rates are optimized to balance multiplexing rates, device accuracies, and samples counts with overall refresh rates for the main LabVIEW application.

After the START rig has achieved *steady state* conditions at the operating point of interest, data is acquired for approximately 1 minute. This 1-minute length of data is then averaged together to produce a single data point for each piece of instrumentation. This single data point, which represents the average value across the 1 minute of data acquisition, is used for post-processing operations and efficiency calculations.

2.4 TEST ARTICLE DESIGN AND FABRICATION

2.4.1 Overview and Casting Process

The purposes of the CLEEN II program were to advance the technologies for better fuel efficiencies in the turbine portion of an engine. The GTF engine series was selected as the baseline test bed with the expectation that new technology advancements achieved in this program would be useful in future engines of this model line. As such, the blades used for baseline comparison testing were actual production blades for this engine. The new technologies were incorporated into the specially made technology, or tech blades.

As the baseline blades were sourced directly from the production blade program and their performance has been well documented in numerous hours of actual on-wing flight time, details will not be given in this section regarding the design considerations or manufacturing processes for these blades. This section will instead focus on the design of the tech blades, how they differ from the baseline blades, and the manufacturing of these new specialty blades for the CLEEN II program.

The FAA CLEEN technology blade introduces significant design changes relative to the baseline production HPT first blade to improve thermal and aerodynamic performance. These design features include leading-edge, pressure- and suction-side skin cores for a multi-wall internal cooling geometry, tip-vortex control via tip bowing, multiple tip-surface squealer pockets, and reduced cooling-hole count for reduced Electric-Discharge Machining (EDM) costs.

The blades were cast by P&W's Rapid Prototype Casting Lab (RPCL) in East Hartford, Connecticut, using advanced technology ceramic cores. Throughout the various steps of development of this blade, learning was attained for how to properly cast advanced airfoils. Learning from this development program was directly transferred to future HPT blade designs.

2.4.2 Core Configurations

The CLEEN tech blade consists of a variety of internal cooling feature configurations for a rainbow wheel of testing. It should be noted that the external shape of all the tech blades was common. The first batch of castings produced does not have crossovers between core passages. The last batch of castings produced possess six crossovers between the 2nd and 3rd pass of the serpentine core passages. The crossovers were intended to re-energize the OD cavity where the cavity is was starved of flow due to core manufacturing non-conformances. Again, the blades with these different core con- figurations have the same external shapes, and there is no visual difference between the two when looking at the external surfaces of the parts. The resulting machined blades from these castings then have four coating configurations: blades without coating, blades with primer only, blades with primer and PTFE, and blades with black paint (for IR emissivity). This results in a total of eight different finished machin--ed blade configurations in the turbine disk for testing.

2.4.3 Design Considerations

Aero/Durability optimized designs are aimed at maximizing the use of internal convection and film cooling for increased turbine performance and long life with less cooling flow. Key to the design of the Tech blade was to carry out multi-disciplinary workflows and optimizations that introduce physics-based tools with heat-transfer predictive capability in the aerodynamic design process. The external airfoil loading is shown in ***Figure 2-23***, which can also reduce heat transfer coefficient at the leading edge of the airfoil.

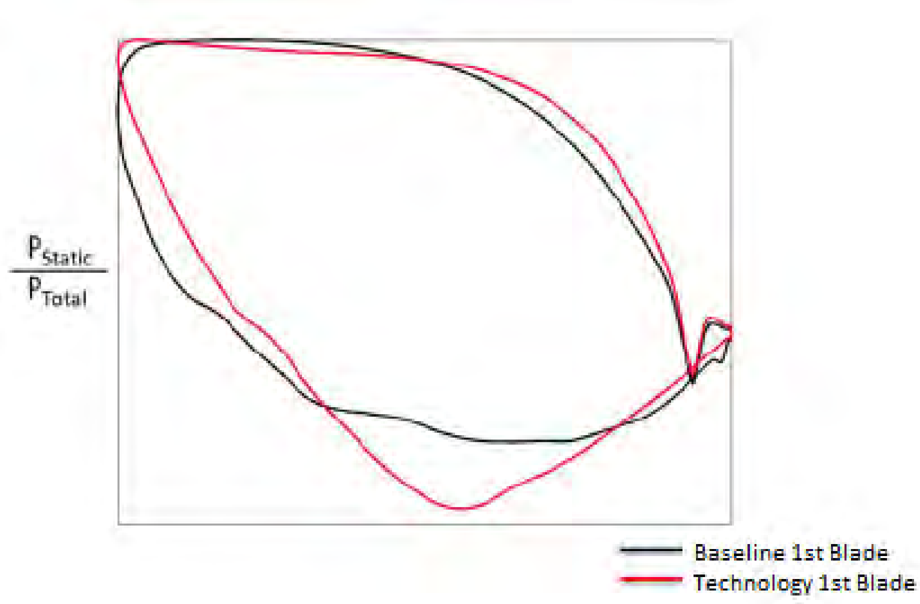

Figure 2-23. *Comparison of Loadings at 50% Span*

Non-axisymmetric endwall contouring (EWC) was applied to the blade-hub flowpath to reduce secondary flow losses.

CFD-predicted radial profiles of total pressure and temperature at the exit plane of the single stage turbine are plotted in ***Figure 2-24***. Profiles are shown for both the baseline and tech blade configurations here. The main differences evidenced by these plots is that the tech blade is predicted to alter the radial profiles more evidently in the outer half of the span than the inner half. In fact, the tech blade radial profiles are predicted to nearly match those of the baseline blade in the inner half of the span.

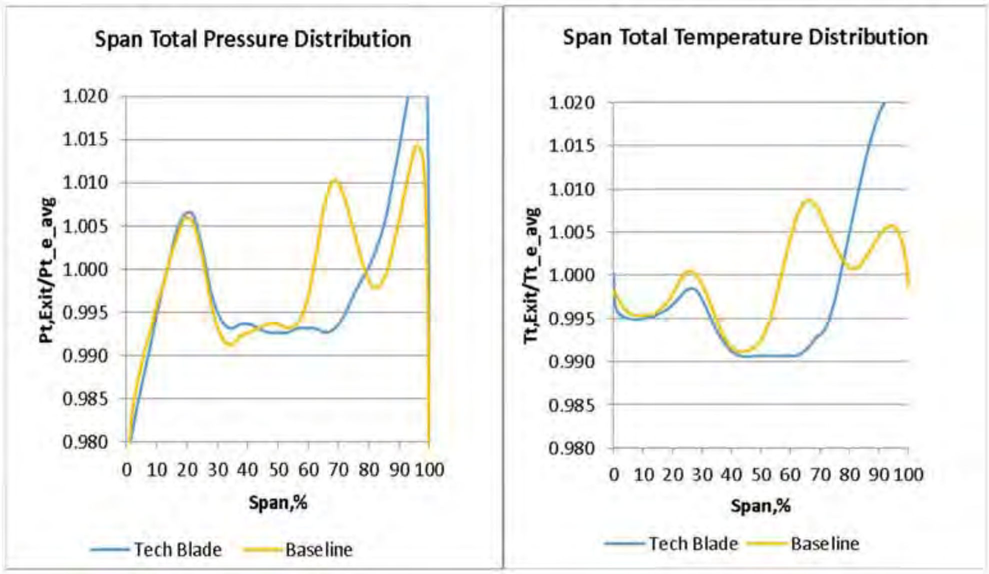

Figure 2-24. *Comparison of Exit Pressure and Temperature Distribution*

2.4.4 Hardware Inspections

Typical inspection methods for multi-wall castings include a combination of CT and ultrasonic (UT) scan techniques. The CT scanning is necessary for the internal locations where the UT probe cannot be used. CT scanning is Computed Tomography — a computer processed combination of x-rays at various angles to produce *virtual slices* through the part. As the tech blade is an atypical double-wall design, CT scan was more appropriate for wall thickness checks and was the primary method used. There were 47 total inspection points, including the leading edge, internal multi-wall, concave side, convex side, and trailing edge inspection points.

Aside from min-wall checks at specified radial sections, full-sweep CT scans were used as well. The full scan allowed the HPT team to view issues like kiss-in, where skin core and internal cores intersect as well as core break, which may not have been detected with the fixed radial sections. Kiss-ins were evident towards the tip of the blade, causing pressure equalization in the individual cores, resulting in deviation from the design intent. Core break, also evident towards the tip, resulted in restriction of flow to exit the tip. The full CT scanning of all hardware allowed the IPT to select the best parts from the group for the rig test as well as allow RPCL to identify areas where additional improvements/adjustments and possibly bumpers (cores positioning features) were needed.

The detail radius of the tip of the blade was designed to match the tip of the baseline rig blades. The baseline rig assets were product relevant development engine blades that were stripped of their metallic and ceramic coatings and were then re-coated with primer or primer and PTFE of various thicknesses, to provide IR capability in the START and maintain similarity to the tech blades. The baseline blades themselves had a tip radius which was a function of machining. This radius was machined from the blades after they were installed in the development rotor, were shimmed out, and then underwent a grinding process for the rotor.

The tech blades were designed to have the same tip radius but did not undergo a grinding process in the rotor. The tech blades were detail ground only, and any variation in sizing in the individual rotor slots added to the machining tolerance variation in each blade that can then impact clearance between the blades and Blade Outer Air Seal (BOAS). Through detailed bench measurements, Penn State verified that, while shimmed in the rig rotor, the tech-blade-tip radii were equivelant to the baseline blades at cold conditions.

Furthermore, the capacitance probes in the START record measurements of the tip clearance between each individual blade in a wheel, and the BOAS. Capacitance probe data for the baseline blades showed that individual blade tip clearances vary by about .003 in. across the baseline blades in the wheel. Given the differences between coated and uncoated blades and the differing thickness of coatings, these variations were expected and also shown to be minimal, illustrating the tight tolerances held during construction of the rig.

2.4.5 Changes from Design Intent

Casting single-crystal airfoils for use in turbine engines is notoriously difficult and it was therefore no surprise that casting the tech blades, a first-time casting for this design, with several brand-new features, presented challenges and delays. Careful attention was paid to the necessary rig-to-engine corrections and additional bookkeeping to discern accurate back-to-back thermal and performance comparisons. These rig-to-engine corrections enable the use of the tech blades to gain useful insights related to future products.

2.5 RIG OPERATION AND TEST EXECUTION

With all necessary equipment becoming available and the necessary preparatory tests and calibrations completed in the latter half of 2019, aero-efficiency testing began in August 2019 with the baseline blade. The IR equipment was then assembled into the rig and the baseline IR tests were completed at the end of the year. A swap was done to install the tech blades, and the IR tests completed in early 2020. This was followed by a change of configuration back to the aero efficiency equipment, and the tech blade aero tests were completed in March of 2020.

Overall, the rig performed very well during the IR testing, so the information in this section will focus on the aero-testing which showed a few issues during the initial tests in August, and then more severe issues in March, which eventually required a repeat of those tests. The executed test program is outlined in ***Table 2-3***, where the efficiency tests are divided into round A (original tests) and B (repeat tests).

Table 2-3. *Executed Test Program*

Test Round	*Blade*	*Test Dates*
Efficiency-A	Baseline	August 2019
IR	Baseline	December 2019
IR	Tech	February 2020
Efficiency-A	Tech	March 2020
Efficiency-B	Tech	August 2020
Efficiency B	Baseline	September 2020

A couple of minor issues presented themselves during the August 2019 baseline blade aero testing. With the 360 degree traverse, data gathering was limited to 350 degrees instead of the full 360-degree sweep. This was quickly remedied by moving limit switch. Additionally, a localized temperature variation was apparent when plotting the temperature data. This was traced to a slightly recessed BOAS cap plug. Both these issues were comparatively minor and were addressed prior to running the efficiency tests for the tech blades in March 2020.

During the first test campaign of the baseline blade in August 2019, data from the 360 degree traverses, visualized as full-annular plots, revealed unexpected, very localized regions of high temperature and pressure near Top-Dead-Center (TDC) (***Figure 2-25***). After conducting a thorough root-cause analysis, it was found that a port for IR camera access port in the BOAS was not plugged in a flush manner (see ***Figure 2-26***). When each rake traversed past this circumferential location, the effective blade tip clearance was increased by up to 0.050" (See ***Figure 2-26***(a)). In addition to this hardware deviation issue, the test team learned that the traverse stop-switch prevented achievement of a full 360 degree traverse. The resulting gaps in data are shown in ***Figure 2-25***. These issues were rectified when the tech blade was run and 2nd test campaign.

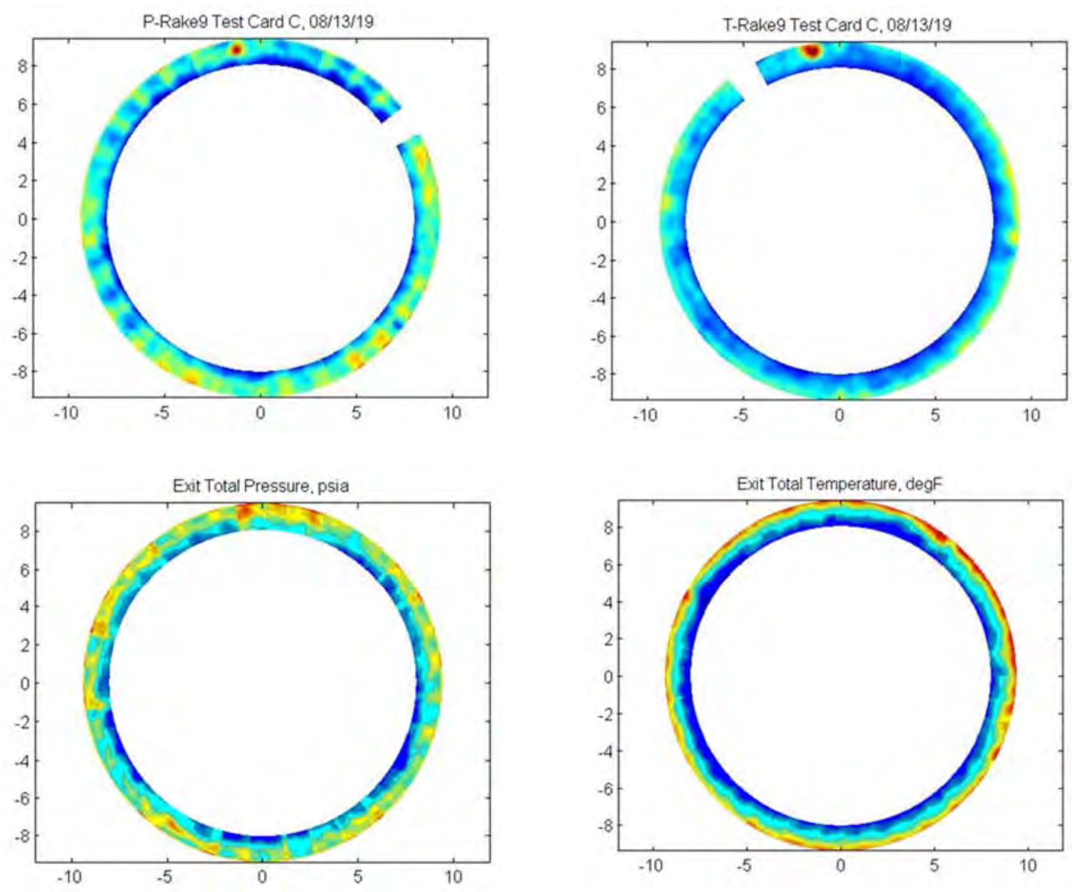

Figure 2-25. *Baseline Traverse 9-point and 10-point Probes Reading Contours*

Figure 2-26. *Thermal Imaging Access Port Plug*
Originally slightly recessed, now shown flush-coated for 1st test campaign tech blade efficiency and subsequent 2nd Test Campaign Baseline Blade and Tech Blade

Just after completion of the tech blade efficiency tests in March 2020, the COVID-19 pandemic caused a shutdown of the START facility for several months. During this time, data processing continued, and it became apparent that there was an issue with some aspects of the rig, causing widely varying efficiency data. The efficiency data had been very stable during the August 2019 test, and within the stated objective of this rig of achieving +/- 0.10% repeatability. The March 2020 tech blade efficiency data showed a much larger amount of variability at +/- 1.38%.

The investigation into what was causing the variation was hampered by the inability to go into the rig to do any tests. However, during the shutdown it was possible to continue scrutinizing the data and eventually the issue was traced to a failing power supply in one of the upstream Scanivalve pressure units (***Figure 2-27***). The START facility was reopened in June 2020 and testing confirmed this hypothesis, with the power supply on this unit drifting significantly throughout the day, indicating a failing piece of hardware (***Figure 2-28***).

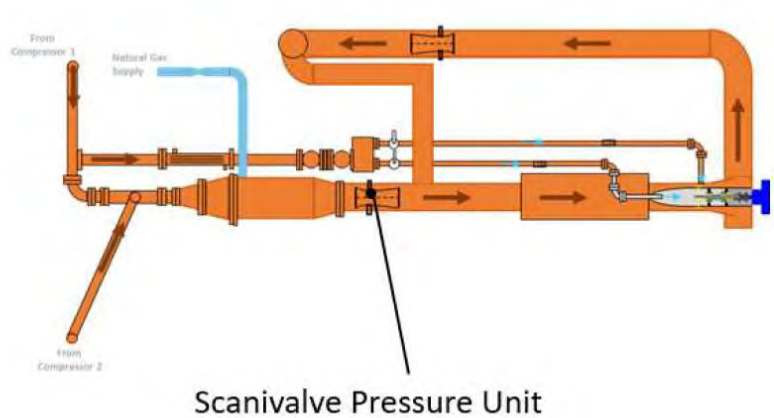

Figure 2-27. *Location of the Scanivalve Pressure Unit — Upstream of the Test Section*

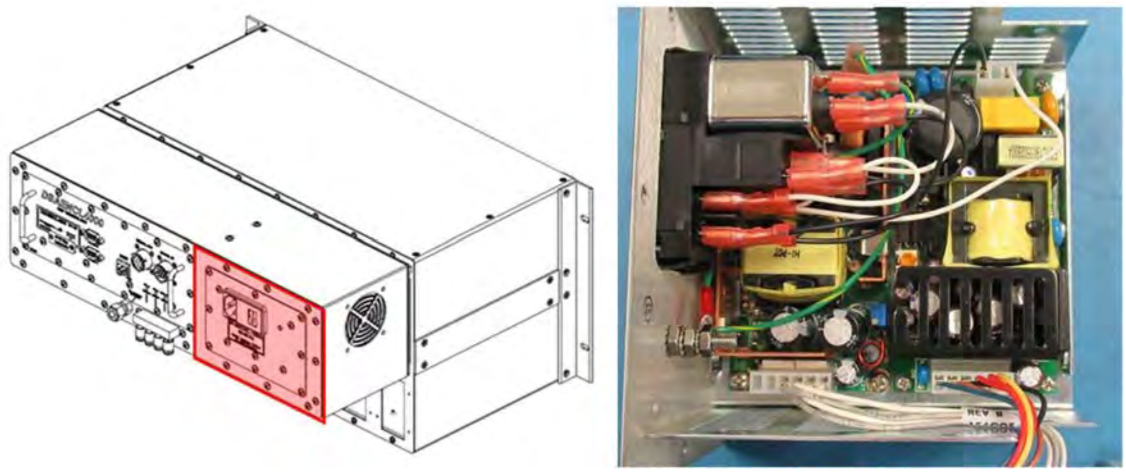

Figure 2-28. *Detail of the Failing Power Supply Hardware Component*

With the issue now known, a plan was developed to repair and upgrade the START facility and complete a set of repeat tests to ensure the best quality aero-efficiency data for the system level performance assessment. Facility repairs were conducted from June through July of 2020, with additional monitoring added as well as procedural changes designed to increase the repeatability further (such as modification to the thermal soaking procedure).

These upgrades were completed at the end of July 2020, and the repeat tests began in early August. The tech blades were already in the rig and so testing began with those blades. At the end of August a swap was done to install the baseline blades back into the rig, and those repeat efficiency tests were completed by the end of September. The new repeat data achieved the goal of improving the quality and repeatability of the efficiency tests, and providing better back-to-back results for assessment. Both tech and baseline blade test now achieved less than +/- .05% variability. More detailed discussion of this and the rest of the results is present in Section 2.6.

2.6 PERFORMANCE TEST RESULTS

2.6.1 Introduction

With completion of turbine and instrumentation design work, hardware fabrication, rig construction activities, and facility/instrumentation shakedown by late 2019, performance testing for the CLEEN II program kicked off in August of that year. Initial testing focused on the baseline blade design. Once the tech blades were available a few months later, they were first used for IR testing, and as such, the tech blade aero testing was scheduled in March, 2020. During March, 2020, an issue was discovered with an instrumentation power supply in the rig, yielding inconsistent test results. Also, at this time the worldwide COVID-19 pandemic caused a temporary shutdown of the rig facilities. After determining the cause of the data issues during the shutdown, the rig was reopened in June, 2020 with a plan to improve the facility and repeat the performance-related tests. The repeat testing was concluded in September, 2020. This repeat testing allowed for an improved back-to-back assessment of stage efficiency for the tech and baseline blades due to improved repeatability and data quality.

2.6.2 Post-Test Hardware Measurements

Part of the process of both the engine-to-rig and design-intent-to-as-cast performance bookkeeping is to incorporate detailed inspection data into the analysis. For aeroefficiency, several types of hardware measurements were performed after testing supported the bookkeeping processes. These measurements included:

1. As-cast CT scanning and CMM measurements of both the airfoil profiles at several spans

2. Measurement of blade flow areas (throat areas of the blades when installed and shimmed to simulate centripetal loading)
3. Measurements of blade-tip radii to support understanding of running clearances.

Most of the inspection measurements were taken after testing was completed in September 2020. Both sets of blades were sent from the PSU START facility back to P&W in Connecticut to undergo flow testing of the internal passages (for durability) as well as CMM measurements. CMM requires the blades to be installed in the disk and shimmed to simulate being under centripetal load. This work was completed and the results were available for integration into the analysis by the end of October 2020.

2.6.3 Performance Testing, Analysis, and Results

2.6.3.1 Test Matrix

The test team made a recommendation of rig running conditions as listed in Table 5.1 after completing rig operability/verification for the proposed test matrix. This was accomplished by varying the Speed Parameter (SP) and Pressure Ratio (PR) by ±5%. Since the facility exhaust duct arrangement limits the downstream static pressure of test section, PR levels more than 5% above ADP could not be achieved. Also, related to the speed parameter variation, the mechanical speed of the magnetic bearing system was limited to approximately 11,000rpm, which limited the maximum achievable values to be just 2% above ADP. As a result, the team decided to extend the lower range of PR and SP variation so that a minimum of three points would be conducted to characterize the shape of the efficiency lapse curves.

2.6.3.2 Pre-test Analysis

The blades were cold flow tested to generate hot flow curves which are used in the secondary flow modeling. CFD analysis was done to estimate the rpm factor between static and rotating hardware. In the flow model of ***Figure 2-43***, the inlet pressure and temperature at the TOBI, purge, Aft Wheel Space (AWS), operating inlet, and vane trailing edge were used as boundary conditions for each test card. In order to better match the flow measured in the rig, the TOBI, purge, and AWS knife-edge (KE) areas were calibrated, which resulted in a representative flow model for each test card measured.

The isentropic turbine efficiency, η, was calculated based on measured mixed-stream mass-flow rates and thermodynamic properties (pressure and temperature) acquired from the 360 degree traversing rakes for the turbine test section control volume.

$$\eta_{th} = \frac{\left(\dot{m}_{main}h_{main} + \sum_i \dot{m}_{TCA_i}h_{TCA_i}\right)_{inlet} - \left(\dot{m}_{main} + \sum_i \dot{m}_{TCA_i}\right)h_{exit}}{\left(\dot{m}_{main}h_{main} + \sum_i \dot{m}_{TCA_i}h_{TCA_i}\right)_{inlet} - \left(\dot{m}_{main}h_{main} + \sum_i \dot{m}_{TCA_i}h_{TCA_i}\right)_{exit,ideal}}$$

Equation 1

Supplementary quantification and validation of turbine efficiency is also available via Equation 1 by replacing the actual work in the numerator of Equation 2 with the extracted power, as measured by the turbine shaft torque meter, τ, and the rotational speed, Ω.

$$\eta_{th} = \frac{\Delta H_{shaft} + \sum_i \Delta H_{TCA,pump_i} + \Delta H_{HPX}}{\left(H_{main} + \sum_i H_{TCA_i}\right)_{inlet} - \left(H_{main} + \sum_i H_{TCA_i}\right)_{exit,ideal}}$$

Equation 2

For the main gas path flow and each individual cooling flow, the measured temperatures and pressures were combined with additional fluid property details to accurately calculate specific total enthalpy, ht. The total enthalpy was determined via a P&W proprietary gas property table. All the efficiency data presented in this test report are based on the P&W data-reduction process.

Similarly, the mass flow rate, $\dot{m}$, for each fluid stream (main gas path and each cooling stream) was calculated using Venturi equations based on ASME-standards MFC 3M and PTC-19.5. The torque-based efficiency formulation in Equation 2 can be directly compared with the thermal efficiency from Equation 1. The torque value for Equation 2 was measured using a Torque-meters, Ltd. phase-shift torque meter with 0.1% full-scale accuracy relative to 516 ft-lbf range. Additionally, redundant torque measurements were also available from a load cell attached to the turbine dynamometer. Shaft rotational speed was measured with a laser tachometer using a once-per-revolution TTL signal converted to operating speed with 0.1 rpm resolution.

Temperatures and pressures acquired from the stage-exit traverse system can be characterized using information from either the 9-point or 10-point measurement rakes, along with the combination of the two rakes. Area-averaged measurements from these independent temperature and pressure rakes are typically within 0.1°R and 0.02 psia of each other. The impact of these variations on integrated efficiency calculations represents ±0.02 percentage points by selecting paired rakes (i.e., Pt-9 and Tt-9 or Pt-10 and Tt-10), but general characterization of overall stage performance is quantified using the arithmetic mean of pressures and temperatures from both rakes. Based on the above accuracy range of individual contributors to the efficiency equation, the uncertainty of efficiency based on measure data is ±0.4%.

2.6.3.3 Test Data

Turbine performance tests were conducted from August 2019 to September 2020 for both the baseline and tech blade configurations. This testing resulted in approximately 50 days of data collection with the conduction of over six-hundred 360 degree performance traverses. As mentioned earlier, the first campaign began with the baseline blade in August, 2019, followed by the tech blade testing in early 2020. The tech blade testing ended abruptly due to the COVID-19 pandemic-related restrictions. Although the quality of these data sets met the quality standards for the CLEEN II test matrix, variations of the BOAS material and differences between first vane leakage levels between the two configurations raised concerns regarding the relevance of the data.[1]

The joint PSU/P&W team made the recommendation to retest after having conducted thorough evaluations of data acquired in this phase. The P&W program office and Validation Discipline recommended repeat testing to minimize uncertainty engendered by hardware issues and cooling-flow differences between the two configurations.

From August to September 2020, the repeat testing for both the tech and baseline blade configurations was more efficiently executed due to learning gained during the earlier testing.

2.6.3.3.1 Exit Traverse

The turbine exit total pressures and total temperatures were measured by 4 different rakes: two total-temperature rakes (9-point and 10-point each) staggered in radial span, 180 degrees apart circumferentially. Likewise, total-pressure rakes were employed with the same arrangement. All four rakes were mounted on a 360 degree traversing mechanism which enabled the recording of the full-annulus flow field for each test condition. ***Figure 2-29*** shows the measured total-temperature profile (Tt vs span), scaled by the average value, for both the baseline and tech blades, at the pseudo aero design point, i.e., Test Card C0 (without vane trailing edge cooling flow).

The data shown here are for the design intent TOBI flow level. One should remember that in this arrangement, the tech blade, which under flows by approximately 20 percent due to manufacturing non-conformances,

[1] Lemmon, E. W., Bell, I.H., Huber, M. L., and McLinden, M. O., 2018, NIST Standard Reference Database 23: Reference Fluid Thermodynamic and Transport Properties- REFPROP, Version 10.0, National Institute of Standards and Technology, Standard Reference Data Program, Gaithersburg, MD.

drives more front cavity leakage flow into the main-gas path at the ID just upstream of the blade. It is this redistribution of flow that is believed to cause the marked and unexpected reduction in the total-temperature profile in the ID region compared to the baseline blade. This is clearly evidenced in the data shown in ***Figure 2-29*** between 0 and 50 percent span. This trend was not expected based on the design feature differences between the baseline and tech blades.

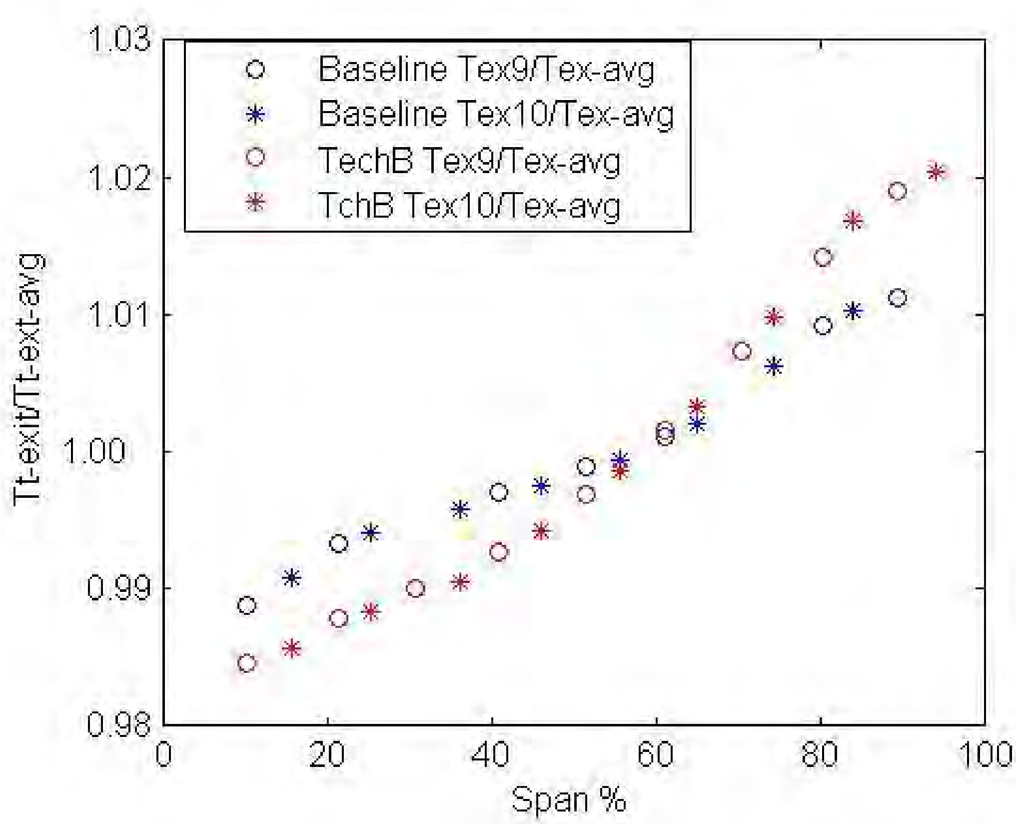

Figure 2-29. *Scaled Turbine-exit Total-temperature Profiles for the Baseline and Tech blade Configurations With Design-intent TOBI-flow Level*

As reviewed earlier, testing was also conducted for both the baseline and tech blades with minimum TOBI flow, i.e., Test Card A4. Similar to the plot shown in ***Figure 2-29***, ***Figure 2-30*** displays the scaled turbine-exit total-temperature profiles with the minimum TOBI flow level. Here, a more sensible (as predicted) result is revealed, whereby the tech blade configuration produces a total temperature profile shape very similar to the baseline in the ID region of the span. This is more in keeping with the aforementioned CFD predictions for these radial profiles.

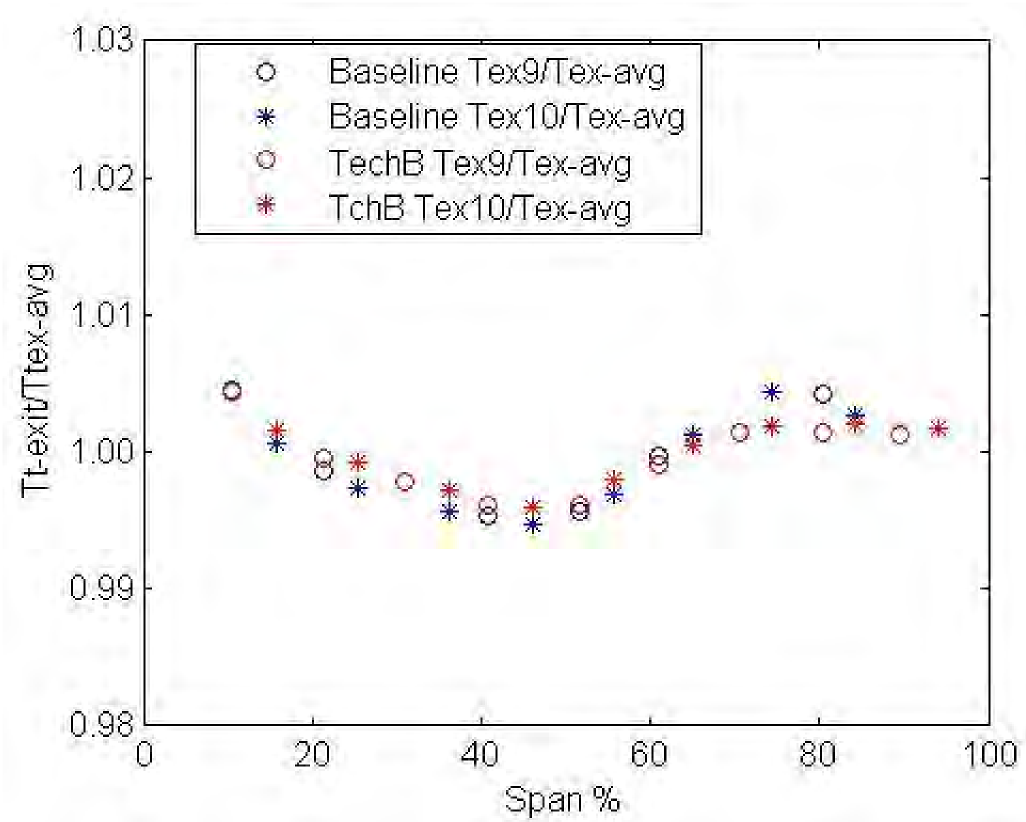

***Figure 2-30.** Scaled Turbine-exit Total-temperature Profiles for the Baseline and Tech blade Configurations With Minimum TOBI flow Level*

Figures 2-32 and ***2-31*** show an example of the full-wheel aerodynamic exit traverse data collected for each test point for the baseline blade configuration. Both total temperature and pressure are recorded by the traversing system for the full 360 degrees of the exit duct behind the turbine stage. These data are then area averaged across the entire measurement domain and employed to calculate the pressure ratio and efficiency of the stage. It is worth noting that there are non-negligible variations around the circumference of the exit duct which would not be accurately captured and factored into the efficiency calculation if less than the full 360 degrees was traversed.

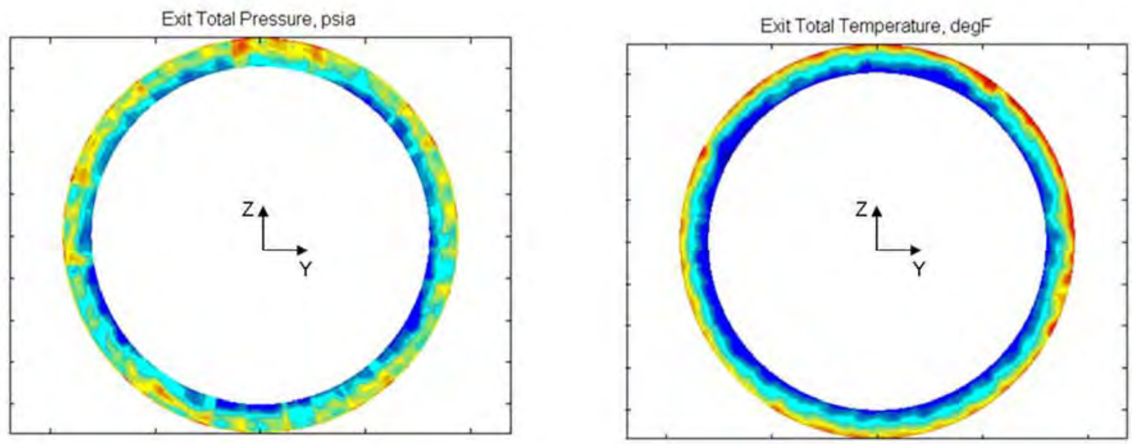

Figure 2-31. *360-degree Exit Total Pressure and Total Temperature Contour (Tech Blade Retest, August 2020)*

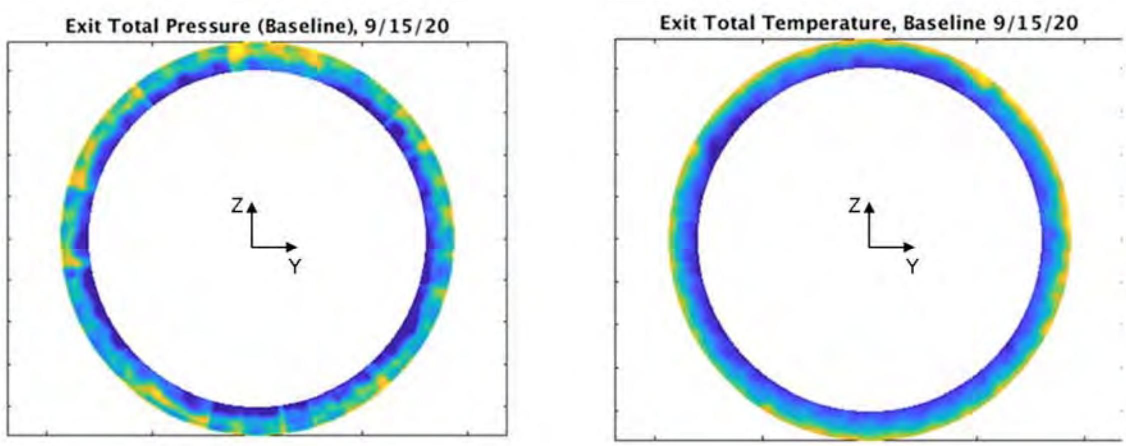

Figure 2-32. *360-degree Exit Total Pressure and Total Temperature Contour (Baseline Retest, Sept 2020)*

Figure 2-31 shows an example of the full-wheel aerodynamic exit traverse data collected for each test point for the tech blade configuration. While the color scales are not precisely the same as the images shown for the baseline blade data, similar variations in the circumferential direction are present and highlight the need to capture the full annular flow field when measuring efficiency in such a rig.

2.6.3.4 Post-Test Analysis

2.6.3.4.1 Comparison With Post-test Analytical Prediction

The measured rig efficiency, as described in the data reduction section, is calculated via a mixed-stream, control volume approach. Following the second, repeat testing campaign, post-test analyses have focused on relating the measured efficiency data from the rig to engine-specific applications.

As mentioned earlier, the under flowing tech blade drove a redistribution of the blade cooling flow supplied by the TOBI. The main effect was that the flow emanating from front cavity upstream of the tech blade was notably increased compared to design intent, while the cooling flow to the main body of the tech blade was reduced relative to design intent.

Because the tech blades were found to be flowing notably less than design intent and lower than the baseline blade, a higher TOBI supply pressure was required to target the same TOBI flow rate. The impact of this higher supply pressure for the TOBI flow in the tech blade testing is two-fold:

1. The ideal work term in the denominator of the mixed-stream efficiency calculation is increased, thereby decreasing the turbine efficiency.
2. The front cavity flow between the vane and blade increased to accommodate the increased TOBI flow. This cavity flow entering the main gas path is more detrimental to efficiency than the main-body cooling flows of the blade.

So, this mal-distribution of TOBI flow, along with the higher supply pressure for the TOBI flow do not represent engine relevant conditions and therefore must be corrected when relating the rig data to an engine application.

When applying relevant corrections to the engine-to-rig efficiency bookkeeping as well as accounting for geometry deviations, the predicted efficiency for the baseline blade configuration is 0.25% lower than the measured efficiency. Following the same methodology, the efficiency prediction for the tech blade in the rig is 0.08% lower than the measured efficiency.

2.6.3.5 Performance-Related Conclusions

A back-to-back comparison of bookkept efficiency levels for the baseline and tech products suggests that the tech blade configuration improves stage efficiency by 0.11% over the baseline blade design. This is in line with expectations of a small efficiency improvement for the tech blade based on pre-test predictions

Key learning from the test campaign includes the recommendation of using individual TOBIs sized separately for each blade configuration (lower flow rate for tech blade with same supply pressure). This would mitigate challenges associated with the bookkeeping required to relate the test data back to product relevance. Additionally, the current 360-degree traversing device blocks access for the installation of a radial-circumferential traversing cobra probe down-stream of the HPT. Rectifying this interference with design changes would allow for use of the cobra probe to collect flow-angle data at the turbine exit to gain.

2.7 DURABILITY TEST RESULTS

2.7.1 Introduction and Background

The CLEEN II program objective set forth to quantify cooling benefit associated with the advanced durability technology in a turbine airfoil. The cooling efficiency of such technology airfoil design was then compared to that of a baseline airfoil design. The baseline airfoil design used herein was representative of a P&W legacy airfoil in current commercial applications. In order to quantify the cooling benefit, the thermal response of the blade i.e. blade temperature, was measured as a function of the cooling air delivered to the airfoil in a controlled turbine rig environment.

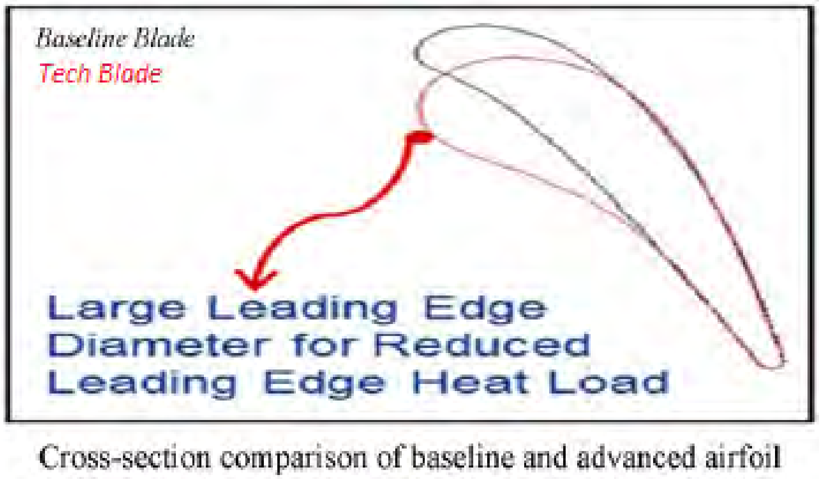

Figure 2-33. *Cross-section Comparison of the Baseline and Technology Airfoil Designs Evaluated for the CLEEN II Program, Not to Scale*

The rig assembly, test articles preparation, thermal measurement set-up and calibration was completed by 3Q 2019. The baseline airfoil tests and technology airfoil tests were then executed in 4Q 2019 and 1Q 2020 respectively. Post-processing of the acquired data including mapping of the IR thermal image data from 2D camera space to 3D part space was completed in 2Q 2020. This effort also entailed *stitching* of multiple IR camera views to generate a complete map of the airfoil P/S temperature distribution for each respective blade.

During each phase of testing, the rig inlet total pressure radial profile, total temperature radial profile, cooling flow temperature and mass flow were carefully controlled and measured to ensure consistency between test runs. The rig inlet pressure profile was measured during initial baseline airfoil efficiency tests in 3Q 2019. This pressure profile was used across all post-processing presented in this durability report. However, the rig inlet total temperature radial profile was updated during each phase of durability tests due to difference in rig temperature between durability and aero tests. The cooling air mass flow, temperature and pressure were measured in real-time during each test run.

Following completion of all tests, the test articles were sent to P&W in 4Q 2020 for post-test evaluation and data-matching. This durability post-test inspection entailed geometry inspection of the cooling features and airflow measurements and the measured data were incorporated into the overall durability cooling efficiency analysis.

2.7.2 Test Matrix

Table 2-4 shows the durability test matrix summarizing the target rig conditions. The test matrix included a total of six test conditions (herein also referred to as *test cards* A through F). These test cards represented different levels of cooling flow to the 1st Blade airfoil (TOBI Flow) and the upstream 1st Vane T/E slot. Different levels of Vane T/E slot flow were represented in test cards A, B, and C than in test cards D, E, and F. The cooling air to the 1st blade airfoil was also varied across test cards A, B, and C and similarly across test cards D, E, and F.

Table 2-4. FAA CLEEN II Durability Test Matrix Target Rig Conditions

Pt Inlet	Tt Inlet	Speed Parameter	Vane T/E Flow	TOBI Flow	TOBI Rail Hole Flow	
$psia$	$°R$	$\frac{N}{\sqrt{T}}$	$\%w4$	$\%w4$	$\%w4$	TEST CARD
41.3	860	367	1.90	**8.37**	1.825	A
41.3	860	367	1.90	**6.92**	1.825	B
41.3	860	367	1.90	**5.48**	1.825	C
41.3	860	367	**0.95**	8.37	1.825	D
41.3	860	367	**0.95**	6.92	1.825	E
41.3	860	367	**0.95**	5.48	1.825	F

Variation of the 1st Vane T/E flow was important in order to account for the mixing effect between the main gaspath air and vane cooling flow, which subsequently influences the temperature profile upstream of the 1st blade. In contrast, variation of the TOBI flow enabled quantification of the airfoil thermal response to cooling flow for each of the blade airfoil designs.

The target rig inlet total pressure and total temperature were measured using a single probe at midspan in real-time during IR data collection.

2.7.3 IR Data Acquisition and Mapping

A specially developed acquisition software was used to collect phase-locked thermal images of rotating blades. This software includes a number of controls including the image integration time. From a previous test campaign with similar camera hardware, the integration time was found to be a key parameter governing the signal-to-noise ratio in thermal images. Methods were developed to improve signal quality and test execution efficiency. Integration time works similarly to exposure time in photography, where long exposure time allows for good quality images, however, it does introduce blurring as the blades speed past at over 10,000 RPM. An optimization process was done to find the best integration time resulting in the highest quality image before too much blurring occurred.

The methods developed to optimize noise and integration time were largely successful; however, in any focal plane that are bad pixels that need to be accounted for. The bad pixels are caused by manufacturing defects of the sensor itself, where not every pixel responds to radiant energy in the same manner, and some pixels simply do not respond at all. The manufacturer of the IR detector claims an array operability specification of 99.5%, indicating that as many as 0.5% of all pixels in the array may not function correctly. These bad pixels will appear as a very high or very low value relative to neighboring pixels. Standard image processing methods were used to address these issues.

With the image acquisition and processing completed, the next step is the mapping process which involves transforming the thermal image data into a space where it is usable for analysis.

2.7.3.1 2D to 2D Image Mapping

To compare the experimental results with numerical predictions, both must be in the same coordinate system. The acquired infrared images are 2D, while the predictions are fully 3D. Through the use of image mapping, the 2D IR images are transformed into 3D part space. The process of converting 2D images to 3D maps is also referred to as photogrammetry and through applications in computer vision, animation, and geographic information systems (GIS), among others, the techniques to relate 2D images and 3D objects are well known and are covered in detail in various textbooks.

The goal of transforming 2D images to 3D part space is not novel; other researchers have used the technique for nose cones in hypersonic wind tunnels, airfoils for fixed-wing and rotary-wing aircraft, and blade cooling in a cascade facility. All of these studies used stationary hardware and most used a single camera view, so capturing images in a rotating environment called for some new and clever setup of instrumentation and post processing.

A computational subroutine to perform the 2D to 3D image mapping procedure was written and during development several methods were tested to find the most effective and efficient ways to perform the 2D to 3D mapping. The captured IR images were phase-locked to a particular blade view. Due to the discretization of phase to capture images, methods to identify orientation in camera space through the use of known markings (fiducial markings) are required. To describe the 3D part locations, a geometric CAD file is used as the target and image features are linked to specific 3D coordinates which can be used to create a transfer matrix which is used to transfer thermal values from the image into the 3D part space. This process is repeated for other camera views and the final mapped images stitched together on the 3D blade surface. Examples are shown in ***Figures 2-34*** and ***2-35***.

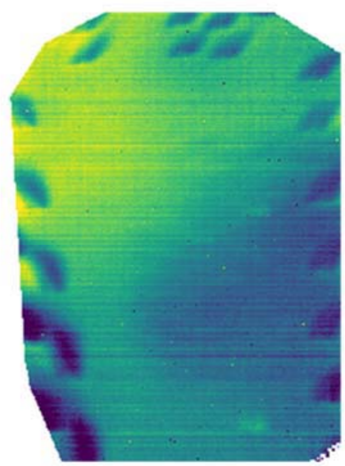

Figure 2-34. *Example 2D Thermal Image Acquired with IR system of Leading Edge and Pressure Side*

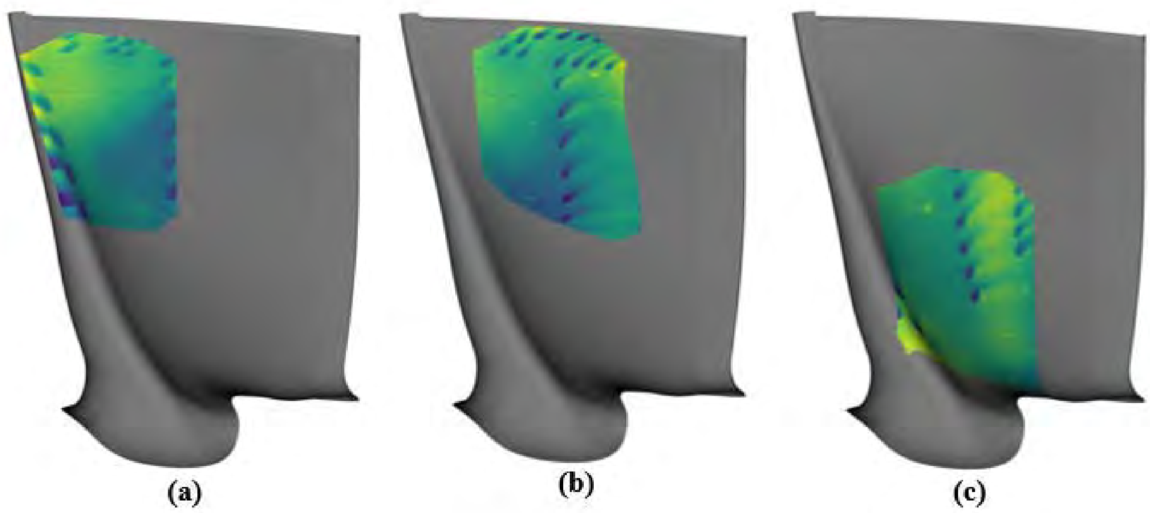

Figure 2-35. *Mapped Results for Different Blade Regions for Baseline Blade*

2.7.4 Test Data

The durability test data acquisition was carried out between Nov 2019 and January 2020, with the baseline airfoil measurements taken first. During these tests, the airfoil surface temperature was measured using an IR probe while the rig gaspath and cooling flow conditions were measured in real-time using thermocouples, pressure taps and venturi meters.

Figure 2-36 shows the measured cooling air mass flow and temperature for different test runs executed for test card A. Each of these test runs were executed on different days and confirms repeatability of the rig test conditions. Repeatability between test cards and test runs was ensured at target mass flows, main gaspath temperature and pressure conditions. The cooling air temperature fluctuated depending on the test card flow level. This variation in cooling air temperature was a potential contributor to variation in measured airfoil surface temperature between test cards and therefore had to be accounted in the data analysis.

.

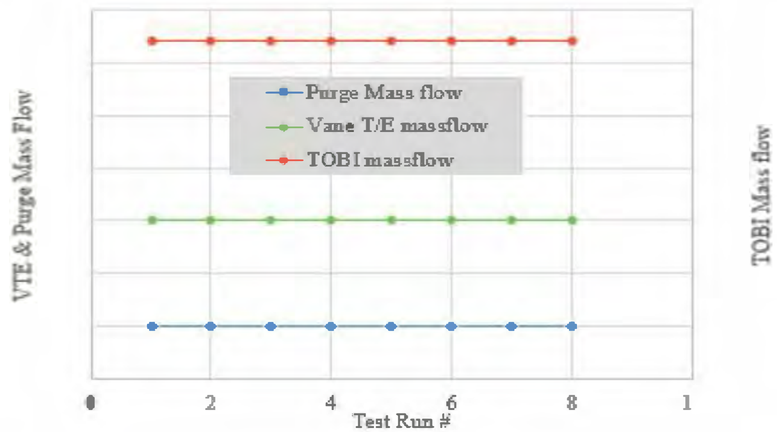

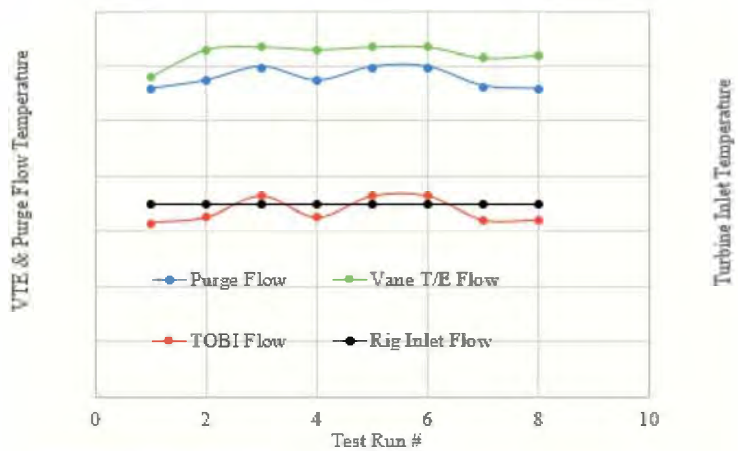

Figure 2-36. *Repeatability of Rig Test Conditions Between Runs for Tech Airfoil Test Card A*

In addition to the observed variation in cooling air temperature, the rig inlet total temperature radial profile was found to be sensitive to the level of cooling air mass flow to the vane T/E as shown in ***Figure 2-37***. The cooling flow to the vane T/E cooled the outer radius of the rig passage thereby inducing a radial temperature gradient near the outer wall of the main gaspath. This gradient in radial total temperature profile was steeper for higher vane T/E mass flow condition (test cards A, B, and C) compared to the lower vane T/E mass flow condition (test cards D, E & F). This variation in rig inlet total temperature radial profile was also a potential contributor to variation in measured airfoil surface temperature between the two sets of test cards and therefore needed to be accounted in the data analysis.

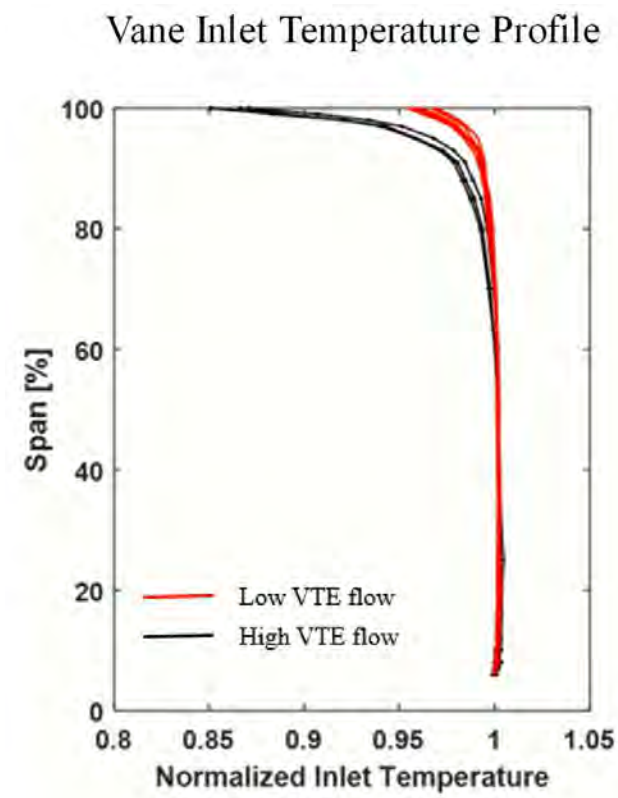

Figure 2-37. *Rig Inlet Total Temperature Radial Profile Variation With 1st Vane T/E Cooling Mass Flow*

The measured airfoil surface temperature was mapped to the 3D part model as shown in ***Figure 2-38***. Overall, the data showed decreasing airfoil surface temperature with increasing TOBI cooling flow for both baseline and tech airfoils. Furthermore, each of the airfoil designs had a unique temperature distribution footprint which was indicative of the influence of the internal core design.

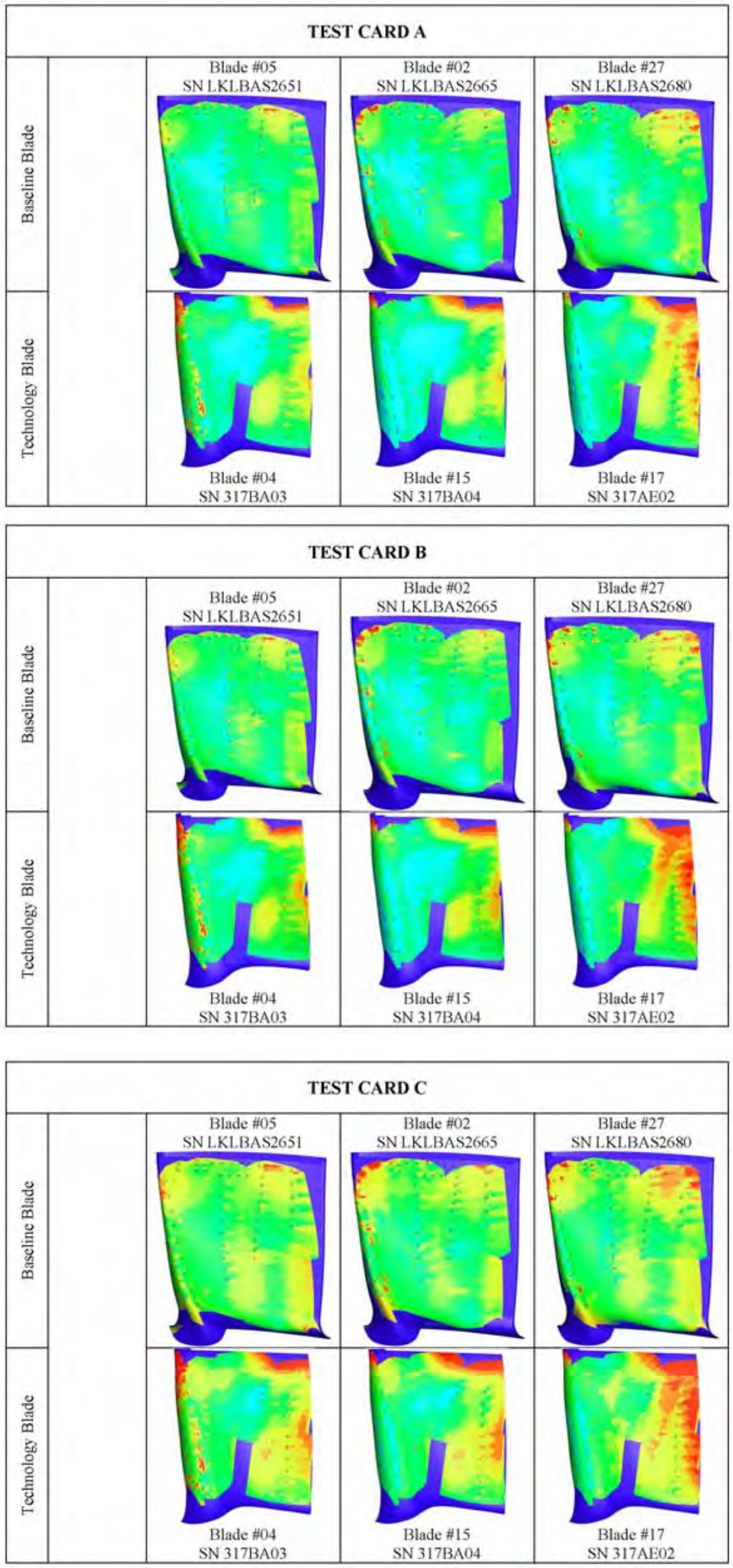

Figure 2-38. *Rig Data Summary for Baseline and CLEEN II Tech Airfoil*

There exists a significant difference in cooling hole layout on the airfoil P/S between the baseline and technology airfoil, with the latter having fewer film-cooling holes. However, despite the reduced film-cooling, the tech blade showed equivalent or lower surface temperature on the forward-P/S region of the airfoil compared to the baseline airfoil for each test card. However, the aft-P/S region, approximately downstream of the mid-chord, showed higher temperature for the tech airfoil compared to the baseline airfoil.

At this point, it should again be noted that significant modifications were applied to the tech blade T/E tip flag core passages in order to adjust overall blade flow due to manufacturing/design oversight (***Figure 4-12***). The elevated temperature in this region of the tech airfoil was in-line with the pre-test durability predictions. Because the flow circuit deviated from the design intent in these areas, the technology benefit in the T/E and tip flag regions could not be quantified with meaningful accuracy in these regions from these test results.

2.7.5 Post Test Inspection

Following completion of all the rig tests in 4Q 2020, the blades were sent to P&W facility for inspection. This was necessary in order to obtain geometric and airflow characteristics for each of the airfoils. The post-test inspection process included visual inspection of the part coating, external geometry, film-cooling holes and bench top airflow. Each core on the part was air flowed independently to determine its flow characteristic and the measured flow data was used to data match the durability model. The total blade airflow data showed that the tech airfoils were under-flowing on average relative to its design intent. In contrast, the detailed individual core airflow data indicated the pressure side skin cores in some parts were under-flowing while in others were over-flowing relative to design intent.

2.7.6 Overall Cooling Efficiency Analysis

In order to quantify the overall cooling efficiency benefit for the tech airfoil relative to the baseline airfoil, consideration had to be given to the aforementioned variations in rig boundary conditions which could potentially influence the measured airfoil temperature. This includes differences in geometry between airfoils which affect cooling flow delivery and rig operating conditions difference between test cards. Therefore, a direct comparison of the airfoil surface temperature differences does not suffice in drawing conclusions on the overall technology cooling benefit.

In the first part of this effort, the impact of variation of the rig inlet total temperature radial profile due to vane T/E flow was accounted by leveraging CFD. A full stage CFD model of the test rig was executed to determine the interstage temperature profile upstream of the 1st blade as shown in ***Figure 2-39***. This interstage temperature profile was then non-dimensionalized into a profile factor which is a function of the vane T/E flow temperature and rig inlet temperature as shown in the equation below. This allowed for the blade inlet profile i.e downstream of 1V, to account for the 1V T/E flow temperature and the rig inlet profile for each test card/test run.

$$Profile\ Factor = \frac{T_{gas} - T_{t4.1,Avg}}{T_{t4.0} - T_{1V\,TE}}$$

where

$$T_{gas} = Local\ average\ gas\ temperature$$

$$T_{t4.1,Avg} = Station\ 4.1\ average\ gas\ temperature$$

$$T_{t4.0} = Station\ 4.0\ average\ gas\ temperature$$

$$T_{1V\,TE} = Upstream\ 1V\ trailing\ edge\ slot\ flow\ temperature$$

In order to account for core manufacturing deviations and resulting flow deviations, the flow splits through each airflow core at rig conditions was determined for each test card. The flow model used to generate these cooling air flow splits had been data-matched using the post-test airflow data for each airfoil. In addition to that, the external airfoil surface was discretized into regions based on internal core design directly influence the surface temperature of that region. This allowed for the measured surface temperature to be directly correlated to the amount of cooling air delivered to that region of the airfoil.

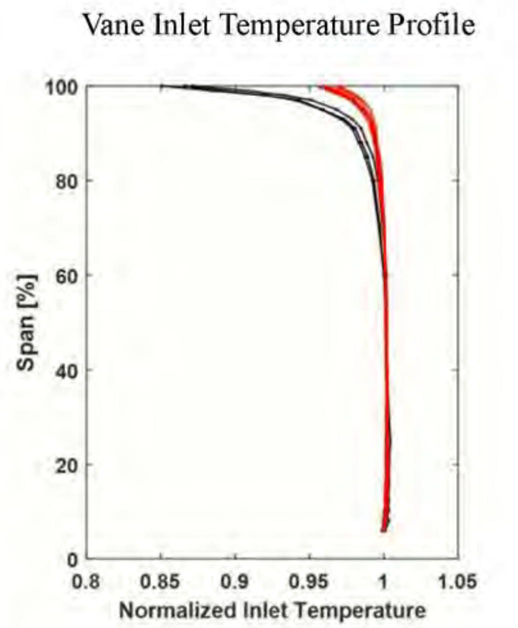

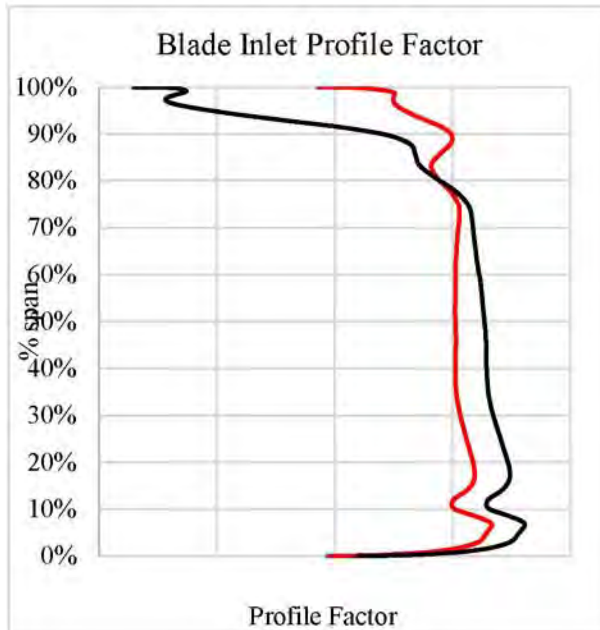

Figure 2-39. *Effect of START Rig Inlet Radial Temperature Profile on Interstage Temperature Profile Factor Upstream of 1st Blade as Predicted Using CFD*

Finally, the airfoil surface temperature was nondimensionalized into cooling effectiveness (Phi Φ) which accounted for cooling air temperature and blade upstream temperature. The cooling effectiveness (Phi Φ) was then correlated to the core flow heat load parameter (Beta β) to generate a cooling technology curve for each airfoil surface region. The cooling technology efficiency was assessed for only the P/S skincore regions of the tech airfoil relative to the forward P/S region of the baseline airfoil.

Figure 2-40 shows the generated cooling technology curve derived from the measured airfoil surface temperature. The technology curve confirms increased overall cooling effectiveness on the airfoil P/S of the tech airfoil compared to the baseline airfoil. This confirms that the tech airfoil requires less cooling flow to achieve a target blade temperature compared to the baseline airfoil, hence the CLEEN II tech cooling benefit.

$$Phi,\ \emptyset = \frac{T_{41} - T_{surf}}{T_{41} - T_{cool}}$$

$$Heat\ Load\ Parameter = \frac{W * C_{p_{coolingAir}}}{H_{gas} * A_{surf}}$$

where:

$$\boldsymbol{T_{41}} : Blade\ inlet\ Temperature$$

$$\boldsymbol{T_{surf}} : Blade\ surface\ Temperature$$

$$\boldsymbol{T_{cool}} : Core\ Supply\ Temperature$$

$$\boldsymbol{W} : core\ mass\ flow$$

$$\boldsymbol{C_{p_{coolingAir}}} : Cooling\ Air\ Heat\ Coefficient$$

$$\boldsymbol{A_{surf}} : External\ Surface\ Area$$

$$\boldsymbol{H_{gas}} : External\ Surface\ Heat\ Transfer\ Coefficient$$

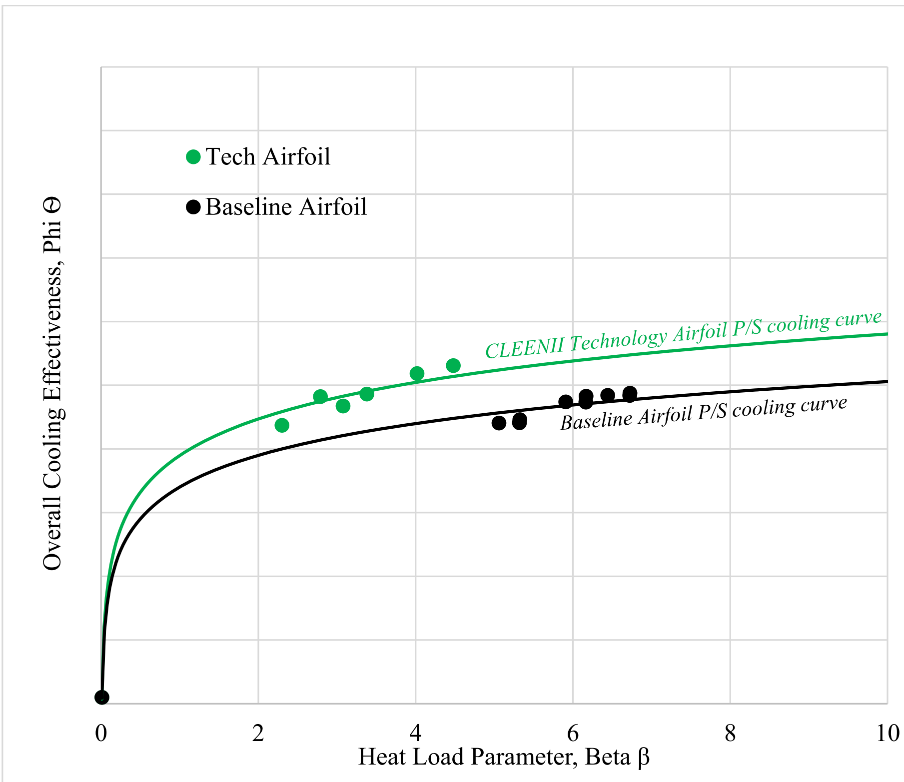

Figure 2-40. *Cooling Technology Curve for the Baseline and Tech Airfoil P/S*

Figure 2-41 shows the projected CLEEN II airfoil P/S cooling efficiency benefit derived from the technology curves. At any given Phi Φ, the difference in Beta β between the two technology curves can be used to estimate cooling credit to the airfoil P/S resulting from CLEENII technologies. The tech airfoil showed a cooling efficiency benefit of 27.5% relative to the baseline airfoil based on the measured data.

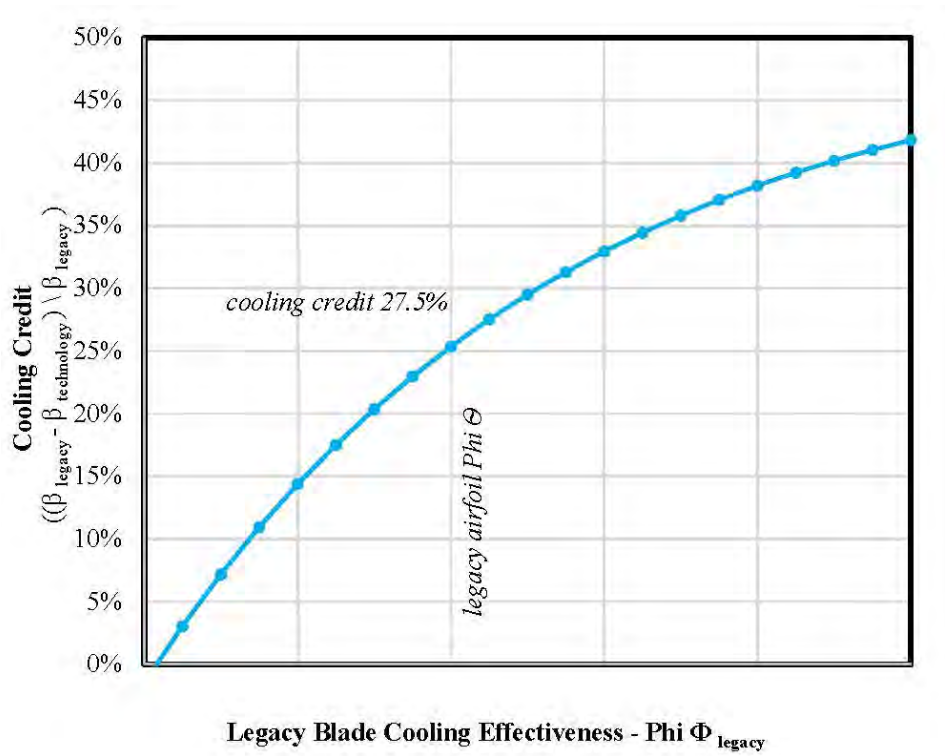

Figure 2-41. *CLEEN II Airfoil P/S Technology Cooling Credit Curve Relative to Baseline Airfoil*

2.7.7 Durability Summary, Conclusions, and Future Opportunities

The FAA CLEEN II program set out to demonstrate advanced cooling technologies packaging and application on a turbine airfoil and associated cooling efficiency benefit. To this end, the P&W durability team leveraged both passive and active advanced cooling concepts on a 1st blade design. Passive cooling was incorporated through an inter-disciplinary collaboration between turbine aero and durability to design an optimized external airfoil geometry to reduce and redistribute external heat load. The airfoil was also designed to allow packaging of advanced convective cooling technologies internally.

This advanced double wall airfoil was used to benchmark, learn and advance manufacturing process at P&W for future commercial products. The airfoil used in this CLEEN II testing contained manufacturing non-conformances which were accounted for in the overall program objective to quantify the cooling benefit. The negative learning at the time of test article production was since carried forward to positively impact current manufacturing process at P&W which is an enabler for use of advanced cooling concepts for durability.

Advanced infrared thermal imaging architecture and data processing algorithm was developed to enable measurement of blade P/S temperature in a rotating turbine environment. Additive manufacturing was leveraged to support the thermal imaging architecture in the turbine within precision accuracy of ~+/-2.5°F. Temperature measurements taken on the CLEEN II technology airfoil were compared to those from the baseline P&W airfoil and indicated a P/S cooling efficiency benefit up to 27.5%.

The success from the current program has provided insight for potential opportunities for future work in advance turbine cooling technology. Specifically, a similar study on the blade S/S and tip regions which are critical to turbine performance is recommended. Furthermore, airfoil heat flux measurement is recommended in order to quantify heat load redistribution.

2.8 CONCLUSION

The FAA CLEEN II cooled-rig test campaign represents the first cooled turbine test in this new experimental facility, as well as the first cooled HPT first-stage test run by P&W with modern designs. While the benefits of this collaboration are many, with details presented in the body of this report, the main findings are as follows:

1. Following application of bookkeeping steps to account for hardware non-conformances and boundary condition issues, the tech blade design was shown to provide a performance benefit of 0.1% compared to the baseline design. The results are very close to the predictions and considering the experimental and predictive uncertainties the test is a success for P&W.
2. Substantial learning was garnered regarding multi-stream efficiency measurements in a complex, cooled HPT first stage, such as the importance of accurately controlling and measuring the boundary conditions of each fluid stream which affects the efficiency calculation.
3. The importance of detailed hardware inspection data to support accurate performance bookkeeping between test configurations and for translation of the results to product applications.
4. The importance of test data quality criteria and risk-reduction testing standards to avoid the need for re-testing and for maximizing data accuracy and repeatability.
5. Finally, this work allowed extensive learning and process development for the execution of cooled-turbine performance and durability testing, without the undue schedule pressures tied to engine program funding.

In addition to the achievements of the aero-efficiency tests and the learning gained from this program, the durability assessment was also very successful. The specific durability goals of the CLEEN II program were achieved in testing out new double-wall cooling architectures and advancing manufacturing readiness. The anticipated reduction in cooling flow required was also achieved and increased cooling efficiency of 27.5% was demonstrated.

Along with these successes in the CLEEN II objectives, the rig was upgraded to allow for state-of-the-art image gathering capabilities, and the temperature data gathering that this equipment allows will continue to advance the understanding of turbine blade cooling properties well into the future. There are already several more tests planned for the START rig which continue where CLEEN II left off and offer even greater understanding and advancements in blade technology.

3. HIGH-PRESSURE COMPRESSOR CORE TECHNOLOGIES TESTING

3.1 INTRODUCTION

Development of the Next Generation Product Family (NGPF) HPC began circa 2005. The HPC has been used on the highly successful GTF products developed at Pratt & Whitney. As the product has matured, and compressor development learning has been acquired, opportunities for technology insertion to further improve the compressor performance have been desired.

The CLEEN II program supported the testing of a full compressor rig design that incorporated several advanced technologies. The data acquired has successfully provided insight to the effects of various technologies applied to the compressor. Overall, the test data has showed a better than expected efficiency improvements across the full power range as well as improved high power stability.

3.2 HPC CORE TEST OBJECTIVES

The primary test objectives for the CLEEN II program are to:

- Mature and de-risk advanced GTF HPC technologies
- Fully characterize the advanced GTF HPC

The technologies included in the CLEEN II compressor design include:

- Reaction Reduction
- Solidity Reduction
- Leakage Reduction
- Surface Finish Improvements
- Aero-Structural Optimization Improvements

To fully characterize the advanced technology HPC, the following effects were tested with the fully intra-stage instrumented compressor:

- Inlet Profile Effects (Axisymetric)
- Distortion Sensitivity (Non-axisymetric)
- Bleed Modification Sensitivities
- Vane Optimization and Sensitivities
- Reynolds Number Sensitivity
- Transient Operation Effects

3.3 HPC TEST SETUP

3.3.1 Rig Configuration Overview

The HPC technology rig was developed as a joint program with MTU Aero Engines AG of Munich, Germany. The HPC Rig configuration included the following features:

- Eight Compressor Stages
- Intermediate Case Struts
- Variable Vanes
- Bleeds

- Diffuser Strut

Test capabilities included:

- Ability to add, change, or remove inlet screen
- Traverse Probes at HPC inlet to capture circumferential variation across passage
- Traverse Probes at HPC exit to capture circumferential variation across passage
- Turbulence probes at inlet

3.3.2 Instrumentation

The HPC was fully instrumented in order to gain as much knowledge as possible about the internal and overall functionality of the HPC. The instrumentation included:

- Case temperatures and pressures
- Static pressure kulites
- Strain Gages
- Clearance Measurements
- Accelerometers
- Resolvers
- Kielheads for internal total pressure & total temperature measurements

The HPC inlet was characterized using a traverse probe. Multiple locations for the total pressure (Pt) and total temperature (Tt) sensors were used to provide additional confidence in efficiency calculations. Wall static instrumentation on the Intermediate Case (IMC) verifies that the HPC matches engine boundary conditions.

Every vane stage in the HPC includes kielheads in order to understand the detailed stage matching. The resolvers provide the feedback that variable vanes are operating in the commanded angles. The kulites are used to determine when and where the compressor instability initiated. The kielhead pressures and temperatures allow a stage-by-stage mapping of the compressor to understand the stage matching as well as detailed radial profiled information. The clearances for each rotor were measured throughout the test. Rotor stresses could also be observed through the non-contacting timing system.

Multiple circumferential locations at the exit plane measurement of total pressure and total temperature allowed for higher confidence in efficiency calculations. The exit pressure traverse was used to understand the circumferential variation, including detailed wake information..

3.4 TEST PROGRAM

The Major Test Program Elements of the HPC Technology test were the following:

- Optimize Stator Vane Schedule (SVS)
- Define performance (efficiency/stability) across full operating envelope
- Define performance and surge line sensitivity to:
  - — Vane Angle
  - — Rotor tip clearance
  - — Inlet profile
  - — Inlet distortion

— Bleed variation

— Reynolds Number

The test started with running speedline characteristics across from idle to design speed to obtain efficiency/stability information at very tight clearances. The *break-in* and *rub-in* procedures were performed in order to *nibble* or take small increments of rub in order to safely set the clearances to the desired level. The break-in was accompanied by post-run compressor borescope inspections to verify clearance levels.

A Design of Experiments (DOE) was run at multiple speeds in order to optimize the vane setting to balance efficiency and stability margin capability. Once the optimum vane settings were determined for idle through overspeed conditions, the HPC was mapped out at the various conditions to obtain efficiency lapse rates and stability margin.

Inlet profile studies were then performed. In an engine environment, the operation of the Low Pressure Compressor (LPC) affects the profile entering into the HPC. The HPC must be able to maintain stability margin for various profile entering the HPC, and therefore it is important to understand the implications of an altered inlet profile. Non-circumferential uniform distortion can also enter the HPC and therefore a 180-degree distortion test was run.

Sensitivities of individual, variable vane angles, the impact of stage proportionality, and bleed variation were all captured across the full compressor operating map. Throughout the development of an engine, it is necessary to adjust variable vane angles bleed levels, thus it is imperative to understand these sensitivities and impacts.

Reynolds number variation was also tested in the rig campaign. As the altitude of the engine varies from sea level up to the mission altitude, the Reynolds number varies substantially. This tends to alter efficiency and stability margins. Tests of Reynolds Number impact allows for full operational envelope understanding.

3.5 BASELINE RESULTS

3.5.1 Performance

3.5.1.1 Efficiency

The efficiency benefit of the CLEEN II research is based on providing benefits from not just improved aerodynamics, but knowledge of the boundary conditions, and improved mechanical design features that support improved aerodynamics.

The aerodynamics modified to provide a benefit include:

- Reduced reaction
- Reduced solidity
- Airfoil Optimization
- Endwall Optimization

The benefits from the mechanical design features include:

- Reduced leakages
- Improved surface finish
- Improved rub system
- Aero-structures optimization improvements

The non-*aerodynamics* benefits account for about half of the efficiency benefit of the compressor, which confirms the statement of "the devil is in the details."

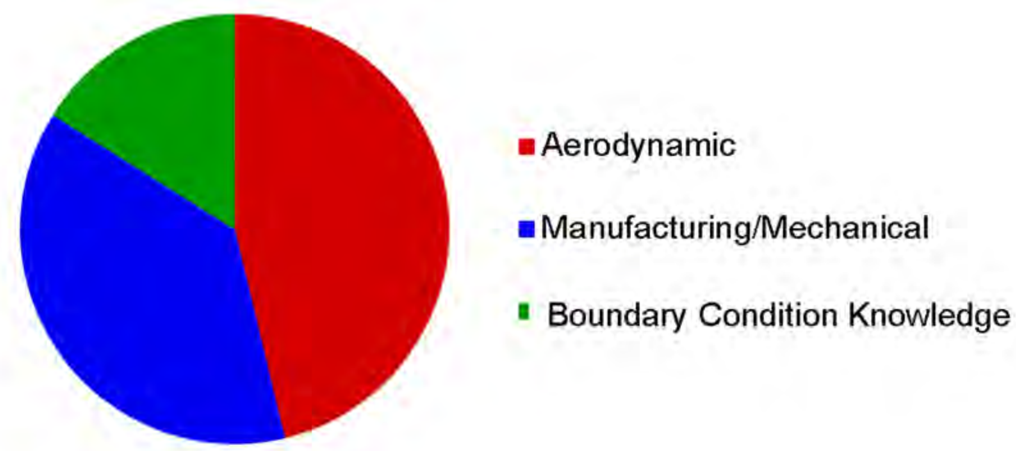

Figure 3-1. *Source of Performance Benefits*

The measured efficiency from the rig needed to be adjusted to account for rig specific boundary conditions in order to project the performance to an engine. As explained earlier, the rig is heavily instrumented in order to gain insight into the internal details of the compressor, but this does incur a loss due to the extra surface area/friction from the instrumentation. The clearances are then adjusted for expected product relevance. Since the test is primariily run with ambient inlet conditions, the effect of the boundary condition needs to be adjusted to a flight condition with an LPC in front of the HPC. Other small concessions such as hardware concessions and inlet profile differences account f or small adjustments as well. ***Figure 3-2*** shows that the instrumentation loss is the largest adjustment made to the measured performance to project to product expectations.

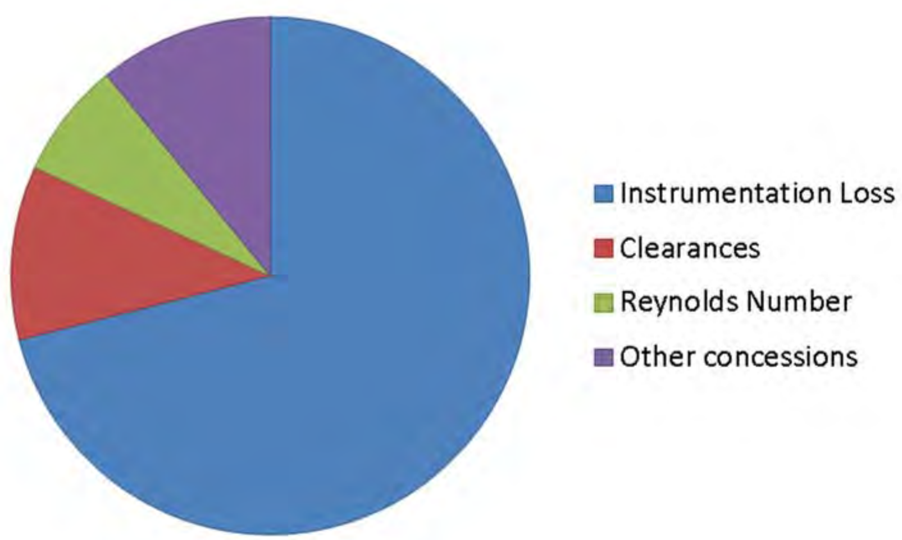

Figure 3-2. *Efficiency Bookkeeping to Measured Expectations*

3.5.1.2 Inter-stage Learning

The stator leading edge kielhead data provide valuable pressure and temperature understanding. ***Figure 3-3*** shows a comparison of the data in green versus the pre-test expectation from CFD in red. The kielhead pressure and temperature sensors provide radial distributions across every stage on stator leading edges. The radial profile data provides insight to if the weakness of the compressor is generated in the inner diameter or the outer diameters of the airfoils. The inter-stage pressure and temperature data can also be used to look at individual quasi (stator leading edge-to-stator leading edge) stage compressor maps of pressure ratio versus corrected flow. ***Figure 3-3*** shows that at high power, CFD had relatively good predictive capability to the stage matching.

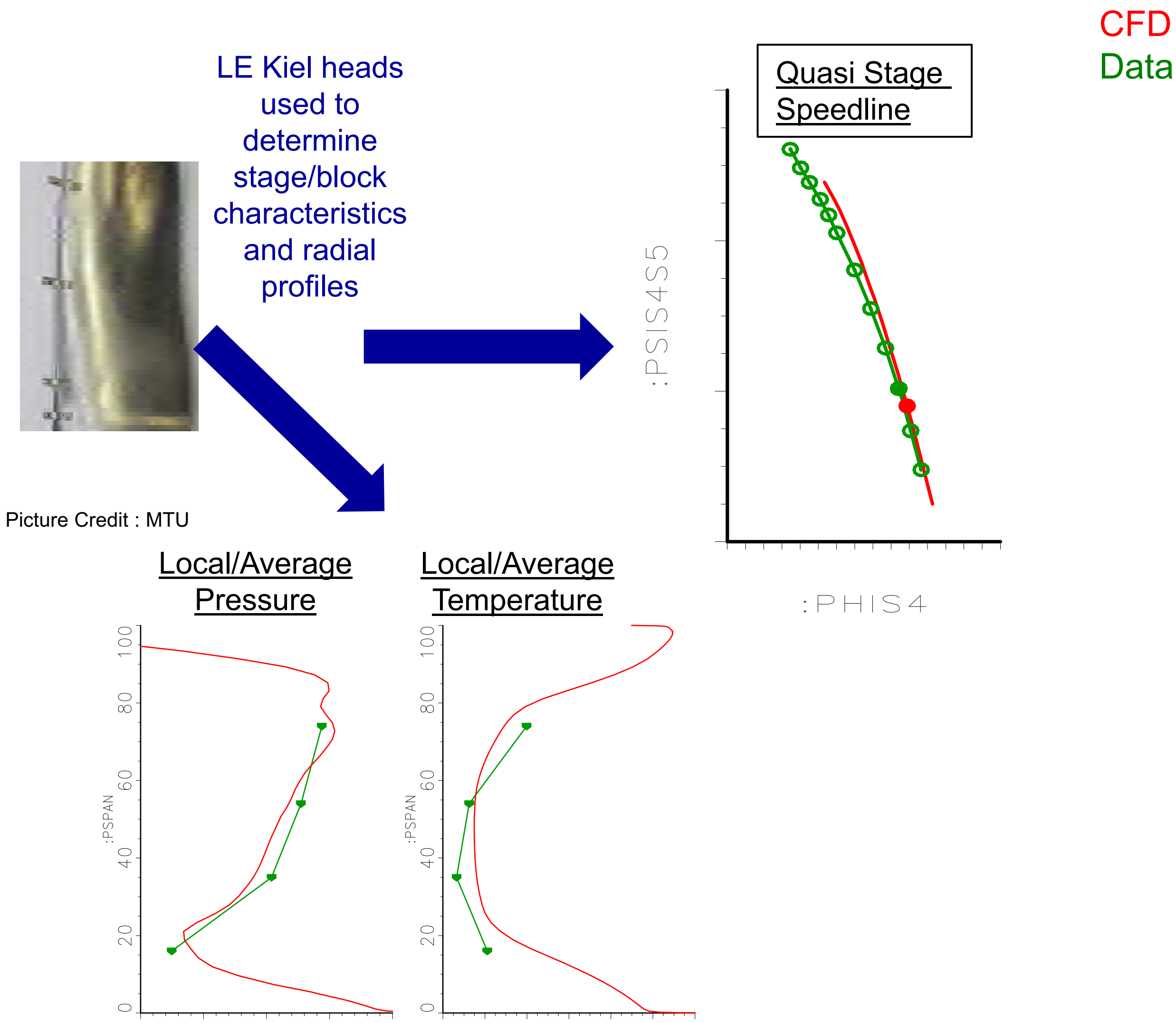

Figure 3-3. *Data Versus CFD Comparison of Inter-stage Pressures*

Figure 3-4 shows the results of a Stator Surface Static Measurement (green) that is transformed into an airfoil mach distribution and compared against CFD (red). At high power, the mach distribution is very well-aligned with expectation. The surface static pressure measurement can be used to determine if the stator leading edge incidences are not aligned with expectations. It can also be used to determine if a stator separates prior to expectation.

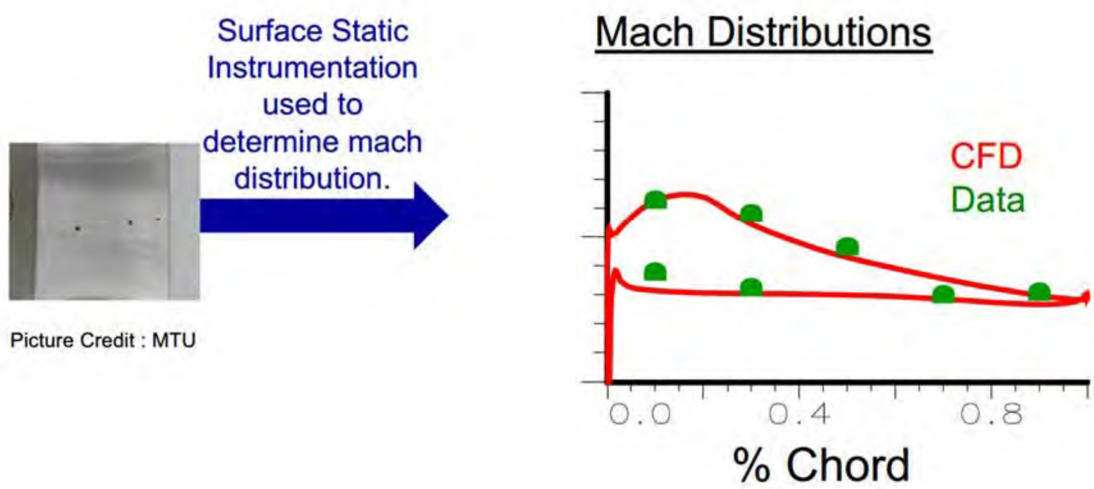

Figure 3-4. *Stator Surface Static Measurement Versus Prediction*

3.5.2 Vane Optimization

Vane optimization was performed to balance the efficiency and stability requirements at various speeds including starting, idle and cruise. The variable vanes are then proportionally tied to the IGV to form curves to meet the needs of the various operating conditions.

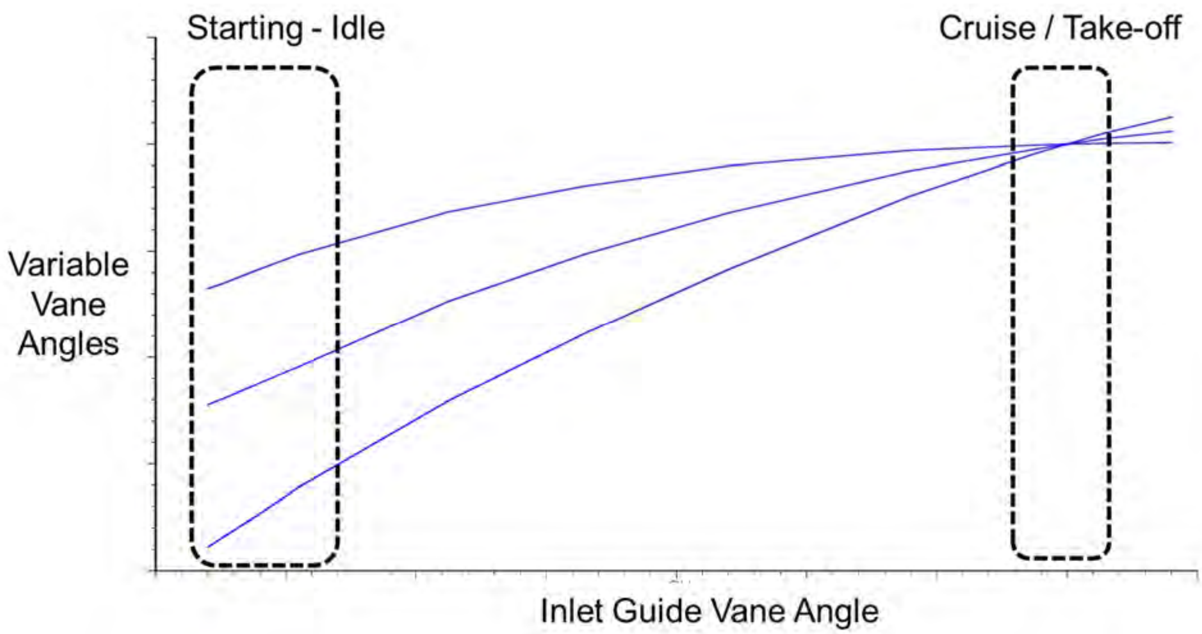

Figure 3-5. *Outcome of Vane Schedule Optimization*

3.6 SENSITIVITY TESTING

3.6.1 Inlet Profile

As mentioned previously, inlet profile studies were then performed. The operation of the LPC affects the profile entering into the HPC. The HPC must be able to maintain stability margin for either profile entering the HPC, and therefore it is important to understand the implications of an altered inlet profile. Non circumferentially uniform distortion can also enter the HPC and therefore a 180 degree distortion test was run.

The inlet profile of the compressor is altered by modifying a screen inserted at the inlet of the rig. The screen is made up of a wire mesh. The mesh creates a radially varying pressure loss. ***Figure 3-6*** shows the radial variation in the inlet profile at high power resulting from the various inlet screen designs.

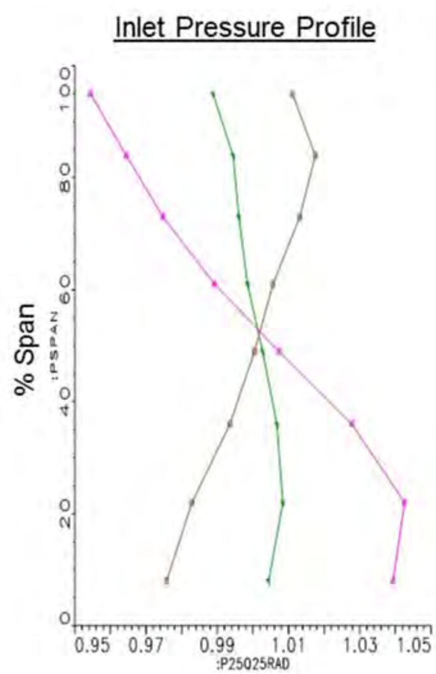

Figure 3-6. *Measured Inlet Profile Variation at Design Speed*

3.7 CONCLUSIONS

In conclusion, the testing performed in 2016 on the HPC technology rig was extensive and allowed for comprehensive learning on the new compressor developed at P&W.

The compressor was fully instrumented in order to understand the internal details of the compressor. Sensitivity testing of vanes, clearances, inlet profiles, bleeds and Reynolds Numbers allowed for further understanding of the benefits and limitations of the new compressor.

The advanced technologies validated under the HPC core testing work has since been incorporated into P&W's product offerings and sets the baseline for all future P&W products.

4. SINGLE-ELEMENT CASCADE TEST INFORMATION

4.1 OBJECTIVES

The SEC test study was designed to bridge the gaps between durability and aerodynamic disciplines, as well as fundamental flat-plate experiments and expensive rig/engine tests. To this end, film cooling effectiveness and aerodynamic losses are measured for a current state-of-the-art airfoil design. Such detailed measurements are necessary to enhance the understanding of the physical mechanisms that govern the intricate interactions between the film cooling jet and the local boundary layer. Measurements are compared between standard and advanced cooling hole shapes at engine-representative operating conditions in order to investigate the effect of cooling hole geometry on performance and durability metrics. The advanced cooling hole shape was developed by executing a hole geometry optimization aimed at maximizing the film effectiveness downstream of the cooling hole on a flat plate. It was subsequently tested in a PSU low-speed, flat plate test facility which confirmed an improved cooling effectiveness at low Mach number conditions.

Furthermore, the generated test data represents valuable, benchmark-quality aero/thermal data, which can be used to improve the predictive capability of next-generation film-cooling modeling using computational fluid dynamics (CFD) solvers.

4.2 TEST PLANNING AND EXECUTION

Before the start of the FAA CLEEN II contract, P&W had initiated the conceptual design studies for SEC testing and determined that the RTRC as the most suitable facility to execute the testing. The SEC provide a number of advantages; namely, comparatively low flow requirements, relevant engine conditions, highly resolved measurements supported by a scaled design and modular rig design which allows for easy testing of multiple airfoil shapes and cooling configurations.

In 2013, P&W completed Phase I of design and construction of the SEC and demonstrated its capability. In the last quarter of 2016, RTRC began to design and build the required modifications specific for the FAA CLEEN II test airfoils target rig conditions. The facility modifications and test article assembly were completed in March 2018. Upon completion of the assembly of the facility and test article, which included several rounds of internal design reviews, the CLEEN II SEC tests were carried out between April 2018 and June 2018. Additional tests were also conducted in November 2018 under P&W IR&D funding to enhance understanding of the preliminary testing results. The final test results were presented to the FAA audience in March 2019 and the final test report in June 2019. The SEC test schedule is outlined in ***Figure 4-1***.

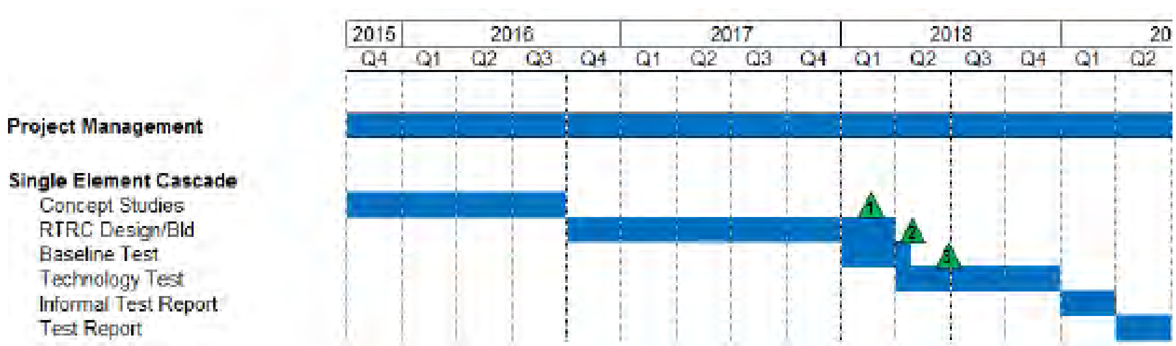

Figure 4-1. *FAA CLEEN II SEC Testing Schedule*

4.3 TEST SET-UP

4.3.1 Cascade Configuration Overview

The basic function of the Single Element Cascade is as follows. Compressor air enters the cascade through a venturi which measures the mainstream mass flow through the cascade. The air is then heated using electrical heaters, after which it enters a larger chamber with a screen for flow conditioning. The flow then passes through a turbulence grid located at the test section inlet which results in approximately 5% freestream turbulence intensity. The air finally goes through the cascade test section where the test airfoil is located before exiting through an ejector system controlled by a series of valves.

IR thermography is used to measure airfoil surface temperature of the cooled airfoils. Measurements of the airfoil surface temperature as well as plenum and the cascade inlet total air temperatures are used to calculate the adiabatic film-cooling effectiveness at a given cooling flow rate. The adiabatic film-cooling effectiveness is defined as:

$$\eta = \frac{T_r - T_w}{T_r - T_c}$$

Equation 1

where T_r is the local recovery temperature, T_w is the measured wall temperature and T_c is the temperature of the cooling air. The airfoil was also spray painted with a thin layer of flat-black paint of known emissivity.

A total of five anti-reflective coated windows were installed along the guidewalls and the endwall and of the test section for IR optical access. The IR windows were positioned such that the entire airfoil surface temperature could be captured using the infrared cameras.

4.4 TEST ARTICLES AND TEST MATRIX

The airfoils tested in the SEC are two-dimensional, prismatic airfoils extracted from a section of a three-dimensional advanced low heat-load airfoil which is also being tested in the FAA CLEEN II PSU START rig. First, a cross-section of the three-dimensional engine airfoil was extracted. The two-dimensional airfoil shape was then scaled up and extruded to cover the span of the cascade. The larger scale allows for better feature resolution of the additively fabricated airfoil and cooling hole shapes while enabling highly resolved surface IR measurements.

To investigate the aero-thermal performance of advanced film-cooling on the SEC airfoil, three rows of film-cooling were strategically placed around the airfoil. The cooling flow to each row was controlled independently since each row is supplied with cooling air via individual plenum. ***Figure 4-2*** shows a cross-section of the test airfoil as well as the location of the pressure-side row — PB, suction-side row — SA, and leading-edge row — SH. Cooling on the leading edge of an airfoil is often also referred to as showerhead cooling.

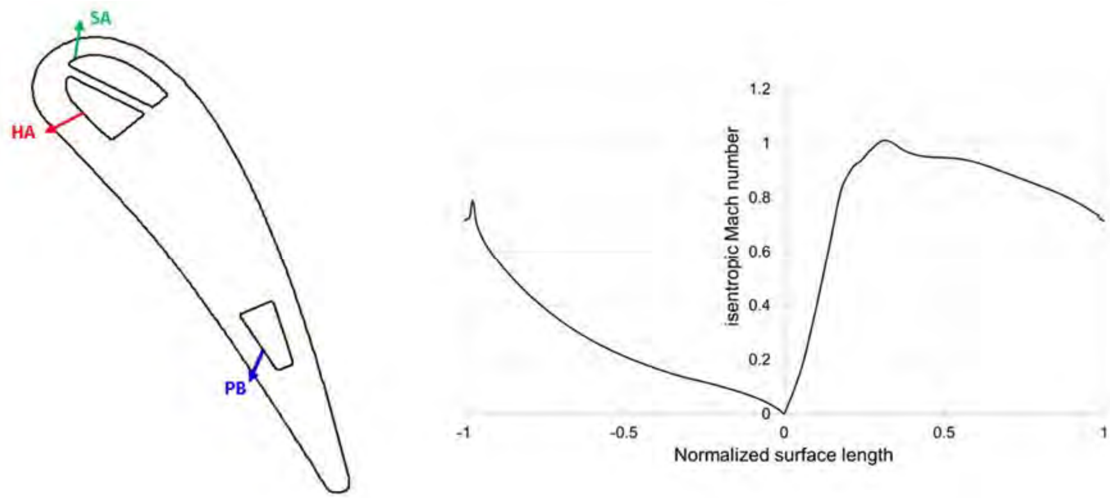

Figure 4-2. *SEC Airfoil Cross Section (left) and Pressure Distribution (right)*
For both images, the location of the cooling rows is also shown.

Two test airfoils, A1 and A2, were fabricated with standard and advanced cooling hole geometries, respectively. To facilitate implementation of internal instrumentation for measuring the plenum total pressure and temperature, each airfoil was assembled from three additively fabricated pieces i.e., the hub, midspan and tip section of the airfoil were additively fabricated separately. The parts at hub and tip were similar between airfoil A1 and A2 airfoil, while the midspan section of the airfoil is unique for A1 and A2 due to different cooling hole shapes. ***Table 4-1*** provides a summary overview of the cooling hole shapes used for each cooling hole row on each test airfoil.

Table 4-1. *Cooling Hole Shapes for SEC Airfoils A1 and A2*

	HA	*PB*	*SA*
A1	Round	Shaped	Shaped
A2	Shaped	Advanced	Advanced

For film cooling testing using airfoils A1 and A2, a total of three blowing ratios were considered: low, medium, high, where the choice of blowing ratios was guided by corresponding real engine applications as well as the PSU rig test. The blowing ratio is defined as the mass flux ratio between the coolant flow and the mainstream gas flow locally at the injection of cooling.

$$BR = \frac{(\rho V)_c}{(\rho V)_g}$$

Equation 2

Note that the cooling hole footprint for the advanced cooling holes is larger than that of the standard shaped hole geometry. In order to maintain the same mechanical coverage (an indicator of the lateral average film-effectiveness of a film-cooled surface) the spanwise hole distance for the advance hole row was increased in order to maintain the same mechanical coverage between airfoils A1 and A2.

4.5 RIG AND TEST ARTICLE MANUFACTURING

The aforementioned rig components as well as test article airfoils were all new and prerequisite equipment requiring design, manufacturing, and integration and/or testing to ensure the SEC rig would function as intended.

Conceptual design work had begun in late 2016, with the manufacturing stage beginning in late 2017. A review of P&W's previous SEC work was conducted prior to beginning design work to allow knowledge gained to be leveraged for the FAA CLEEN II testing. This resulted in improved sealing between the cooling air manifolds and plenums to prevent cross-talk and leakage, maximized uniformity of blowing ration across span, elimination of blind spots due to changed IR window location/sizes, improved IR camera fidelity due to improved multi-point calibration, and improved steady state due to improved flow conditioning grid designs.

As previously mentioned, a total of five anti-reflective coated windows were installed along the guidewalls and the endwall of the test section for IR optical access. The IR windows were positioned such that the entire airfoil surface temperature could be captured using the infrared cameras. The design and manufacturing of these windows benefited from the previous experience from SEC rig and the subsequent design studies conducted thereof. The figure below shows one of the rectangular window sections prior to installation into the SEC rig.

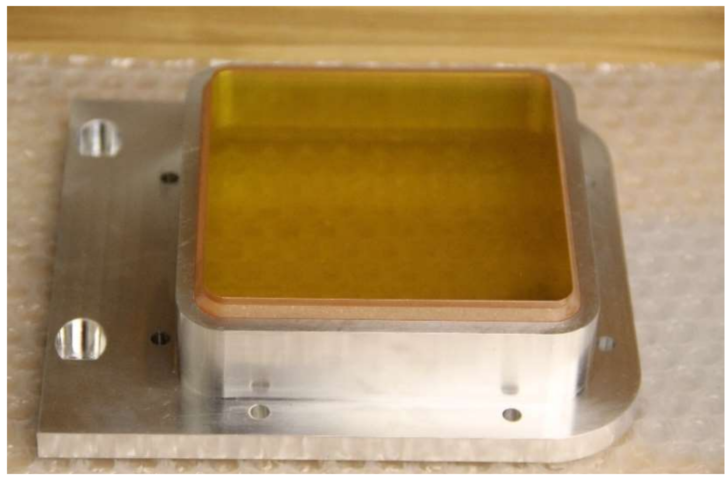

Figure 4-3. *Rectangular Flat Window Manufacturing Component*

A variety of new technologies and features were assessed for inclusion in the airfoil design. Details of this process and selection, as well as discussion of the design elements themselves, were outlined in section 2.4. This process concluded in mid-2017 and an assessment on appropriate additive manufacturing processes was made prior to work beginning on manufacturing the SEC airfoil test articles. The requirements for the additively manufactured airfoil sections included low conductivity for accurate film effectiveness measurements, ability to be hermetic, and accurate and repeatable geometry creation. A review of available data and experience led to a downselect of the appropriate process and material. A variety of benchtop tests and inspections then followed to prove out the suitability of the process and material. The tests included leak tests to confirm non-permeability, white light interferometry of a preliminary featured airfoil design to gauge print quality, and benchtop thermal conductivity measurements.

With the material/process selection and detailed design process now finished, the actual manufacturing of the airfoils began in the second half of 2017. The manufacturing process included not only the 3D printing of airfoils, but also the instrumentation, calibration, flow visualization and other prerequisite tests needed to ensure repeatable and quality data during the test campaign. ***Figure 4-4*** shows one of the uncooled airfoils used for flow visualization and calibration.

Figure 4-4. *Flow Visualization and Calibration Airfoil*

Following all cooled and uncooled tests, visualizations and calibrations, the rig was assembled and prepped for the testing campaigns to begin in early 2018. The assembled and instrumented rig is shown below as well as outline of the SEC schedule. The tests were concluded with the results available prior to full span START Rig rotational testing later on in the program.

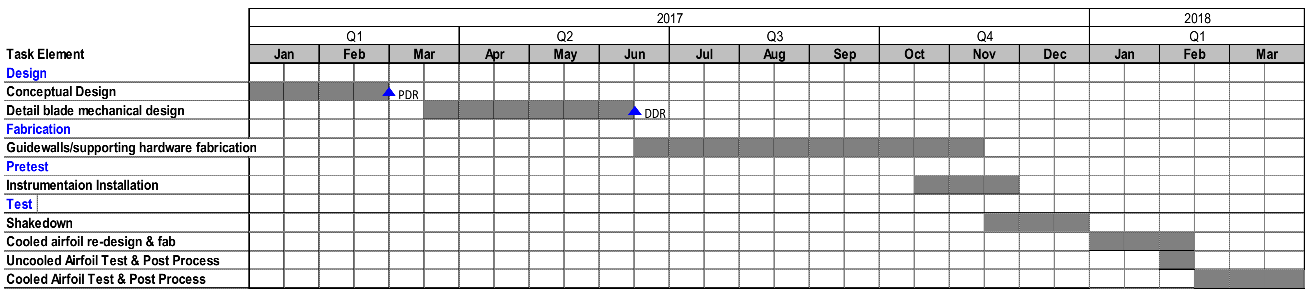

Figure 4-5. *Overview of SEC Design, Manufacturing, and Test Schedule*

4.6 TEST RESULTS

Several uncooled airfoils were tested at the beginning of the experiments in order to verify the intended rig condition and instrumentation functionality. During that process, static pressure taps were placed at midspan around the airfoil surface and cascade guidewalls to establish the intended airfoil loading and Mach Number distribution. The measurements were compared to CFD prediction as shown in ***Figure 4-6***, and a good agreement was observed relative to the design intent (CFD).

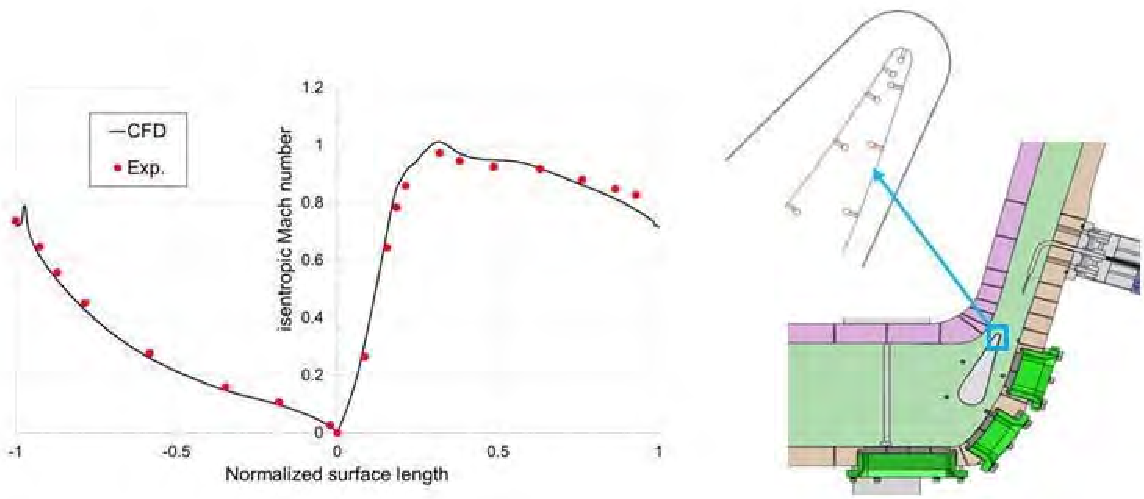

Figure 4-6. *Predicted and Measured Mach Number Distribution on the Airfoil Surface*

A kiel pressure probe traverse downstream of the test airfoil was also used to measure the exit total pressure distribution to establish a baseline for assessing airfoil profile losses and losses due to mixing of the film cooling jets. A typical wake profile from such downstream traverse measurement of the uncooled airfoil is shown in ***Figure 4-7***. Only the data in the loss core indicated by the blue-colored vertical lines in ***Figure 4-7*** is ultimately integrated to obtain an area-averaged downstream total pressure, pt2. The extent of such integration domain is guided by the CFD prediction. Since the upstream total pressure, ptg, is also measured in the rig, an uncooled loss can be defined as follows:

$$L_0 = \frac{p_{tg} - p_{t2}}{p_{tg}}$$

Equation 4

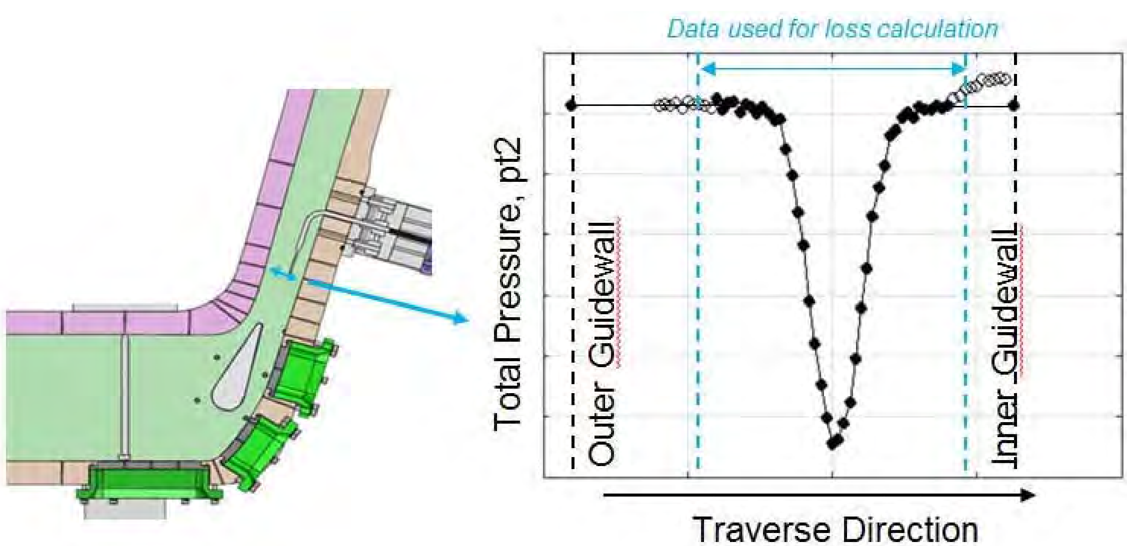

Figure 4-7. *Typical Total Pressure Distribution Measured Downstream of the Test Airfoil*

Measurements of the airfoil profile losses obtained from the uncooled airfoil (PTAP; no cooling holes) as well as the cooled airfoils at zero cooling flow condition (A1, A2) showed very good repeatability. Furthermore, the measured profile loss agreed with the loss predicted by CFD analysis.

4.7 SUCTION-SIDE COOLING

Measurements of the airfoil profile losses obtained from the uncooled airfoil (PTAP; no cooling holes) as well as the cooled airfoils at zero cooling flow condition (A1, A2) showed very good repeatability. Furthermore, the measured profile loss agreed with the loss predicted by CFD analysis. ***Figure 4-8*** presents the measured cooling losses, L_c, for the suction-side row SA (left). Results are plotted over a non-dimensional mass flow ratio, mc/mg. Since the total pressure in the cooling plenum, ptc, as well as the cascade and cooling massflows were also measured, a mass-weighted total pressure loss can be defined as follows:

$$L_c = \frac{(\dot{m}_g p_{tg} + \dot{m}_c p_{tc}) - (\dot{m}_g + \dot{m}_c) p_{t2}}{(\dot{m}_g p_{tg} + \dot{m}_c p_{tc})} - L_0$$

Equation 5

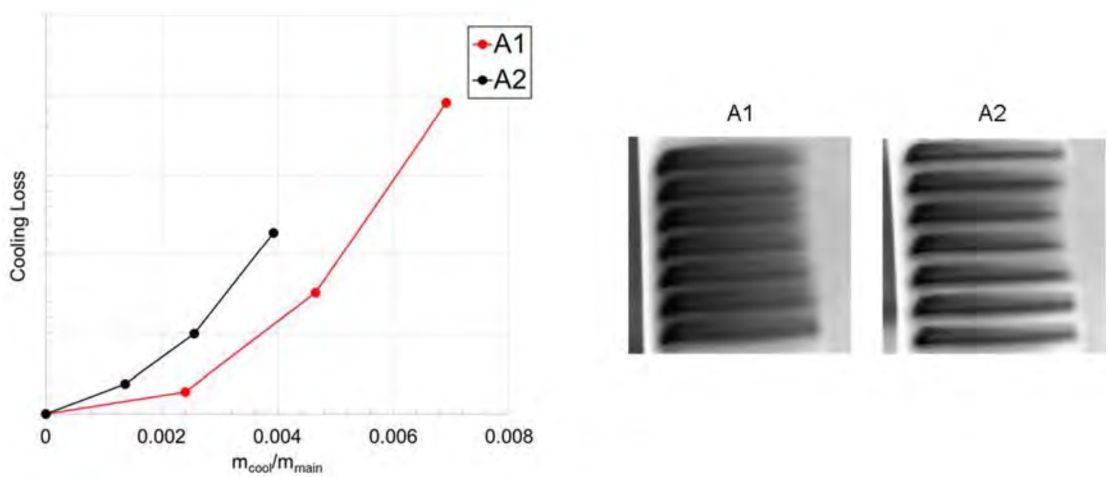

Figure 4-8. *Measured Cooling Losses for Suction Side Row SA (left), Raw IR Data From the Cooling Test at Medium Blowing Ratio, BR (right)*

Subtraction of the uncooled loss, L0, in this equation allows for the additional loss due to cooling to be isolated from the overall profile loss of the airfoil. It can be seen that for any given mass flow ratio, the advanced hole shapes (A2) cause an increased cooling loss compared to the standard shaped holes (A1). The raw IR data presented in ***Figure 4-8*** (right) shows the film-cooling traces on the surface of the airfoil downstream of the shaped and advanced cooling holes at a nominal blowing ratio. These film traces have been mapped to a CAD model of the airfoil for further post-processing and the calculation of overall film effectiveness. It was deduced that the film coming out of each advanced shaped hole in row SA has a wider radial footprint compared to the standard shaped hole. This wider film-footprint enables the film to cool a larger span section com- pared to the standard shaped hole. It can also be seen that there is a clear distinction of film traces coming out of each hole in row SA on airfoil A2 (advanced shaped) while the traces on A1 (standard shaped) are superposed together. This results in regions of lower film-effectiveness between the film traces from each hole on row SA on airfoil A2. Such regions of low film-effectiveness between each discrete cooling hole do not exist for the standard cooling hole row which are tightly spaced. In general, the film-effectiveness and loss results suggest that there is a difference in how the cooling jet mixes with the main gaspath air.

While the results presented in ***Figure 4-8*** show that the advanced shaped holes lead to higher losses, overall less cooling mass flow was required to cool the same surface area with advanced shape cooling holes. This is due to the difference in hole spacing discussed earlier. Accounting for these differences it was calculate that an overall benefit can be realized for the advanced configuration of airfoil A2. However, measurements of film effectiveness also indicate some regions of lower film-effectiveness for A2 which suggests that the hole spacing for the advanced holes might require slight adjustment. This may prevent the full benefit of flow and loss reduction to be realized. Still, the results emphasize the potential of the advanced shaped cooling hole to reduced overall cooling flow levels and improve thermodynamic cycle efficiencies.

4.8 PRESSURE SIDE COOLING

This section discusses the results obtained from testing film-cooling on the airfoil pressure side row PB at three different blowing rates on both airfoils A1 and A2.

The results show that for both hole geometries, the film-core size at the hole exit have is only marginally bigger for the advanced shaped hole compared to the standard shaped hole. As a result, there are larger regions of low film-effectiveness between each film trace on airfoil A2 compared to A1. This region of low film-effectiveness is also much bigger than that previously observed on the suction side of the same airfoil. In addition, the film-effectiveness contour plots also show that the film coming from the advanced holes attenuate faster downstream of the hole exit. Finally, the film from each hole lacks the radial distortion (two-lobed distribution) previously observed for similar holes on the airfoil suction side. Such differences in film distribution on the pressure side relative to suction side allude to a difference in secondary flow structure between holes located on the pressure-side and suction-side of an airfoil. As it is to be understood, the pressure gradients and local Mach number are different at the film injection location for row SA (suction side) and row PB (pressure side) which is likely to alter the jet-in-crossflow secondary flow structure.

Analogous to the suction-side results presented in ***Figures 4-8*** and ***4-9***, measured cooling losses, Lc, for the pressure-side row PB are presented in ***Figures 4-9*** and ***4-13***. ***Figure 4-9*** indicates that, similar to row SA, the advanced hole shapes of airfoil A2 result in increased cooling losses compared to the standard shaped holes of airfoil A1 for mass flow ratios greater than 0.003. For smaller coolant mass flow ratios, the losses are small and very similar between A1 and A2. The IR data also shown in ***Figure 4-9*** (right) for the medium blowing ratio and both airfoils. The measurements show that for both hole geometries, the film-core size at the hole exit have is only marginally bigger for the advanced shaped hole compared to the standard shaped hole. As a result, there are larger regions of low film-effectiveness between each film trace on airfoil A2 compared to A1. This region of low film-effectiveness is also much bigger than that previously observed on the suction side of the same airfoil. In addition, calculated film effectiveness results suggest that the film coming from the advanced holes attenuate faster downstream of the hole exit. The reduction in film effectiveness could be the result of the coolant jet lifting off the airfoil surface rather than staying attached.

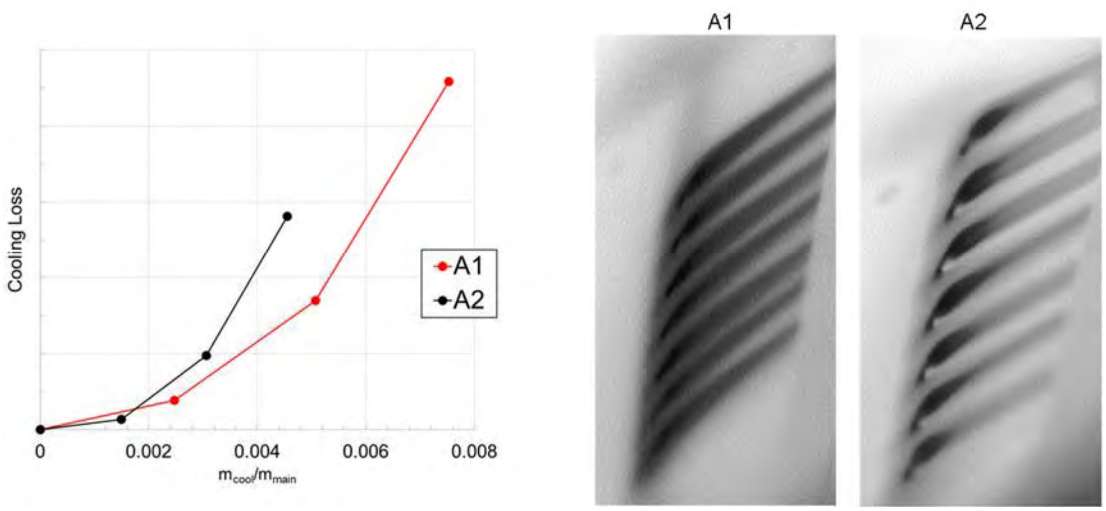

Figure 4-9. *Measured Cooling Losses for the Pressure Side Row PB (left) and Raw IR Data From the Cooling Test at Medium Blowing Ratio, BR (right)*

When comparing the overall surface area that is covered by film from the advanced hole shapes, the same conclusion can be drawn as for the suction-side film: airfoil A2 requires less cooling flow and incurs lower cooling loss for cooling the same surface extent when accounting for difference in cooling-hole spacing. However, since the IR data shows poor film-effectiveness for the advanced shaped hole on the airfoil pressure side, an overall benefit can only be realized after further optimizations of the cooling hole shape, and, in particular, the hole spacing. This would be required to arrive at the best aero-thermal solution that results in reduced cooling losses without compromising the surface film-effectiveness.

Airfoil A2 was selected for a repeatability test after the airfoil had been taken out of the cascade and then reinstalled at a later date. ***Figure 4-10*** shows good a greement and repeatability for the advanced pressure-side cooling hole shapes in airfoil A2, especially at low coolant mass flow rates.

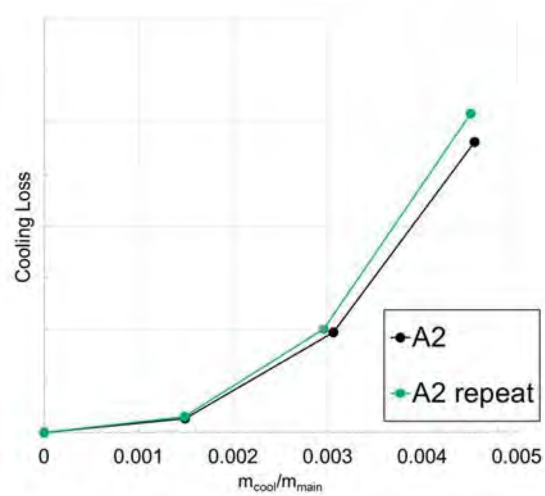

Figure 4-10. *Measured Cooling Losses for the Advanced Pressure-Side Cooling Holes of Airfoil A2 at Different Test Days*

4.9 SHOWERHEAD COOLING

This section discusses the film-cooling results for the leading edge row HA on airfoils A1 and A2. The showerhead cooling is typically required to cool the leading edges of HPT airfoils where the hot gases impinge on the airfoil surface resulting in one of the highest external heat transfer coefficients on an airfoil. Aerodynamic losses for showerhead cooling are believed to be low since the coolant film mixes with the hot gases at a low surface Mach number prior to being accelerated around the airfoil surface. At the same time, the low momentum of the mainstream gaspath air results in large blowing ratios for cooling holes in the vicinity of the stagnation point even at moderate supply pressures. As a result, the cooling jet is always at risk to blow off the airfoil surface, which results in poor film effectiveness.

Figure 4-11 presents the measured cooling losses for the leading-edge film of row HA. ***Figure 4-11*** (left) shows that the cooling losses associated with the two different hole shapes are very similar for small coolant mass flow rates (mc/mg<0.003). For larger coolant mass flow rates, increased losses are observed for the shaped showerhead holes compared to the round holes. The raw IR data also shown in ***Figure 4-11*** (right) indicates distinctly different film-effectiveness distribution for shaped holes, indicating that the cooling jet originating from the shaped leading-edge might lift off the airfoil surface. A similar effect, albeit less pronounced, can be seen for the round cooling holes. Overall, this trend is unexpected. The round holes were expected to show an increased propensity to jet blow off compared to the shaped holes. It is speculated that the reduced hole spacing for the round cooling holes promotes the interaction of adjacent cooling jets, leading to a more favorable blow-off characteristic compared to the shaped cooling holes that are spaced further apart.

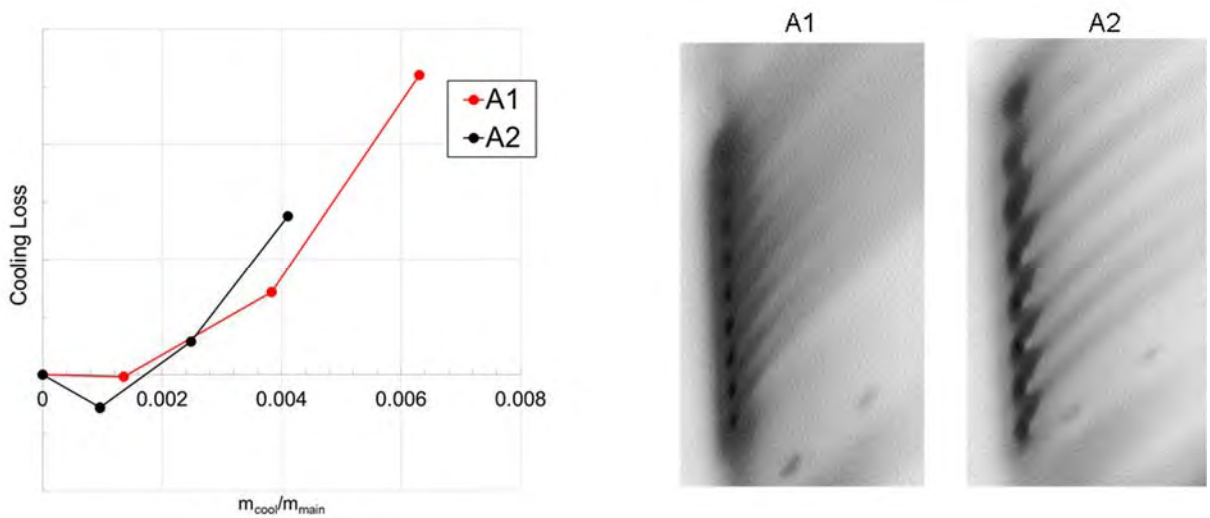

Figure 4-11. *Measured Cooling Losses for the Leading Edge Row HA (left) and Raw IR Data From the Cooling Test at Medium Blowing Ratio, BR (right)*

Film-cooling effectiveness results were reduced from the IR data for round (A1) and shaped (A2) showerhead cooling holes at various blowing ratios. At low blowing ratios, both hole types show relatively uniform film-effectiveness distribution across the airfoil span with attenuation in the streamwise direction towards the trailing edge. Increasing the blowing ratio results in a non-uniform distribution of film-effectiveness for round showerhead holes. Since the mainstream air in the leading-edge region has very low momentum, the high momentum cooling air jets from round holes sweep spanwise on the airfoil surface, especially at medium and high blowing rates. This superposition of film on one side of the airfoil span results in higher film-effectiveness downstream of the leading edge. On the contrary, film from shaped showerhead holes does not show this bias of film to one side of the airfoil span.

This is understood to be due to the lower momentum with which the cooling air exits the diffuser of the shaped cooling hole and therefore immediately swept downstream by the mainstream air.

Due to a difference in hole spacing, the same surface area on the airfoil is cooled with less coolant air for airfoil A2 compared to airfoil A1. While overall cooling loss levels are similar, the shaped showerhead cooling configuration does not lead to improved cooling effectiveness. However, as stated before, these measurements demonstrate sufficient sensitivity to cooling hole shape and its effect on both aerodynamic losses and film-effectiveness to support the theory that there exists an aero-thermal optimum for which the airfoil surface is cooled with reduced coolant mass flow and reduced mixing losses.

4.10 CONCLUSIONS

Single-element cascade testing was carried out under the FAA CLEEN II contract to investigate the aero-thermal performance associated with film cooling of a modern, low heat-load airfoil geometry. The design configurations included a variety of cooling hole shapes located at key locations around the airfoil. Highly resolved measurements of cooling film effectiveness and aerodynamic loss were obtained for standard round and shaped cooling holes as well as advanced cooling hole shapes. The advanced shapes had been developed and optimized for cooling a flat-plate geometry and were previously tested in a PSU low-speed, flat plate test facility. The SEC tests, however, were conducted at relevant operating conditions (Reynold's number, Mach number) emulating an engine take-off condition.

For all cooling rows (suction side, pressure side, showerhead) the measured data suggested that cooling losses increased for the advanced hole shapes. However, at the same time it was recognized that the same airfoil surface area was cooled with less cooling air for the advanced hole shapes. Accounting for these differences suggested that an overall reduction of cooling flow could be achieved to protect a given airfoil from the hot gaspath air. Even without improvements to film effectiveness and mixing losses, the reduced cooling air requirement would result in significant thermodynamic cycle efficiencies. Simultaneously measuring the quantities that are important to assess durability and aerodynamic performance is key to achieve that goal.

Ultimately, the SEC test also successfully generated a comprehensive benchmark data set that can be used to validate state-of-the-art CFD tools. Since CFD is used for cooling-hole optimizations, these validation activities play a key role in improving solver predictive capabilities and further developing advanced cooling technologies. Moreover, CFD will be exploited to enhance the understanding of physical mechanisms associated with different cooling hole shapes.

5. OVERALL SYSTEM LEVEL BENEFITS

The ultimate motivation for the component improvements under the CLEEN program is engine performance benefit at the system level. The PW1100G-JM performance model shows baseline performance compared to performance with the benefits of the compressor and turbine technologies mentioned in the previous sections.

The assessment is performed at ADP, which is cruise thrust, 35,000 ft Alt/0.78 Mach/ISA temperature. These benefits combined result in 1.4% reduction (improvement) in specific fuel consumption at ADP.

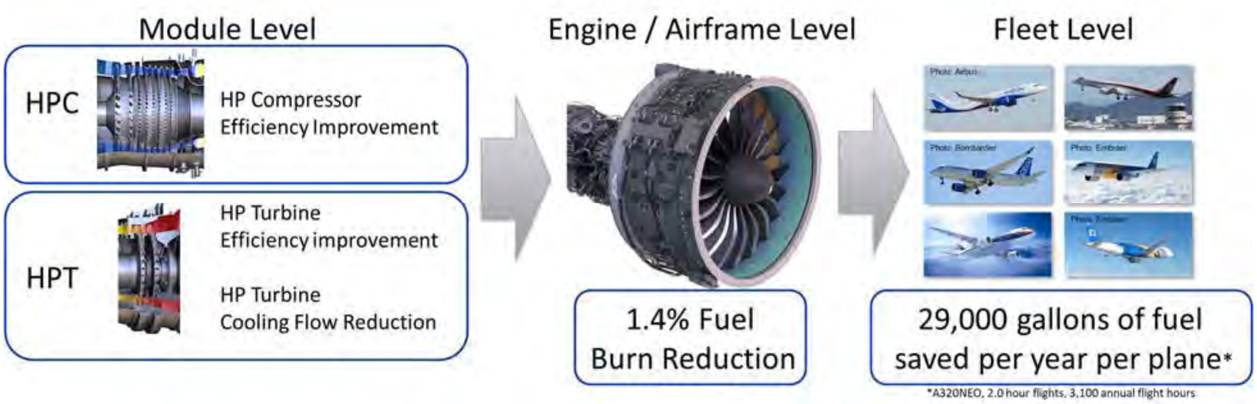

Figure 5-1. *CLEEN II Technologies System Level Impact*

Based on the A320neo average flight of 2 hours and the average number of hours flown in one year, the 1.4% cruise SFC improvement would save, on average, 29,000 gallons of fuel per year per airplane.

The turbine cooling flow reduction significantly contributes to the overall benefit, which might be less intuitive than that of the component efficiency increases. Engines bleed air from the high compressor to secondary air pipes to cool HPT vanes and blades. Since cooling air circumvents combustion. The HPT *tech blade* achieves the same component life in the hot environment with less cooling flow, improving the thermal cycle efficiency. Future system analysis work might show other advantages of how cooling flow reduction technology can contribute to system metrics:

1. Hold flow same as baseline and reduce maximum temperature at the airfoil to improve time on wing.
2. Bleed the same flow, reducing flow to the HP turbine, but increasing cooling flow to the LP turbine.
3. Improve compressor stability by possibly redistributing the loading in the HPC with the reduced bleed flow.

6. FUTURE APPLICATION DISCUSSION

P&W is pleased to collaborate with the FAA and their objective to develop continuous lower energy, emissions, and noise technologies for civil subsonic airplanes under the CLEEN initiative. The successful CLEEN I and CLEEN II programs have permitted P&W to develop, design, and validate advanced turbofan engine technologies that are aimed at impacting multiple current and future product lines by reducing the noise, emissions and fuel burn of the current generation of the GTF engine, as well as the next generation of GTF engines.

The recently certified GTF engines already delivers world-class capability in fuel burn, emissions, and noise. The technology portfolios developed under CLEEN I, II and proposed under CLEEN III are projected to continue improving on this state-of-the-art capability to deliver even more performance, noise reduction relative to the Stage 5 aircraft noise standards, nitrogen oxide (NOx) reduction, nonvolatile particulate matter (nvPM) reduction and additional fuel burn reduction. The proposed CLEEN III initiatives, when integrated with the UHB ratio GTF propulsor developed under the FAA CLEEN I program, and core technologies developed under the FAA CLEEN II program,will deliver 26 percent fuel-burn reduction (FBR), relative to a Year 2000 best-in-class aircraft, such as the Boeing 737-800, and achieve 18 EPNdB cumulative noise reduction relative to the Stage 5 aircraft noise standards (assuming approximately 3 EPNdB from airframe improvements). This represents a significant contribution to the achievement of the multiple FAA CLEEN subsonic transport aircraft goals and demonstrates the value of such programs for the country, its residents, the environment and our world.

CLEEEN II Technology, development and facilities, such as the PSU START test facility, has itself spun off additional technology development to continue efforts in defining alternatively manufactured highly efficient turbine blades with advanced cooling capability under the FAA ASCENT Program. This effort, contracted by the FAA to PSU, with support from P&W, will begin the learning and progressive technology development of low cost highly effective turbine blades of the future, while continuing educational development and university centers of excellence.

7. SUMMARY AND CLOSING STATEMENTS

In conclusion, the P&W FAA CLEEN II program was highly successful in demonstrating engine core thermal efficiency technologies with the GTF architecture.

The High Pressure Compressor and High Pressure Turbine rig testing made possible by collaboration between the FAA, PSU, and P&W, were able to demonstrate module level benefits utilizing full-scale hardware that are directly transferable to the GTF engine architecture.

For the HPC, P&W successfully demonstrated a product-like HPC core which in the end overachieved on estimated efficiency goals. P&W continued progress on the HPC design by testing the same core aero in both a ground and flight test engine bringing the Technology Readiness Level of that technology to TRL7.

For the HPT, P&W and the FAA assisted in enhancements to PSU's world-class START facility to enable the successful testing on novel technologies using new instrumentation and measurement methods in a representative engine environment. P&W was able to claim TRL 5 for durability technologies and TRL6 for aerodynamic technologies. The learning gained during the testing was directly transferred to ongoing design and manufacturing efforts for the GTF fleet.

In closing, P&W thanks the FAA for providing the funding and support in the successful execution of this highly successful program on-budget and on-time.